Electric transport and the pseudogap in the 1-2-3 HTSC system, under all-around compression (Review Article)

R. V. Vovk, and A. L. Solovjov

Articles you may be interested in

Electric transport and the pseudogap in the 1-2-3 HTSC system, under all-around compression (Review Article)

R. V. Vovk

V.N. Karazin Kharkov National University, Ministry of Education and Science of Ukraine,
4 Svoboda Sq., Kharkov 61107, Ukraine

A. L. Solovjov[a)]

B. Verkin Institute for Low Temperature Physics and Engineering, NAS Ukraine, 47 Nauka Ave.,
Kharkov 61103, Ukraine
(Submitted June 8, 2017)
Fiz. Nizk. Temp. **44**, 111–153 (February 2018)

The problem of how high pressure impacts various electric transport mechanisms in HTSC compounds $REBa_2Cu_3O_{7-\delta}$ (RE = Y, or another rare-earth ion) is considered. The features of the crystal structure and the effects that structural defects of different morphologies have on the electrical conductivity of these compounds in the normal, pseudogap, and superconducting states, are discussed. A review of the experimental data obtained in studies on the effect of high hydrostatic pressure on the various electric transport mechanisms of $REBa_2Cu_3O_{7-\delta}$ compounds, with varying composition and technical prehistory, is conducted. Different theoretical models devoted to the subject of how high pressure impacts the electrical conductivity of 1-2-3 HTSC system compounds are discussed. *Published by AIP Publishing.* https://doi.org/10.1063/1.5020905

Introduction

The gaps in the understanding of the anomalous properties of layered metal oxide superconductors (cuprates) continue be one of the most central problems in modern solid state physics. Despite the fact that 30 years have passed since high-temperature superconductors (HTSCs) were discovered in 1986 by Bednorz and Müller,[1] the microscopic mechanism responsible for this unique physical phenomenon remains unclear. The HTSC phase diagram is rather complex.[1–4] It contains an antiferromagnetic region, a "superconducting dome," a "strange metal" region, the Nernst effect, and a pseudogap that decreases linearly with increasing oxygen content.[3–5] Under-doped cuprates (UCs) are on the left flank of the "superconducting dome" and exhibit the most unusual and interesting properties in the normal state.[6–10] They are quasi-two-dimensional, highly correlated conductors with a low concentration of charge carriers n_f, and internal disorder. The charge carrier spectrum is characterized by a large (several hundred kelvin) pseudogap, the nature of which remains unclear, despite more than three decades of intensive research (Refs. [2–12] and references therein). UCs are not explained by the Landau-Fermi-liquid theory, and their resistive properties are not even qualitatively described by the Drude model. This has led to the generation of very unusual theories,[13–18] but none of them is able to explain the entire complex of experimental facts.

The pseudogap (PG)[5,7–11] that opens at a certain characteristic temperature $T^* \gg T_c$, where T_c is the superconducting (SC) transition temperature (critical temperature), remains the most intriguing cuprate property. By definition, the PG is a special state of matter that is characterized by a reduced (but not entirely to zero) electron density of states (DOS) at the Fermi level.[19,20] Note the fundamental difference between the pseudogap state and the superconducting state in which a SC gap opens and the DOS is zero.[21] It is believed that having a correct understanding of the PG nature will answer any remaining questions about the superconducting pairing mechanism in HTSCs, which is still debatable (Refs. [4], [5], [7], [9] and references therein). This is important to the search for new superconductors with an even higher T_c.

Despite the seemingly significant progress that has been achieved in recent years when it comes to fundamental research of HTSCs, an adequate solution to one of the most important applied problems still has not been found: the creation of HTSC materials with a high current density in strong magnetic fields. In terms of total critical parameters, not to mention technological qualities, traditional (low-temperature) superconductors still have no rivals. In this aspect, the most important experimental tool for studying HTSCs is the use of extreme effects such as high pressures,[6,22–25] which allow to successfully verify the adequacy of numerous theoretical models, as well as to establish more significant physical parameters of HTSC structures that determine their physical characteristics in the normal and superconducting states. With the exception of a few of our papers,[26,27] no literature has been devoted to examining the effects of pressure on the fluctuation conductivity and the PG in HTSCs.

The role of electron-phonon interaction (EPI) in the formation of Cooper pairs at such high temperatures remains unexplained.[28,29] It is assumed that EPI is probably present in cuprates, but must be strengthened by some additional interaction that is most likely magnetic.[5,7,11] Recent calculations[30] show that the specific nature of EPI in HTSCs causes a strong correlation narrowing of the electron band W. This leads to the chemical potential $\mu \sim W \gg J$, where J is the electron exchange interaction constant. The fulfillment of this condition is decisive in the formation of singlet electron pairs in HTSCs, which are bound by a strong effective kinematic field. However, there are no sufficient experimental results[26–29] to confirm these calculations.

The significant objective difficulties associated with the experimental study of charge transfer dynamics in such systems should also be acknowledged. These difficulties include: the rather complex crystal structure of HTSCs,[31,32] the heterogeneity of structural defect distribution,[33] the presence of intergranular boundaries and cluster inclusions,[34] the inhomogeneity of specific experimental samples,[35] often due to different technological backgrounds, and a number of others. All that has been said above largely determines the fact that the popular objects of experimental research on the different physical properties of HTSCs are 1–2–3 systems, $REBa_2Cu_3O_{7-\delta}$. This is due to several reasons. On the one hand, both point and planar (twin boundaries) defects can be produced quite effortlessly in this system, and their composition can be varied relatively easily by isovalent and non-isovalent doping with element substitution. On the other hand, using single-crystal samples of these compounds makes it possible to obtain experimental objects with a given topology of the defective ensemble, which in turn makes it possible to separate how the structural defects of different morphologies contribute to electric transport. The latter is of a decisive importance both to fundamental research, and to solving the most important applied problems discussed above: obtaining the newest functional materials with high electric transport parameters.

This article is an overview of how high pressure impacts the various electric transport mechanisms in $REBa_2Cu_3O_{7-\delta}$ HTSC compounds. Several theoretical models devoted to this problem are considered. Features related to the crystal structure and phase diagram are discussed, as well as how structural defects having different morphologies impact the electrical conductivity of these compounds in the normal, pseudogap, and superconducting states. A review of the experimental data obtained over the course of investigating the influence high hydrostatic pressure has on the various electric transport mechanisms of $REBa_2Cu_3O_{7-\delta}$ compounds with varying composition and technological background is presented.

1. Features of the crystal structure and specific conductivity mechanisms in 1-2-3 HTSC systems

1.1. The theoretical aspects of describing the pseudogap state in HTSCs

A rigorous theory for HTSCs, similar to the Bardeen-Cooper-Schrieffer (BCS), and the Bogolyubov theory for classical superconductors,[21] is currently absent. Other than Wang & Ching's publication entitled "A Structural-Based Microscopy Theory on High-Temperature Cuprate Superconductors,"[36] we are not aware of any other serious attempts to create a complete microscopic theory of HTSCs. Of the latest studies, Refs. 16 and 37 should be noted, as they contain references to most of the theoretical work devoted to the problem of HTSCs, but these articles draw opposing conclusions. Reference 37 demonstrates it is impossible to describe the existing experimental results for cuprate HTSCs, including those obtained using angle-resolved photoemission spectroscopy (APRES), without accounting for the origin of coupled fermions [we will call them local pairs (LP)[38]] below the pseudogap opening temperature $T^* \gg T_c$. In Ref. 16, Anderson's idea,[13,14,39] which

is based on the resonating valence bond (RVB) model, is taken to a new level. According to the RVB model, at $T < T^*$ electrons with charge and spin stop being well-defined excitations. There is a so-called charge-spin separation, as a result of which charge must be carried by spin-less holons, and spin is carried by charge-less spinons.[13,39] In the RVB model both types of excitations, spinons and holons, contribute to resistivity. However, the holon contribution is assumed to be decisive, whereas because spinons are effectively tied to the magnetic field $\mathbf{H}$, they must determine the temperature dependence of the Hall effect. Naturally, there is no talk of any paired states at $T < T^*$ in this case.

However, in spite of the substantial difference in the approaches to describing the PG state in HTSCs, we would like to note one similarity implicit in both articles: each of them postulates the presence of two types of particles in the sample, after the PG is opened. In the RVB model, these particles are spinons and holons. And in Ref. 37, the particles are electrons and local pairs, which arise at $T < T^*$, and whose nature remains unclear. Indirectly, the presence of two different types of particles in HTSCs under T^* is confirmed by experiments on measuring the magneto-optical Kerr effect in Bi-2223,[10] which, by definition, can only be observed if two varieties of particle are present in the sample. Strictly speaking, these studies reflect two opposite approaches to the understanding of the PG in HTSCs. The first is based on the idea that the PG occurs as a result of LP formation in cuprates (Refs. 3, 7, 9, 37, 40–44 and references therein). The second presupposes that the nature of the PG appearance is non-superconducting or magnetic. The number of such models is extremely high. These include theories that consider spin fluctuations,[45–47] the possibility of exciton,[36] and polaron[48] appearance, charge density wave interaction,[4,49] as well as the abovementioned charge-spin separation.[13,14,16] Our view is that the PG occurs as a result of locally paired (LP) fermions below T^*, but that the pairing mechanism is most likely magnetic.[5,8,10,16] The very abundance of the available models demonstrates that there is no final conclusion as to the PG and the pairing mechanism in HTSCs. This is explained by the extreme complexity of the HTSC crystal structure.

1.2. The features of the crystal structure, and specific conductivity mechanisms in 1-2-3 HTSC systems

The implementation of various electric transport modes has been actively studied at all stages of HTSC research.[50–52] According to modern concepts,[4,5,7,8,11,16] it is precisely the understanding of these systems' very unusual properties in the normal (nonsuperconducting) state that can serve as the key to answering questions related to the physical nature of HTSCs. An important role in the study of these physical phenomena is played by the composition and topology of the defective ensemble,[50,54,55] both of which determine the conditions for the transport current flow and charge carrier scattering mechanisms. In this aspect, the $REBa_2Cu_3O_{7-\delta}$ family compounds (Re = Y or another rare-earth ion) are the most promising in the implementation of such studies, due to the fact that the technology involved in their production is sufficiently developed,[53,55] and the fact that replacing yttrium with isoelectric analogues[56–58] is sufficiently easy.[56–58] Since a significant amount of the experimental work is conducted on ceramic,[35,59] film,[60–62] and textured[63] samples

from different technological backgrounds, many aspects of this issue are yet to be clarified. Suffice it to say that of the more than 700 articles published in the last five years in journals such as Phys. Rev. B, Phys. Rev. Lett. and Physica C or other publications devoted to various aspects of conductivity in HTSCs, less than 15% were carried out using single crystal samples.

However, YBaCuO single crystals always have planar defects, or twin boundaries (TB),[64] whose influence on the transport properties in the normal and superconducting states is insufficiently studied due to the experimental difficulties that manifest themselves in any attempts to determine the contribution of these defects.

This section presents the data on the crystal structure and features of a 1-2-3 HTSC system defective ensemble, as well as a brief analysis of the current state of research related to their electric transport characteristics.

1.2.1. The crystal structure of $REBa_2Cu_3O_{7-\delta}$ compounds

X-ray and neutron diffraction methods[65] have been used to establish that within the limits of $YBa_2Cu_3O_{7-\delta}$ oxygen stoichiometry variation there are two phases. Figure 1 shows the elementary cells of two compositions with minimum and maximum oxygen content ($\delta = 1$ and 0), whereas Fig. 2 shows another version of this representation. The elementary cell of $YBa_2Cu_3O_7$ is orthorhombic ($Pmmm$), and the unit cell of $YBa_2Cu_3O_6$ is tetragonal ($P4/mmm$), i.e., the structure and properties of $YBa_2Cu_3O_{7-\delta}$ are a direct function of the level of doping, which is determined by the oxygen index $7-\delta$.

In both cases, the structure is a derivative of perovskite (Fig. 2) with a tripled lattice period c due to Ba-Y-Ba cation ordering. Two thirds of Cu(2) copper atoms are in a tetragonal pyramidal configuration ($4 + 1$) of oxygen atoms, with the latter being displaced from the basal plane of the pyramids by approximately 0.3 Å along the c-axis. One third of the copper atoms Cu(1) are in the basal planes and have a variable oxygen configuration (Figs. 1 and 2). In the $YBa_2Cu_3O_7$ structure [the Cu(1) coordination number is 4] it is possible to isolate linear chains that are formed by flat squares Cu(1)-O(4), elongated along the b-axis. In the case of $YBa_2Cu_3O_6$, oxygen is entirely absent in the chain planes of CuO and the Cu(1) atoms have an oxygen coordination number of two. As such, the population of oxygen positions
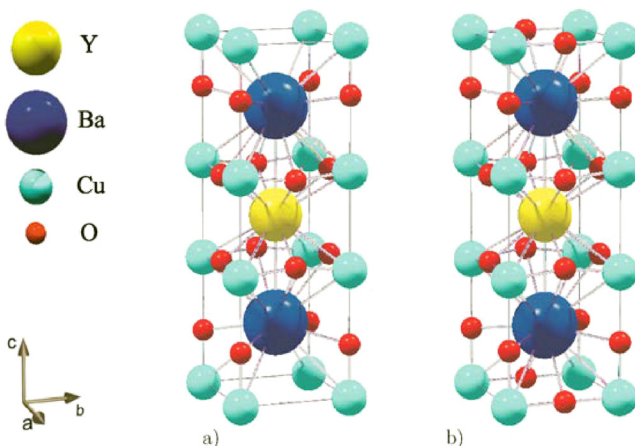

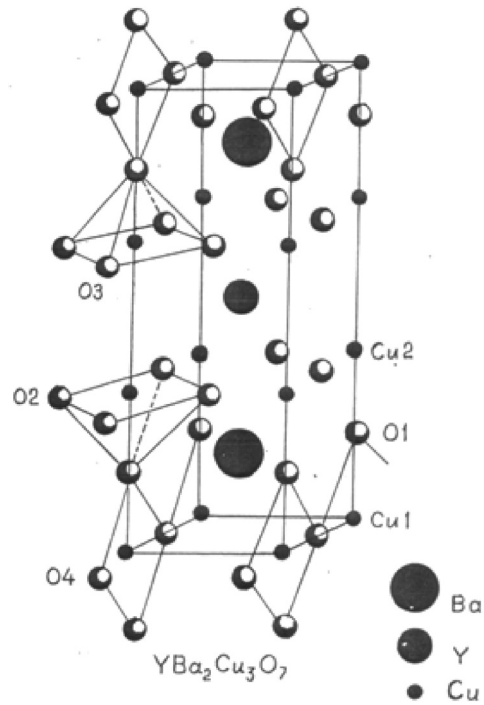FIG. 2. The crystal lattice of the $YBa_2Cu_3O_{7-\delta}$ (Ref. 67) compound.

in the basal plane determines the oxygen non-stoichionetry of $YBa_2Cu_3O_{7-\delta}$ (Refs. 31, 32, and 67; Figs. 1 and 2).

In fact, the elementary cell of $YBa_2Cu_3O_{7-\delta}$ (YBCO) ($V_{cell} \approx 1.74 \times 10^{-22}$ cm^3) is a structural "stack" consisting of seven planes:[31,32,67] two planes of CuO_2; two BaO planes with a Ba atom at the center of the plane; two chain CuO planes and an yttrium Y-layer. As already noted, conductivity is implemented mainly by CuO_2 planes. The role of the chains comes down to supplying the CuO_2 planes with charge carriers, and the Y-layer actually provides the anisotropic motion of charge carriers in such a system.[31] The CuO_2 planes are mirror symmetric with respect to BaO planes, however due to the presence of CuO chain planes and their slight longitudinal bending, the pairwise invariance in the CuO_2 planes is somewhat disrupted. A similar violation of charge symmetry also occurs in other HTSC systems containing CuO_2 planes, such as $Bi_2Sr_2CaCu_2O_x$ (BiSCCO), and can, in principle, limit the increase in T_c with an increasing number of CuO_2 planes in a HTSC system.[31,32,68]

The electronic configuration of cuprates is based on conducting CuO_2 planes located near the Y-layer (Figs. 1 and 2), which, in fact, determine the quasi-two-dimensionality of the HTSC electronic properties. Another component of the electronic structure of cuprates is the one-dimensionality of O-Cu-O chains. HTSC systems always have a CuO_2 plane, whereas the O-Cu-O chains could be absent, which is the case in La_2CuO_4 (for example see Refs. 31 and 68). Another known HTSC structure that is also missing O-Cu-O chains but has CuO_2 planes, is $Bi_2Sr_2Ca_{n-1}Cu_nO_{2n+4}$.[31] The cuprate layers in Bi-compounds form certain stacks (packets) of n layers of CuO_2. Inside each such packet is a strong Josephson interaction between the CuO_2 planes, which is reflected in tunnel experiments,[69,70] in particular.

Most of our experiments were performed on $YBa_2Cu_3O_{7-\delta}$ and $Y_{1-x}Pr_xBa_2Cu_3O_{7-\delta}$ (YPrBCO) single crystals. Therefore,

FIG. 1. The crystal lattice of the $YBa_2Cu_3O_{7-\delta}$ (Ref. 66) compound.

most of the attention will be paid to discussing the $YBa_2Cu_3O_{7-\delta}$ structure, which combines all of the features of copper-oxide cuprates and is one of the most complex and labile among all HTSC systems.[31,32,68,71]

In the ground state (Figs. 1 and 2) (oxygen index 7-δ < 6.4), all cuprates, including YBCO, are Mott insulators with long-range antiferromagnetic (AF) order, in which the electron spins $S = 1/2$ are localized on the copper ions Cu^{2+} (Ref. 71; Fig. 3). The dielectric state is a consequence of strong electron (Hubbard) correlations. The strong Coulomb repulsion U_{dd} at the Cu^{3+} centers leads to the $Cu_{x^2-y^2}$ energy band split into the lower (LHB) and upper (UHB) Hubbard bands, which are separated by the energy (Hubbard) gap $E_g = 1.5$–2 eV.[72] Within the framework of the single-band Hubbard model,[72–74] the LHB is completely filled, whereas the UHB is a free band. In YBCO there is a unique closeness between the d-states of copper and the p-states of oxygen.[32,68] As a result, the band structure of cuprate HTSCs is determined by the strongly correlated electron motion along the d-orbitals of copper, interacting with the p-orbitals of oxygen. However, it should be emphasized that the description of the YBCO dielectric state in terms of Cu $3d_{x^2-y^2}$ and O $2p\sigma$-orbitals cannot be considered entirely correct, since they are highly hybridized.[71,75]

In contrast to $La_{2-x}(Sr,Ba)_xCuO_4$ the charge carriers in YBCO arise as a result of oxygen intercalation.[31,32,68,71] The doping process begins with the filling of vacant places in the chains of the CuO_x base layer, in which oxygen is initially absent [Fig. 1(a)]. This doping stage [(7-y) < 6.2] does not affect the CuO_2 active plane. Upon introduction, oxygen attracts two electrons from neighboring Cu^+ ions, resulting in the formation of O^{2-}. Copper in chains has a variable valence depending on the number of nearest oxygen neighbors. Over the course of doping, a situation in which oxygen does not find positions with two neighboring Cu^+ ions arises in CuO_x. In this case, the necessary electron is taken from the neighboring active CuO_2 plane, which ultimately leads to the hole conductivity in YBCO. Thus, chemical doping is accompanied by a flow of charge between CuO_2 and CuO_x chains, which act as a reservoir of trapped electrons. One of the most fundamental concepts in HTSC physics is the possibility of charge redistribution between the quasi-independent unit cell structures that are separated in space.[31,75,76] At this doping stage the chains are mostly broken, having a minimum length of $l_0 \approx 4$ Å for the Cu^{2+}-O^{2-}-Cu^{2+} configuration. It is important that the transition from tetraphase to orthophase begins at $T = 300$ K and 7-$y \approx 6.25$ in the YBCO structure.[31,32] Note that in orthophase OI' the number of vacancies remains large enough that regardless of the partial ortho-ordering of oxygen along the b-axis, the system remains in a dielectric state even at low temperatures. One of the variants of the cuprate phase diagram is shown in Fig. 2, based on $La_{2-x}(Sr, Ba)_xCuO_4$, where the density of the charge carriers per Cu atom is plotted along the abscissa axis.

At 7-$y \geq 6.4$ and a charge carrier density per copper atom of $n_0 \sim 0.05$, there is a dielectric-metal transition, and YBCO acquires metallic conductivity while also simultaneously becoming a superconductor.[71] A spin glass region exists between the AF dielectric and superconducting

domains, in which long-range AF interaction is preserved, albeit weakened.

As oxygen content increases, the axial distance between the planar copper and apex oxygen Cu(2)$-$O(4) diminishes.[31,32,76] This occurs particularly sharply at the dielectric-metal transition, thus ensuring the efficiency of the electron transfer from CuO_2 to CuO_x, i.e., the doping of CuO_2 by holes. At the same time, as the Cu(2)$-$O(4) length contracts with doping, the copper valence increases from $Cu^{+2.1}$ (7-$y \approx 6.2$) to $Cu^{+2.2}$ (7-$y \approx 7$)[31] (Fig. 3). This suggests that initially the holes in the active CuO_2 layer appear in the copper subsystem. As a result, YBCO passes to the ortho-II phase with alternating filled α_1- and empty α_2-chains.[31,32] At the same time, the planar conductivity becomes metallic, whereas the activation of transverse conductivity along the c-axis depends on T. The number of charge carriers (holes) is still relatively small ($n_0 \approx 0.1$). Only $\sim 1/3$ of all holes are in the chain CuO_x-layer. The remaining 2/3 of the holes fall into the two CuO_2 planes. At 7-$y \geq 6.65$, free α_2-chains begin to be filled and T_c continues to increase. Simultaneously, the charge carrier density n_f also increases rapidly. At optimal doping (OD) (ortho-I phase) (7-$y \approx 6.9$, $T_c \approx 90$ K) $n_0 \sim 0.16$ (Fig. 3), and for each CuO_2 plane there are 0.25 of all holes, while 0.5 holes are already in the chain structure. The planar conductivity increases and attains values of $\sigma_{ab} \approx 10^4$ Ω^{-1} cm^{-1} in the ortho-I phase, whereas the transverse conductivity demonstrates a tendency to metallize.[68,78]

The regime into which YBCO transitions at 7-$y > 6.95$ ($n_0 > 0.16$) can be conditionally referred to as "overdoped."[79] In YBCO, this mode is achieved by additional doping using strontium.[4,80] In this regime, practically all CuO_x-layer chains are filled, and the system is *three-dimensionalized*. A sign of YBCO three-dimensionalization with increasing n_f can be the reduction in the distance between CuO_2 and apex oxygen from 2.47 Å at 7-$y = 6$, to 2.3 Å at 7-$y = 7$, as well as the appearance of a coherent (Drude) component for the transverse optical conductivity, which is tracked in IR optical experiments with highly doped samples in the frequency
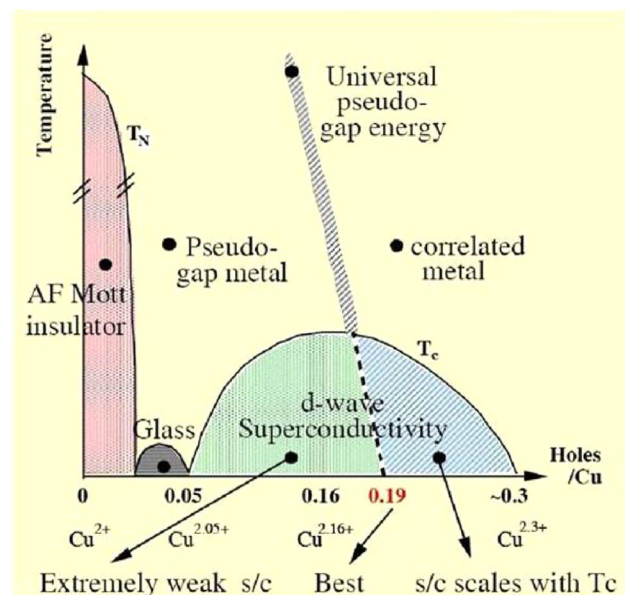

FIG. 3. A version of the HTSC cuprate phase diagram according to Ref. 77.

range of $<1000\,\mathrm{cm}^{-1}$. In this case $\sigma_\perp(T)$ already has a well-pronounced metallic course,[78] however T_c decreases. As the number of charge carriers grows, the band structure of YBCO also undergoes a dramatic change. In the "overdoped" mode the HTSC system becomes an ordinary uncorrelated metal, and the Hubbard gap, together with the correlation A-maximum, disappears.[75]

It should be noted one more time that even with the appearance of a small number of holes, the long-range AF order in HTSC systems quickly disappears. This is explained by the fact that holes, which are mainly introduced into oxygen $2p$-orbitals, effectively destroy the exchange interaction between copper spins.[71,81] However, despite the loss of long-range AF order, strong spin correlations in HTSCs persist up to very high doping levels, which is demonstrated by neutron scattering experiments.[82] This is explained by the fact that Coulomb correlations still make a significant contribution in the metallic 2D-phase. It is precisely these correlations, although they are weakened, that are considered to be the reason behind the conservation of magnetic fluctuations (possibly responsible for the pairing of charge carriers), and also of the Hubbard gap with a charge transfer from oxygen to copper. As a result, the metallic 2D phase is characterized by a number of unusual electrical, optical, and magnetic properties,[45,75,83] and the phase diagram of cuprate HTSCs has the form shown in Fig. 3. All that has been discussed above once again confirms the complexity of the electron and band structure of HTSCs, in particular that of YBCO, as well as their dependence on the level of doping. It should also be noted that different types of structural defects can significantly affect the behavior of HTSCs.

1.2.2. Different types of structural defects in 1-2-3 system compounds

In pure $YBa_2Cu_3O_{7-\delta}$ single crystals, the following structural defects can be observed, depending on the oxygen deficiency and synthesis technology: point defects such as oxygen vacancies that form in the CuO planes, (001) planar defects, twin boundaries, dislocations, and so called $2\sqrt{2} \times 2\sqrt{2}$ structures,[84] observed with an oxygen deficit $\delta = 6.8$–6.9.

Flat defects include twinning planes that form during the "tetra-ortho transition" and minimize the elastic energy of the crystal.[85] The twin boundaries are planes with a tetragonal structure caused by the presence of layers containing oxygen vacancies that are located along the twin boundary[86,87] (Fig. 4). Electron microscopy studies[87] have shown that at the initial stage of the tetra-ortho transition domain nuclei are formed, with two families of coherent interfaces: (110) and ($\bar{1}10$). This can be the reason behind the formation of a "tweed" type structure when close microtwins are overlapped.[87] The period of such a structure depends on the oxygen content and can be stimulated by doping with a trivalent metal—aluminum, in particular.[87,88] At the initial stage of microdomain formation, the TB occurs as a result of the diffusion of structural vacancies in CuO-layers. The propagation of the TB is implemented by the motion of twinning dislocations that are controlled by stresses.

Linear defects (dislocations) are more likely for epitaxial films and textured samples. The source of this type of defect can be misfit dislocations generated by the film-substrate
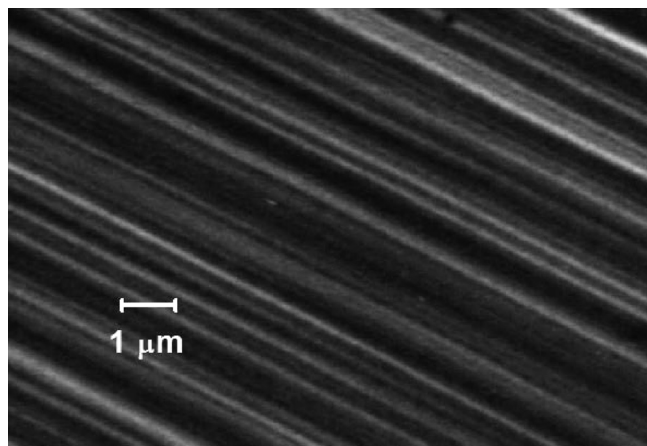

FIG. 4. A photo of a section belonging to a $HoBa_2Cu_3O_{7-\delta}$ single crystal with unidirectional twins.[85]

interface in film samples, and misfit dislocations occurring at the interface between $YBa_2Cu_3O_{7-\delta}$ and $YBa_2Cu_3O_5$ phases in textured fused samples. The dislocation density in the films can reach values of about $1.4 \times 10^8/\mathrm{cm}^2$.[89]

The high density of dislocations in $YBa_2Cu_3O_{7-\delta}$ single crystals can be obtained by growing crystals during a peritectic reaction,[90,91] which is probably due to small inclusions of the $YBa_2Cu_3O_5$ phase. In crystals grown by the solution-melt method, the dislocation density is about $5 \times 10^3/\mathrm{cm}^2$.[92] Note that the dislocation density can be increased by thermo-mechanical processing of the materials.[93]

Point defects (oxygen vacancies) are present in all $YBa_2Cu_3O_{7-\delta}$ samples due to the non-stoichiometric oxygen content. The filling factor is close to one for all oxygen positions, with the exception of CuO(1) [Figs. 1(b) and 2]. Depending on oxygen content, it is possible for superstructures to be formed, given a periodic distribution of oxygen vacancies. In this case the density of oxygen vacancies is relatively large and at $\delta = 0.03$ it is about $10^{26}/\mathrm{m}^3$.

Literature provides reports of a systematic copper deficit in the CuO planes, which can reach values of 0.09 in YBCO compounds.[94] Point defects can also be obtained with doping. As a rule, alloying elements (with the exception of rare-earth elements and Sr) are introduced into the Cu(1) positions.[95] The rare-earth ions and K replace the yttrium atoms, whereas Sr is implanted into the position of the Ba atoms.

Additional defects can be obtained by irradiation.[96,97] Depending on the type of particles and their energy, both point and linear defects (tracks of heavy particles with high energy)[98] can be created, however this is beyond the scope of this review.

1.2.3. The impact of structural defects on the transport properties of HTSCs

It is obvious that the transport properties of HTSC materials will be highly dependent on the structure defects, as well as on the content of oxygen[99] and impurities.[100,101] The resistivity of $YBa_2Cu_3O_{7-\delta}$ single crystals with oxygen content close to the stoichiometric, at room temperature, is ρ_{ab} (300 K) $\approx 200\ \mu\Omega$ cm in the ab-plane and ρ_c(300 K) ≈ 10 mΩ cm along the c-axis.[37,102] In perfect single crystals the electrical conductivity is quasi-metallic in all crystallographic directions.[103–105] However, even a slight deviation

from stoichiometry, $\delta \leq 0.1$, leads to quasi-semiconductor dependence $\rho_c(T)$ while maintaining the quasi-metallic nature of the $\rho_{ab}(T)$ dependence.[77,106] Further decreases in the oxygen content leads to a decrease in the charge carrier density, thermal and electrical conductivity of the YBa$_2$Cu$_3$O$_{7-\delta}$ superconductor, and in the case of an oxygen deficiency $\delta \geq 0.6$, a metal-insulator transition is observed, as noted above.[107] Alloying the YBa$_2$Cu$_3$O$_{7-\delta}$ single crystals with metallic elements, with the exception of the cases specified above, lead to the replacement of copper atoms in the CuO$_2$ planes. At the same time, data on the degree of influence such a substitution will have are largely contradictory. For instance, Ref. 108 reports that according to different authors, an increase in ρ_{ab} in YBa$_2$Cu$_{3-z}$Al$_z$O$_7$ at $z = 0.1$ can be less than 10%, or that it can double at the same Al concentration. The reason for this discrepancy is probably the nonuniform distribution of Al over the crystal volume, since because the single crystals are grown in corundum crucibles, the introduction of Al occurs in an uncontrolled manner. The broad transitions to the superconducting state with $\Delta T_c \approx 2$ K serve as evidence of the nonuniform Al distribution. There is also a significant spread in the parameters of the superconducting state. Whereas alloying YBa$_2$Cu$_3$O$_{7-\delta}$, has almost no effect on the transport characteristics of the normal and superconducting states[109,110] as yttrium is replaced with rare-earth elements.

An exception is the replacement of yttrium with praseodymium Pr atoms, because it has its own magnetic moment $\mu_{Pr} = 3.56\ \mu_B$ and $\mu_{eff} \sim 2\ \mu_B$ in PrBCO. In the range of concentrations $y \leq 0.05$ in a Y$_{1-y}$Pr$_y$Ba$_2$Cu$_3$O$_{7-\delta}$ (YPrBCO) superconductor, the density of charge carriers n_f and ρ_{ab} weakly depend on the concentrations of Pr.[111,112] At $y > 0.2$ there is a sharp decrease in n_f, and at $y > 0.3$ the temperature dependence of the resistivity $\rho(T)$ acquires a semiconductor character. At the same time, T_c decreases rapidly.[113] Eventually Y$_{1-y}$Pr$_y$Ba$_2$Cu$_3$O$_{7-\delta}$ becomes an insulator at $y > 0.7$.[111] This behavior arises as a result of the Fehrenbacher-Rice (FR) energy band, due to the formation of a highly hybridized $4f$-Pr–$2p_\pi$-O (PrIV) state. The increase in resistance and the decrease in T_c are a result of the decrease in the number of free charge carriers in the CuO$_2$ planes, which are localized in the FR band.[114] The calculations performed within the framework of the FR theory, with allowance for p–f hybridization,[115] have shown that a decrease in the charge carrier density n_f in YPrBCO with increasing Pr concentrations, occurs as a result of the holes transitioning from the $pd\sigma$ band of the CuO$_2$ planes into the FR band. This process has little effect on the CuO chains, whose number of holes remains practically constant.[113,116] As a result, the oxygen concentration in YPrBCO also remains the same. Therefore, the study of YPrBCO allows for a direct examination of how HTSC properties change with changes in n_f.

It should also be noted that the properties of PrBCO single crystals are significantly dependent on the method according to which they are prepared. When using standard methods of growing HTSC single crystals from melts, such as spontaneous crystallization from solutions in a melt, the Bridgman method, the zone melting method, and the Kyropoulos and Czochralski processes, PrBCO, as noted above, is an insulator, although it is isostructural to YBCO. However, if the traveling-solvent floating-zone (TSFZ)

method is used at reduced oxygen partial pressure, it is possible to obtain superconducting Pr123 systems with $T_c > 100$ K under a pressure of ~ 8 GPa.[117] This most likely occurs as a result of a noticeable change in the structural parameters of the single crystals, which in turn leads to the shielding of the Pr intrinsic magnetic moment.[117]

As already noted, YBa$_2$Cu$_3$O$_{7-\delta}$ has twin boundary planar defects (Fig. 4). The impact these defects have on the transport properties in the normal state are studied in Refs. 118 and 119, which demonstrate that the twins are effective charge carrier scattering centers. According to Ref. 118, the mean free path of electrons in single crystals l is estimated to be $\sim 0.1\ \mu$m, which is an order of magnitude smaller than the inter-twin distance. Therefore, the maximum increase in $\rho(T)$ due to scattering can be 10%. This is approximately the same increase in resistance that was observed with current flowing across the twins, in comparison to the resistance with current flowing along the twins[85,119] (Fig. 4). It should also be noted that the TBs, being an additional source of anisotropy and acting as powerful pinning centers, can have a significant effect on the magnetoresistive properties (pinning and magnetic flux dynamics), as well as on the magnitude of the critical current in HTSC materials.

Let us emphasize that the external pressure has significant effects on the crystal structure of HTSCs,[120,121] appreciably changing the defect distribution across the sample. Various aspects of these effects are considered in Sec. 4.

2. Normal and excess conductivity of HTSC compounds REBa$_2$Cu$_3$O$_{7-\delta}$ having different defect structure morphology

2.1. The properties of a system with low charge carrier density

Circling back to the cuprate phase diagram (Fig. 3), it is worthwhile to emphasize once again that one of the main differences between HTSCs and *ordinary* metals is a reduced charge carrier density n_f that is about an order of magnitude smaller even with optimal doping. Only in a strongly overdoped mode is n_f so large that it becomes necessary to account for electron-electron interaction (EEI), and the behavior of the system becomes Fermi-liquid (FL).[61,71,122] The fact that the enhancement of the EEI leads to the $\rho \sim T^2$ dependence that is typical for a FL and observable in "overdoped" cuprates,[72,106,123] as opposed to the linear $\rho \sim T$ that is typical for cuprates in a normal state with optimal and low-level doping[7,61] (Fig. 5) can be considered completely established. However, we should underscore that the PG is specifically observed in systems with a reduced n_f (Fig. 3), and that the properties of such systems are extremely specific.[61,124,125]

2.1.1. The BEC-BCS transition in HTSCs and the local pair model

In the classical theory of superconductivity, it is assumed that the chemical potential $\mu = \varepsilon_F$ (ε_F is the Fermi energy), and that it actually does not depend on anything, which is only valid in the high-density fermion limit, characteristic only of ordinary superconductors.[21] In systems with a low charge carrier density, μ becomes a function of n_f, T, and the energy of the bound state of two fermions $\varepsilon_b = -(m\xi_b^2)^{-1}$, wherein m is the fermion mass with a quadratic dispersion law $\varepsilon(k) \sim k^2$, and ξ_b is the coherence length
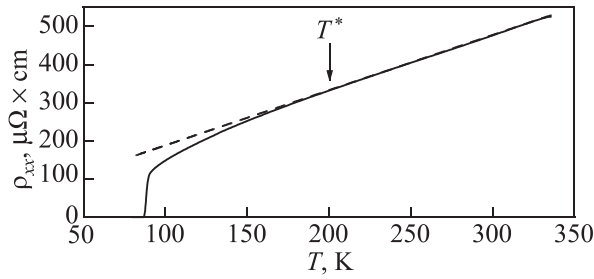
FIG. 5. The temperature dependence of resistivity measured in the *ab*-plane of a YBCO film with $T_c = 87.4$ K (sample F1, solid line). The dashed line is the dependence $\rho_N(T) = \alpha T + b$, extrapolated to the low-temperature region.[61]

(the scattering length in the *s*-channel). Thus, ε_b becomes an essential physical parameter of the interacting Fermi system and determines the quantitative criterion of a dense $\varepsilon_F \gg |\varepsilon_b|$ ($\mu = \varepsilon_F$ is classical "weak" superconductivity) or "dilute" $\varepsilon_F \ll |\varepsilon_b|$ ($\mu = -|\varepsilon_b|/2$ is an HTSC system with strong coupling) Fermi liquid.[126–129] It should be stressed that in systems with a reduced n_f, the quasiparticle behavior in the high-temperature region near T^* can be described using Bose-Einstein condensation (BEC), whereas BCS theory operates in the SC state.[3,5,7,9] Thus, the theory predicts a change in the properties of HTSCs when the charge carrier density varies with doping, and also a BEC-BCS transition with decreasing temperature in systems with a given n_f,[126,129–131] occurring at $T^* > T_{\text{pair}} > T_c$. This situation is illustrated in Fig. 6 from Ref. 131.

It can be seen (curves 3–5) that as T decreases, the BEC regime ($\mu/|\varepsilon_b| < 0$) shifts to the BCS mode, the temperature of which, T_{pair}, rises with an increasing n_f. And for a very small n_f (curve 3), a return to BEC is possible, but already below T_c.

We share the point of view that the pseudogap occurs as a result of the formation of local pairs below T^*.[3,37,40] Moreover, it is assumed that $T \leq T^*$ LPs exist as strongly coupled bosons (SCB).[3,7,126–129] SCBs are very small ($l \sim \xi_{ab}$) non-interacting pairs with an exceptionally strong
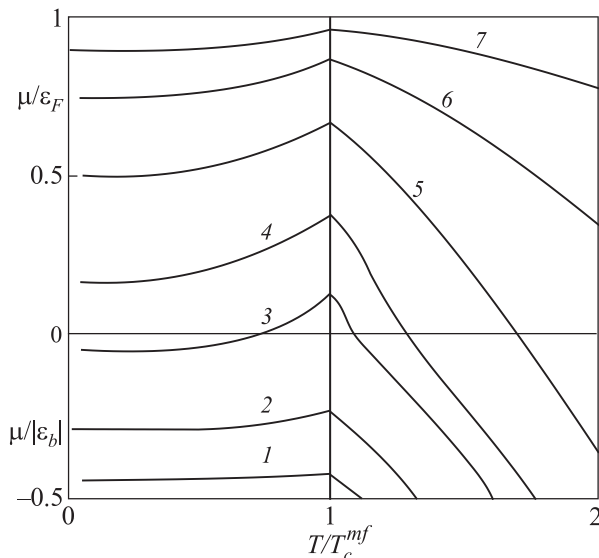

FIG. 6. The dependences $\mu(T)$ for varying $\varepsilon_F/\varepsilon_b$: 0.05 is the BEC limit (1); 0.2 (2); 0.45 (3); 0.6 (4); 1(5); 2 (6); 5 (7); ≥ 10 is the BCS limit (upper curve).[131]

bond $\varepsilon_b \sim \xi_{ab}^{-2}$ that is not destroyed by thermal fluctuations. Here, $\xi_{ab} = \xi_{ab}(0)(T/T_c - 1)^{-1/2}$ is the coherence length in the *ab*-plane, the value of which is very small: $\xi_{ab}(0) = \xi_{ab}(T^*) \sim 5$ Å for OD YBCO, and $\xi_{ab}(T^*) \sim 15$ Å for weakly doped YBCO.[61,132,133] It is assumed that it is precisely this small value of $\xi_{ab}(T^*) \sim 15$ Å that makes the pairing in HTSCs possible at such high temperatures. To compare, for aluminum $\xi_{ab}(0) \sim 16\,000$ Å. Accordingly, the coupling in such a pair is extremely small, and the pairs in Al are destroyed even at $T_c \sim 1$ K.[21]

It is possible to logically explain almost all phenomena that are observed in HTSCs at $T \leq T^*$ using the LP model. As such, a decrease in $\rho(T)$ is generated by the fact that the SCBs can carry current without dissipation. A decrease in the DOS[19,20] and an increase in the Hall coefficient $R_H \sim 1/(en_f)$[134,135] can be explained by the obvious decrease in the density of normal charge carriers n_f that occurs due to SCB formation. It should also be noted that according to the theory,[126–129] stable strongly coupled bosons that obey BEC can only be realized in systems with a low n_f. In the "overdoped" mode there are no SCBs, and as a result, there is no PG (Fig. 3). However, the question of what exactly constitutes a local pair in the SCB state, i.e., at the temperature ranging from T^* to T_{pair}, remains unanswered. According to different models, these can be excitons,[36,136] polarons,[48] bipolarons,[48,137,138] waves of charge[139] or spin[45,49] density, fluctuating antiferromagnetic clusters,[140] hypothetical holon-spinons, introduced by the RVB model,[13,16,21,39] or simply coupled electrons—similar to a Cooper pair, but with exceptionally strong coupling.[30,37,46,141] However, by definition, non-interacting SCBs cannot condense into the SC state. Therefore, the theory suggests that at $T \leq T_{\text{pair}} \sim 130$ K (for YBCO) these formations are transformed into fluctuation (but not coherent) Cooper pairs (FCP), whose coherent behavior rapidly increases as T_c is approached.[3,41,42,70,125] This behavior is a specific property of cuprates, due to their exceptionally short coherence length in HTSCs, though it increases rapidly with decreasing T.[3,5,7,9,126–129] The BEC-BSC transition temperature, T_{pair}, is clearly observed in a number of experiments.[61,142,143] However, the details of such a transition are also not completely clear.

Our calculations show that in well-structured YBCO films with different n_f and, as a consequence, with T_c ranging from 87.4 to 54.2 K, $T_{\text{pair}} \approx 133$ K, i.e., it does not depend on the level of doping.[7,61,62] Moreover, for all samples this temperature corresponds to $\xi_{ab}(T_{\text{pair}}) \sim 18$ Å. Thus, when the size of the pairs $\xi_{ab}(T) < 18$ Å, the LPs behave like SCBs. At $\xi_{ab}(T) > 18$ Å the LPs begin to overlap and transform into FCPs.[3,7] As the temperature drops further and $\xi_{ab}(T)$ increases, one more nontrivial effect is observed in HTSCs. Below T_{01} [≈ 115 K for YBCO and ≈ 130 K for Bi2212 (Ref. 125)] there is a region of superconducting fluctuations, in which, as will be shown below, excess conductivity [Eq. (1)] obeys the classical 3D Aslamazov-Larkin theory[144] and the 2D Maki-Thompson theory.[145] This means that below T_{01} the phase rigidity of the superconducting order parameter, predicted by the theory in Ref. 40, is preserved, and therefore, so is the superfluid density n_s, which is confirmed by experiments.[41,42] This means that in the temperature range from T_c to T_{01} LPs largely behave as superconducting, but incoherent pairs (short-range phase correlations).[3,8,9,40–42]
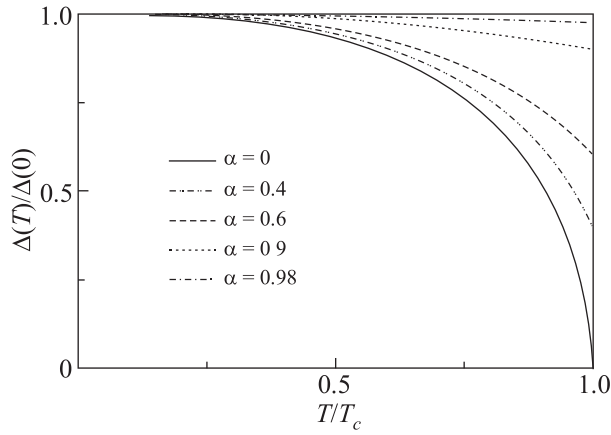
FIG. 7. The dependences of $\Delta(T)/\Delta(0)$ on T/T_c at different values of the PG parameter, α. $\alpha = 0$ corresponds to the BCS limit, $\alpha = 0.98$ corresponds to the BEC limit.[146]

This leads to a specific behavior of cuprates, wherein the SC gap at T_c does not vanish, which is what follows from BCS theory,[21] but transforms instead into a PG.[70,125] This is shown schematically in Fig. 7.[146] It can be seen that as n_f decreases (increase in PG and the α parameter) the dependence $\Delta(T)/\Delta(0)$ deviates even further from the classical BCS dependence (solid curve with $\alpha = 0$) and does not vanish at $T = T_c$, which is completely inexplicable from the perspective of classical superconductivity.

Figure 8 shows the result of an experiment confirming this, in which the internal tunneling effect was examined when current was passed across a structure consisting of 10 layers of Bi2223.[70] The points correspond to the tunnel maxima on the $dI/dV(V)$ dependences obtained for different T. It can be seen that the SC gap Δ does not vanish at T_c, but rather smoothly turns into a PG. Furthermore, it can be seen that, as predicted by theory,[3,146] $\Delta^*(T_c) = \Delta(0)$ for all three of the test samples. It is also clear that the features of the tunnel spectra are well observed only up to $T_{pair} \sim 150$ K, up to which short-range correlation interaction remains between the pairs.[70,125,147] Above 150 K the tunnel maxima are

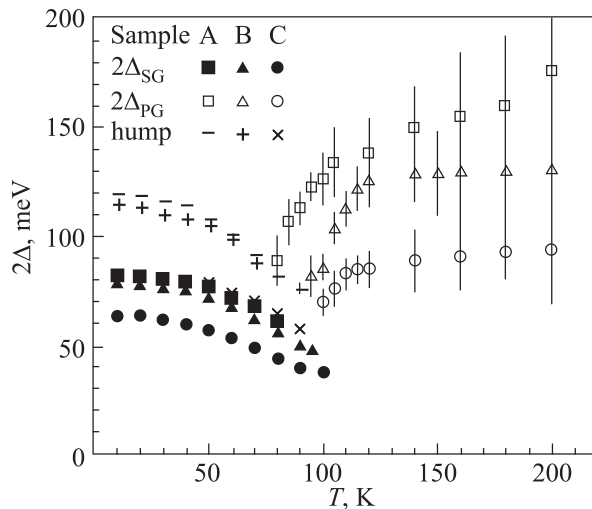FIG. 8. The SC gap $2\Delta_{SG}$ and pseudogap $2\Delta_{PG}$ in Bi2223 as functions of T: A ($\blacksquare$, $\square$) is for weakly doped ($T_c = 82$ K), B ($\blacktriangle$, $\triangle$) is for OD ($T_c = 96$ K), and C ($\bullet$, $\circ$) is for "overdoped" ($T_c = 105$ K) samples. The additional notations correspond to blurred maxima that are observed in the SC state at high V, and have yet to be explained.[70]

completely blurred,[70] since any correlation interaction in the SCB system is completely absent.[3,7,125–129]

It is also worthwhile to note that in tunneling experiments the transition from the SC to the PG mode always occurs smoothly.[69,70] For example, this same result is given by ARPES measurements for the $(BiPb)_2Sr_2CuO_6$ (Pb-Bi2201 with $T_c \sim 21$ K) single crystals in the antinodal direction ($\varphi = 0°$) of the Brillouin zone.[148] However, as shown by the later results of this[149] and other groups,[150,151] the BiSCCO system has a set of angles $\varphi \sim (45–35)°$, in which the ARPES signal is equal to zero in the PG state. These are so-called Fermi arcs (Refs. 150, 151 and references therein), which have yet to be observed in YBCO systems.[5]

2.1.2. Fluctuation conductivity and the 2D-3D crossover in HTSCs

No matter which HTSC property is being measured, whether it is resistivity, the Hall coefficient, the Knight shift, which is the frequency shift at nuclear magnetic resonance, they all change significantly upon transitioning through the pseudogap (PG) opening temperature $T^* \gg T_c$.[5,7,124] In resistive measurements the PG manifests itself as the deviation of the resistance measured in the ab-plane $\rho_{ab}(T) = \rho(T)$ from the dependence that is linear at high T, toward smaller values (Fig. 5). This leads to the appearance of an excess conductivity $\Delta\sigma(T) = \sigma(T) - \sigma_N(T) = [1/\rho(T)] - [1/\rho_N(T)]$, or

$$\Delta\sigma(T) = \left[\rho_N(T) - \rho(T)\right]/\left[\rho(T)\rho_N(T)\right], \qquad (1)$$

wherein $\rho_N(T) = \alpha T + b$ is the sample resistance in the normal state, extrapolated to the low temperature region.[143,152,153] According to the nearly antiferromagnetic Fermi liquid (NAFL) model,[45] the linear dependence of $\rho(T)$ above T^* corresponds to the normal HTSC state, which is characterized by the stability of the Fermi surface.[4,8,45]

According to modern ideas,[5–7] the small coherence length and quasi-layered structure of HTSCs lead to the appearance of a wide fluctuation region on the $\rho(T)$ curves near T_c, where $\Delta\sigma(T)$ obeys classical fluctuation theories (Refs. 144, 145, 154–156 and references therein). At the same time, a change in the content of oxygen, impurities, and structural defects has a significant impact on the formation of $\Delta\sigma(T)$, and therefore, on the realization of different regimes in which fluctuation conductivity exists above the critical temperature.[6,50–52,61] According to currently available ideas, the region in which the FLC exists can be conditionally divided into three characteristic temperature intervals, defined by the ratio of the coherence length perpendicular to the ab-plane $\xi_c(T)$, to the size of the crystal cell along the c-axis d, and the distance between the conducting CuO_2 layers in HTSC d_{01}:

(1) A narrow section in the immediate vicinity of T_c is the so-called "beyond 3D" mode;[50–52,61]
(2) $\xi_c(T) > d$ is the region of 3D fluctuations (closer to T_c);
(3) $d > \xi_c(T) > d_{01}$ is the region of 2D fluctuations (furthest from T_c).

The mechanism responsible for the appearance of the first regime is still unclear. It is assumed that it corresponds to so-called "first-level pairing."[50–52] The 3D-region matches the mode at which $\xi_c(T) > d$ and Josephson interaction

between pairs is realized for the entire volume of the super-conductor. It is assumed[40–42] that in this region the main contribution to the FLC comes from Cooper pairs that occur spontaneously at $T > T_c$, as a result of classical Aslamazov-Larkin (AL) fluctuation pairing. According to Ref. 144, this contribution to the HTSC can be written as

$$\Delta\sigma_{3DAL}(T) = \left[e^2/32\hbar\xi_c(0)\right]\varepsilon^{-1/2}, \qquad (2)$$

where $\varepsilon = (T - T_c^{mf})/T_c^{mf}$ is the reduced temperature; T_c^{mf} is the critical temperature in the mean-field approxima-tion,[6,61,152,153] which separates the FLC region from the region of critical fluctuations or the SC order parameter fluc-tuations Δ directly next to T_c (where $\Delta < k_BT$), not consid-ered in the Ginzburg-Landau theory.[21] The method for determining T_c^{mf} is examined in Sec. 4.2.2. It should be emphasized that $\Delta\sigma_{3DAL}$ is observed in all HTSCs without exception, including magnetic FeAs superconductors,[157] and is practically independent of the sample defect structure.

Since $\xi_c(T) = \xi_c(0)\varepsilon^{-1/2}$ decreases with increasing T, the region of 3D FLC, where $\xi_c(T) > d$, is observed only up to $T \sim T_0$, above which $\xi_c(T) < d$.[156] However, in the tempera-ture range $T_0 < T < T_{01}$ it is still greater than the distance $d_{01} \sim 4$ Å (for YBCO)[85] between the internal conducting CuO_2 planes. As a result, $\xi_c(T)$ still connects the internal planes via Josephson interaction, and the system is in a quasi-two-dimensional (2D) state.[60,145,156] The FLC in real HTSCs near T_c will be considered in detail in Secs. 4 and 5. In this case, the degree of inhomogeneity in the sample structure becomes important. The question of how the struc-tural defects impact the FLC regime in film samples of the $YBa_2Cu_3O_{7-\delta}$ compound is studied in Refs. 50–52, 61, and 158. In this case it was shown[7,60] that for samples having a perfect structure, the dominant contribution to the FLC in the 2D-region comes from the Maki-Thompson (MT) fluctu-ation mechanism,[145] which is defined as result of the interac-tion between the fluctuation pairs and the normal charge carries. According to the Hikami-Larkin (HL) theory, devel-oped specifically for HTSCs, the MT contribution to the FLC can be represented as

$$\Delta\sigma_{MT}(T,H) = \frac{e^2}{8\hbar d(1 - \alpha/\delta)}\ln\left\{\frac{\delta}{\alpha}\frac{1 + \alpha + \sqrt{1 + 2\alpha}}{1 + \delta + \sqrt{1 + 2\delta}}\right\}\varepsilon^{-1}. \qquad (3)$$

Such a contribution is determined by the decoupling pro-cesses in a particular sample, i.e., it depends on the lifetime of the fluctuation pairs τ_φ (Ref. 145)

$$\tau_\varphi\beta T = \pi\hbar/8k_B\varepsilon = A/\varepsilon, \qquad (4)$$

where $A = 2.988 \times 10^{-12}$ s K. The multiplier $\beta = 1.203\,(l/\xi_{ab})$ (where l is the mean free path, ξ_{ab} is the coherence length in the ab-plane) corresponds to the case of the pure limit $(l > \xi_{ab})$, which is always realized in high-temperature superconductors.[7,60]

In the presence of various defects in the sample, the dependence $\Delta\sigma(T)$ is determined by the Lawrence-Doniach (LD) model,[154] which is also a special case of the HL theory:

$$\Delta\sigma_{LD} = \left[e^2/(16\hbar d)\right](1 + 2\alpha)^{-1/2}\varepsilon^{-1}. \qquad (5)$$

In Eqs. (3) and (5)

$$\alpha = 2\xi_c^2(T)/d^2 = 2\left[\xi_c(0)/d\right]^2\varepsilon^{-1} \qquad (6)$$

is the coupling parameter, and

$$\delta = \beta(16/\pi\hbar)\left[\xi_c^2(0)/d^2\right]k_BT\tau_\varphi \qquad (7)$$

is the decoupling parameter. The LD model provides a good description of the experiment on granulated YBCO films,[153] and films with defects.[158] Respectively, in well-structured HTSCs above $T_0 > T_c$ $\Delta\sigma(T)$ is determined by the 2D MT contribution (3). Thus, at T_0, a 3D-2D (AL-MT) crossover is observed.[145] It is obvious that at a crossover temperature $\xi_c(T_0) = \xi_c(0)\varepsilon_0^{-1/2} = d$, which also makes it possible to determine[60,61]

$$\xi_c(0) = d\sqrt{\varepsilon_0}. \qquad (8)$$

It is also worthwhile to note that the MT contribution is not observed in BiSCCO.[152] In bismuth HTSCs near T_c the FLC is also described by the 3D AL contribution, and above T_0 it is described by the 2D AL theory

$$\Delta\sigma_{2DAL}(T) = \left[e^2/16\hbar d\right]\varepsilon^{-1}. \qquad (9)$$

Thus, the classical fluctuation theory of AL and the HL theory developed for HTSCs, both based on the concept that incoherent FCPs exist in cuprate HTSCs at $T > T_c$, provide a good description of excess conductivity $\Delta\sigma(T)$ only up to a temperature $T_{01} \sim 15$ K above T_c. This result, $T_{01}/T_c \approx 1.18$, is obtained on well-structured two-layer YBCO-PrBCo films.[159] Accordingly, above T_{01}, where $\xi_c(T) < d_{01}$, the superconducting and normal charge carriers are located directly in the conducting CuO_2 planes, between which there is no Josephson interaction.[156] For this reason, above T_{01} the fluctuation theories do not describe the experiment, as clearly seen by the results given in Secs. 4 and 5. Therefore, it is obvious that $\xi_c(T_{01}) = d_{01}$, and, as noted above, it is the temperature T_{01} that determines the SC fluctuation region above T_c: $\Delta T_{fl} = T_{01} - T_G$.[159] Accordingly $T_G > T_c^{mf}$ is the Ginzburg temperature,[160–162] up until which $\Delta\sigma(T)$ obeys the fluctuation theories.

As noted above, T_{01} is precisely the temperature to which the phase rigidity of the SC order parameter wave function, and therefore the superfluid density n_s, are con-served in HTSCs,[3,9,40] which is experimentally con-firmed.[41,42] Therefore, the question of the temperature T_{01} is very important. At $T > T_{01}$ the fluctuation conductivity decreases faster than predicted by fluctuation theory. It was assumed that the reason for this is an underestimation of the contribution made by short-wave order parameter fluctua-tions, while it increases with rising temperature. The studies by Varlamov and co-authors[163,164] conducted microscopic calculations of $\Delta\sigma(T)$ with consideration of all the order parameter components. A comparison of the experimental data and the theory[163,164] was carried out in Ref. 57. In this case the agreement with the theory is obtained up to temper-atures of about $T \approx 1.35\,T_c$. However, as before, with addi-tional temperature increases, $\Delta\sigma(T)$ decreases more rapidly than follows from the theory.[163,164] Unfortunately, as already

mentioned, currently there is no strict theory that would describe excess conductivity across the entire temperature range from T_c to T^*, and in particular from T_{01} to T^*. It seems that it is precisely in this region that with rising temperature the local pairs transition from FCPs to SCBs (the earlier-mentioned BCS-BEC crossover), which is confirmed by numerous experiments.[7,19,20,41,42,124,142,143] This behavior is typical for the PG mode in HTSCs, which is discussed in more detail within the next section.

2.1.3. The pseudogap in high-temperature superconductors

Another property inherent to systems with low charge carrier density is the pseudogap, which occurs in cuprate HTSCs at $T^* \gg T_c$ (Refs. 3, 5, 7, 8 and references therein). NMR[19] and ARPES[20,143] studies have convincingly demonstrated that in cuprates at $T \le T^*$ there is a decrease not only in resistance, but also in the density of electron states at the Fermi level (DOS). As noted above, a state with a partially reduced DOS above T_c is a pseudogap by definition.[4,5,7,19,20] Thus, had there been no decrease in the DOS, which precipitated the discovery of the PG in HTSCs, the temperature dependence of resistivity would remain linear up to T_c, which is what happens in classical superconductors.[19] It follows that the excess conductivity $\Delta\sigma(T)$ that manifests as a result of the pseudogap opening, must contain information about the PG. In order to extract it, a special method of analysis[7,62,142] based on the local pair model[3,125–131] has been developed.

As already noted, the number of theoretical models used to describe the PG is exceptionally high (see Refs. 3, 5, 7, 9, 125–129, 165, 166 and references therein). At the same time, not counting our studies, the number of articles devoted to studying the temperature dependence of the PG in HTSCs is very small.[69,70,146,167,168] In our opinion, this is due to the absence of a rigorous theory and corresponding equations that would describe the temperature dependence of the PG. Obviously, in order to extract information about the PG from excess conductivity, one must have an equation that would describe $\Delta\sigma(T)$ in the entire temperature interval from T^* to T_c, and would contain the Δ^* parameter in explicit form. In cuprates Δ^* is considered to be a parameter of the pseudogap, which, as noted above, most likely opens up as a result of local pair formation below T^*. Thus, $\Delta^*(T)$ must reflect the behavior of the LPs at a temperature decrease from T^* to T_c.[7,61,62,167]

In the absence of the corresponding rigorous theory, the equation for $\Delta^*(T)$ was proposed in Ref. 62, taking into account the formation of LPs below T^*

$$\sigma'(T) = A_4 \frac{e^2\left(1 - \dfrac{T}{T^*}\right)\exp\left(-\dfrac{\Delta^*}{T}\right)}{16\hbar\xi_c(0)\sqrt{2\varepsilon_{c0}^*}\,\text{sh}\left(2\dfrac{\varepsilon}{\varepsilon_{c0}^*}\right)}. \quad (10)$$

Here $(1 - T/T^*)$ determines the number of pairs formed below T^*, and $\exp(-\Delta^*/T)$ is the number of pairs destroyed by fluctuations below T_{pair}.[7,61,62] Solving Eq. (10) with respect to Δ^*, we obtain

$$\Delta^*(T)$$
$$= T\ln\left[A_4\left(1 - \frac{T}{T^*}\right)\frac{1}{\sigma'(T)}\frac{e^2}{16\hbar\xi_c(0)}\frac{1}{\sqrt{2\varepsilon_{c0}^*\,\text{sh}(2\varepsilon/\varepsilon_{c0}^*)}}\right], \quad (11)$$

where $\sigma'(T)$ is the experimentally measured temperature dependence of excess conductivity for a particular sample. In addition to $\sigma'(T)$, T^*, T_c^{mf}, ε and $\xi_c(0)$, determined based on resistive and FLC measurements, Eqs. (10) and (11) include a scaling coefficient A_4 and a theory parameter ε_{c0}^*.[62,168] However, within the LP model all parameters can be experimentally determined, as will be discussed in detail in Secs. 4 and 5.

Figure 9 shows the temperature dependences of the PG, $\Delta^*(T)$, obtained using the LP model for four well-structured YBCO films with different charge carrier densities and consequently a T_c, ranging from 87.4 K (sample F1, top curve) to 54.2 K (sample F6, bottom curve).[61,62,142] Each of the curves has four singular points marked with dashed lines for sample F1. These are T^*, $T_{\text{pair}} \approx 133$ K, which corresponds to a maximum on all curves, T_{01}, corresponding to the minimum Δ^*T near T_c, and T_c^{mf}, which is always slightly higher than T_c.[62,159] It can be seen that in this case T_{pair} does not depend on the level of doping. Moreover, it is shown that for all samples $\xi_{ab}(T_{\text{pair}}) \sim 18$ Å.[62] Thus, we can assume that 18 Å is the critical size of the pairs in YBCO. Above T_{pair}, where $\xi_{ab}(T) < 18$ Å, the LPs will behave like SCBs, and below, where $\xi_{ab}(T) > 18$ Å, they transform into FCPs.[3,7,62,142]

Figure 10(a) shows the temperature dependence of spectral weight at the Fermi level, $W(E_F)$, obtained using the ARPES (angle resolved photoemission spectroscopy) method based on an analysis of the energy distribution curves (EDC) for the single crystal $(Bi,Pb)_2(Sr,La)_2CuO_{6+\delta}$ (Bi2201).[143] Figure 10(b) shows the dependence $\Delta^*/\Delta^*_{\text{max}}$ for the same sample, calculated by us using the local pair model (dots).[142] It can be seen that our T_{pair} (maximum on the curve $\Delta^*/\Delta^*_{\text{max}}$) coincides with the T_{pair} obtained using ARPES measurements. It is also clear that $W(E_F)$ smoothly
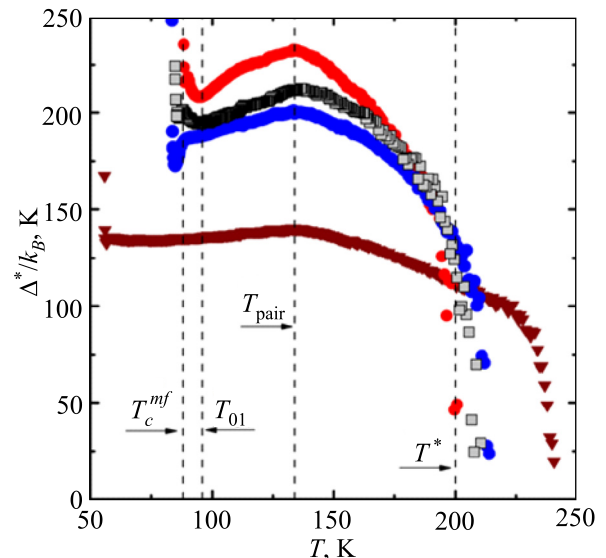

FIG. 9. The temperature dependence of the PG $\Delta^*(T)$ for well-structured YBCO films with different nf, and as a result, $T_c = 87.4$ K (sample F1, upper curve ●), 81.4 K (F3, ■), 80.3 K (F4, ●) and 54.2 K (F6, ▼). The dashed lines indicate T^*, T_{pair}, T_{01} and T_c^{mf} for F1 sample.[61,62]

passes through T_c. Therefore, it is assumed *a priori* in Ref. 143 that, since below T_c there are SC pairs in the sample, these pairs will also exist above T_c, i.e., in the PG temperature range all the way until T_{pair}. These results completely coincide with our ideas as to the existence of the FCPs in the $T_c - T_{pair}$ temperature range.[7,62,142] What happens in the interval $T_{pair} - T^*$, where $W(E_F)$ shows a linear dependence on T, is not discussed in Ref. 143. It is obvious that at T_{pair} the LP properties change, i.e., in accordance with the above, as the temperature increases the FCPs transform into SCBs (theory-predicted[126–131] BCS-BEC transition). It is logical to assume that the $T_c - T_{pair}$ interval is a region in which SCBs exist in the sample. Indeed, in the normal state above T^*, where there are no pairs, the dependence $W(E_F)(T)$ becomes nonlinear right away. The same happens with $T \leq T_{pair}$, where the SCBs transform into FCPs, i.e., once again, the SCBs are gone.

Also, Fig. 10 shows the dependence of the spectral gap (empty squares), determined using the EDC maxima at different temperatures,[143] which, unlike our $\Delta^*(T)$, is in no way correlated with the dependence $W(E_F)(T)$. Thus, a comparison of the results of our analysis and the corresponding ARPES experiments performed on a single sample shows that the LP model can be used to provide a reasonable explanation of all observed features of the temperature dependence $W(E_F)$, which confirms the correctness of our approach to analyzing the PG.[62,142]

3. High-pressure induced redistribution of labile oxygen and longitudinal electric transport in REBa₂Cu₃O₇₋δ (RE = Y, Ho) single crystals with different oxygen content

An important aspect of increasing the critical characteristics of HTSCs is the change in the parameters of the crystal
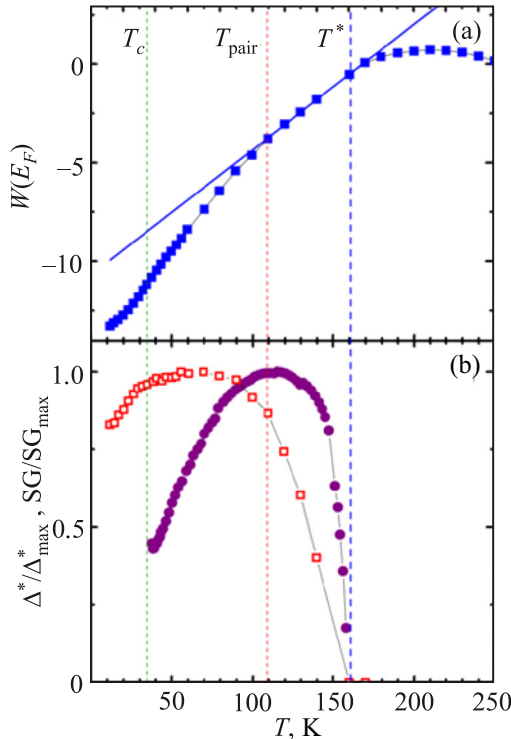

FIG. 10. The temperature dependence of the spectral weight at the Fermi level $W(E_F)$ (■) for a Bi2201 sample with $T \sim 32$ K; (b) is the PG dependence $\Delta^* T$ (●) calculated using the LP model, and the spectral gap (□) obtained using ARPES measurements for the same sample.[142]

lattice, in particular, the change in Cu-O and Cu-Cu distances in the *ab*-plane.[31,32,169] Indeed, as shown in Ref. 169, there is a clear correlation between the change in T_c during the annealing process and the change in the $d_{Cu(2)-O(4)}$ distance. It was shown that smaller lattice parameters correspond to a greater degree of oxygen ordering. The reverse also seems logical, that greater ordering in the oxygen-vacancy system should correspond to smaller lattice parameters. One of the most important methods for clarifying this issue is the application of high hydrostatic pressures. As noted above, in Refs. 22–25 and 170 it was shown that in determining dT_c/dP, the two effects associated with a decrease in the unit cell volume and oxygen redistribution should be separated. In this section we will try to briefly discuss each of these mechanisms.

Section 3.1 provides a brief overview of the theoretical and experimental studies on the evolution of electric transport characteristics in HTSC compounds during the application of pressure. Experimental studies that recorded the true and relaxation effects of pressure are listed, and a model of labile oxygen diffusion migration is briefly described. Section 3.2 shows the original authorial results of studies on the effects of high hydrostatic pressure up to 1.1 GPa on the conductivity in the *ab*-plane of a YBa₂Cu₃O₇₋δ single crystal with reduced oxygen content, and Sec. 3.3 is about the influence of pressure and planar defects on the fluctuation conductivity in single crystals with optimal composition and a given topology of twin boundaries.

3.1. The "true" and "relaxation" pressure effects in YBa₂Cu₃O₇₋δ single crystals with oxygen deficiency

3.1.1. The impact of pressure on the phase state of 1-2-3 system compounds

A set of studies on the different physical properties of high-temperature superconducting 1-2-3 system compounds based on yttrium, show the presence of a nonequilibrium state at some degree of oxygen deficiency in such structures. An important role is played by external factors such as temperature and high pressure,[22–25,50,169–172] leading to a change in the lattice parameters and inducing processes of labile oxygen redistribution, which, in turn, impact the critical parameters of the superconductor.

One of the first and most detailed experimental studies of how pressure affects the T_c in YBa₂Cu₃O₇₋δ (YBCO) (1-2-3 system) was undertaken in Refs. 23 and 24. It follows from the generalized data that the pressure derivative dT_c/dP is positive and is essentially dependent on the concentration of charge carriers n_f. It reaches a maximum in samples with a reduced n_f and $T_c \sim 25$ K, and tends to a minimum when T_c reaches the highest value of $T_c \approx 90$ K and n_f corresponds to optimal doping.

According to Ref. 50, the critical temperature as a function of pressure $T_c(P)$ for a YBCO system can be written as

$$T_c(P) = T_c + \frac{T_c}{T_c^{max}} \Delta T_c^{max}(P) + T_c^{max}(P)$$
$$\times \beta \left[2(n^{opt} - n) - \Delta n(P) \right] \Delta n(P), \quad (12)$$

wherein T_c^{max} is the maximum T_c for this compound, $\Delta T_c^{max}(P)$ is the increase in T_c under pressure, $\beta = 1/(n^{min} + n^{max})^2$ and $n^{opt} = (n^{min} + n^{max})/2$. At $P = 0$ n^{min} is the

minimum number of holes per CuO_2 plane at which superconductivity is manifested, equal to 0.05; n^{max} is the maximum number of holes at which superconductivity disappears, and n^{opt} is the number of holes per CuO_2 plane at which $T_c = \Delta T_c^{max}$, ≈ 0.25 (Fig. 3). Accordingly, $\Delta n(P)$ is the increase in charge carriers under pressure, for the specific sample.[31,32,50]

In this expression, the second term characterizes the change to T_c under pressure, caused by the changes to the lattice parameters, the electron-phonon interaction, linkages between layers, etc., as the so-called "true" pressure effect. The third term is provided by the change to the number of holes under pressure—which is the "relaxation" effect, related to the redistribution of labile oxygen. When summarizing the theoretical and experimental data available to date, we can conclude that separating "true" and "relaxation" pressure effects is important.

3.1.2. "True" pressure effect

One possible explanation for the features along the $T_c(P)$ dependence in the 1-2-3 system was proposed by the Saiko-Gusakov theoretical model,[173,174] which associates the superconducting transition temperature change with the singularities of apical O(4) atom dynamics, which form a bi-stable sublattice controlled by the application of external pressure and changes in oxygen non-stoichiometry. According to Refs. 173 and 174, the birth of a 90-degree phase upon application of pressure to a 60° phase sample, or the alternation between these same phases with varying degrees of oxygen non-stoichiometry, is caused by the "switching" of the frequency mode that dominates in BCS pairing by transforming the bi-stable potential of apical oxygen atoms. With decreasing x, the pressure required for converting the system to a 90° phase also decreases. Thus, a significant increase in T_c under pressure is interpreted as an extended transition from a 60° phase to a 90° phase. Indeed, as can be seen in Fig. 11, which shows the $T_c \sim d \ln T_c / d \ln V$ (T_c) diagram of $YBa_2Cu_3O_{7-\delta}$ crystals with $\delta \leq 0.1$, $\delta \approx 0.45$, and $\delta \approx 0.5$, calculated with allowance for the bulk moduli [100 GPa for $\delta < 0.1$ and 115 GPa at $\delta > 0.1$ (Ref. 175)], the dependences $d \ln T_c / d \ln V$ (T_c) for $\delta \approx 0.45$ and $\delta \approx 0.5$ exhibit a kink that can indicate a transition from the 60° phase to the 90° phase, differing with respect to dT_c/dP.
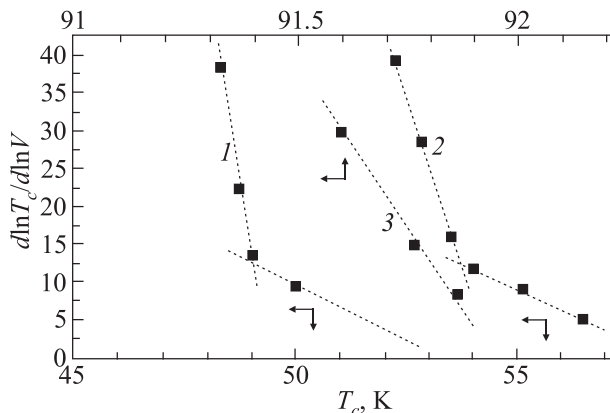

FIG. 11. The diagram of $T_c \sim d \ln T_c / d \ln V$ (T_c) $YBa_2Cu_3O_{7-\delta}$ crystals with oxygen deficiency $\delta \approx 0.5$ (1) and 0.45 (2), as well as a sample with composition close to stoichiometric $\delta \leq 0.1$ (3), calculated with allowance for bulk moduli [100 GPa for $\delta < 0.1$ and 115 GPa for $\delta > 0.1$ (Ref. 175)].

However the anomalous increase in dT_c/dP obtained in Ref. 25, from 1.5 to 2.5 K/kbar in the low pressure region up to 1.2 Kbar, at an insignificant difference in oxygen content in samples with $T_c \approx 45$ and 50 K, as well as a change in the sign of dT_c/dP with the application of uniaxial pressure along different crystallographic directions,[176] apparently does not allow one to unequivocally explain the singularities of the $T_c(P,\delta)$ dependences using only this theoretical model.

It is likely that the features in the behavior of $T_c(P,\delta)$ dependence are the consequence of several mechanisms, one of which being generated by changes to the band structure subjected to uniform compression. The observed linear connection between $d \ln T_c / d \ln V$ (T_c) and $d \ln T_c$ can be derived using the Labbe-Bok model,[177] which accounts for the contribution a logarithmic singularity makes to the density of states of a half-filled band. According to Ref. 177, T_c is given by expression

$$T_c = D \exp\left(\frac{-1}{\lambda^{1/2}}\right), \tag{13}$$

where D is the width of the singularity, λ is the electron-phonon interaction constant. Then, for the volume dependence of T_c we have

$$\frac{d \ln T_c}{d \ln V} = \frac{d \ln D}{d \ln V} + \frac{1}{2\lambda^{1/3}} \frac{d \ln \lambda}{d \ln V}. \tag{14}$$

From here

$$\frac{d \ln T_c}{d \ln V} = a_1 \ln T_c + a_2, \tag{15}$$

where

$$a_1 = -\frac{1}{2} \frac{d \ln \lambda}{d \ln V}; \quad a_2 = \frac{d \ln D}{d \ln V} - a_2 \ln D. \tag{16}$$

The kinks along the $d \ln T_c / d \ln V$ dependences can be related to the cluster structure of the sample, which is confirmed by the presence of steps on the resistive transitions to the superconducting state. As was shown in Ref. 178, the observed stepped form of the resistive transitions indicates a non-stoichiometric ratio of oxygen and vacancy concentrations, which leads to the formation of a mixture of phase clusters that are characterized by different oxygen content and ordering thereof, and accordingly, have different critical temperatures dT_c/dP.

The relatively weak effect pressure has on the T_c of optimally doped samples can be explained using a model that presupposes the presence of a van Hove singularity in the charge carrier spectrum.[179] As is well known, for crystals with $T_c \sim 90$ K the Fermi level lies in the valley between two peaks of the density of states, while the density of states at the Fermi level $N(E_F)$ essentially depends on the orthorhombic distortion $(a - b)/a$.[179] An increase in the ratio $(a - b)/a$ causes an increase in the distance between DOS peaks, and therefore, a decrease in $N(E_F)$ and T_c. A reduction in $(a - b)/a$ leads to the convergence of the DOS peaks, and an increase of $N(E_F)$ and T_c. The following regularities in changes to T_c have been observed in studies investigating the impact of uniaxial compression along the a- and b-axes

on the critical temperature of single crystals with T_c ~ 90 K:[176] when a load along the *a*-axis is applied, the critical temperature increases, whereas if a load is applied along the *b*-axis, it decreases. Under the influence of hydrostatic pressure the value of the ratio $(a - b)/a$ varies slightly, since it is determined only by the difference in the compression moduli along the *a*- and *b*-axes. Therefore, a change in the critical temperature with respect to hydrostatic pressure is relatively small.

For crystals with $T_c \sim 60$ K the Fermi level is shifted from the middle of the band and is located away from the van Hove singularity. Therefore, if the critical temperature is primarily determined by the density of electron states, then its increase under hydrostatic pressure means that under pressure, the Fermi level must shift toward the DOS peak.

3.1.3. Phase separation and the relaxation effect of pressure

Driessen *et al.*[23] were the first to establish an important feature: the baric derivatives dT_c/dP of the start and end of the YBaCuO SC phase transition have opposite signs in the 0–170 kbar pressure range (Fig. 12).

At the same time, the low temperature phase corresponds to the negative derivative $dT_{cf}/dP < 0$, and the high temperature phase is consistent with the positive derivative $dT_{c0}/dP > 0$. Thus, the application of high pressure leads to a broadening of the temperature interval $T_{c0} - T_{cf}$ that corresponds to the realization of fluctuation paraconductivity at $T > T_c$.

As we know based on existing literature,[23,125] in HTSC cuprates the dependence $T_c(x)$ is sufficiently well described by a universal parabolic dependence

$$T_c = T_c^{max}\left[1 - A(x - x_{opt})^2\right], \tag{17}$$

where T_c^{max}, A, x, and x_{opt} are the pressure functions. In YBCO the concentration of charge carriers can vary with changes to the oxygen concentration (Fig. 13[180,181]) via cat-ionic substitution or pressure application.

This dependence correctly describes $T_c(x)$ for compounds such as $YBa_2Cu_3O_{6+x}$, $Y_{1-x}Ca_xBa_2Cu_3O_6$, $La_{2-x}Sr_xCuO_4$, $La_{2-x}Sr_xCaCu_2O_6$ and also for $(Ca_xLa_{1-x})(Ba_{1.75-x}La_{0.25+x})Cu_3O_y$ at different oxygen concentrations *y*. The critical temperature depends not only on the concentration of charge
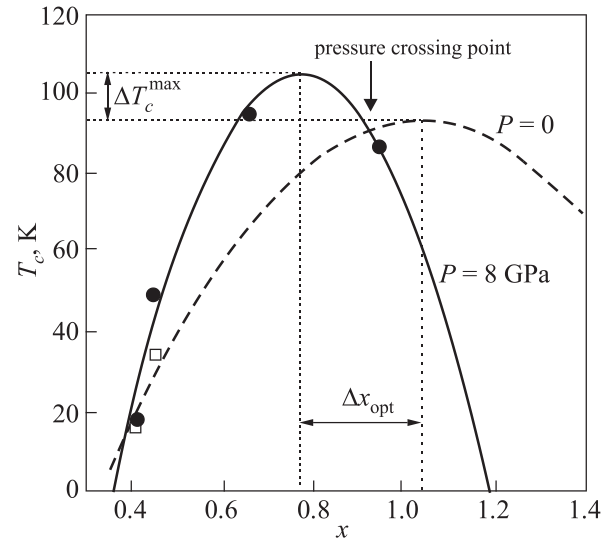
FIG. 13. T_c as a function of oxygen content *x* for $YBa_2Cu_3O_{6+x}$ at a pressure in the range of 0–8 GPa. The parabolic approximation of the experimental data is taken from Refs. 180 and 181.

carriers, but also on the bond strength in CuO_2 planes, as well as on the pressure-induced structural phase transformations and relaxation processes. At the same time, an interesting effect associated with the ordering of labile oxygen in the lattice is observed: an increase in the pressure reduces the defect mobility and simultaneously increases the degree of oxygen-vacancy ordering. This effect is clearly manifested in YBCO samples with a reduced oxygen content,[181] in which the value of dT_c/dP depends strongly on the temperature at which the pressure is applied.

It is worthwhile to add that Abrikosov's studies on fluctuation effects[182] have suggested the formation of superconducting filaments, or so-called "stripes" in one selected crystallographic direction, i.e., one-dimensional superconducting channels. Such channels occur far from the percolation threshold and can increase the superconductivity of the sample. For a lower carrier density ($x_1 < x < x_{opt}$) at $T < T^*$, fermions begin to unite into local pairs (complex bosons), which condense only at T_c (Figs. 3 and 13).[126–130] For high carrier concentrations ($x_{opt} < x < x_{max}$), both characteristic lines eventually merge and $T^* = T_c$. Meaning that in this case, the formation of Cooper pairs occurs at the same temperature as the superconducting condensate (Figs. 3 and 13).

In the local pair model,[183] the pressure derivative dT_c/dP changes in different ways on either side of the point corresponding to the optimal carrier concentration. The hopping integral *t* increases with increasing pressure. Therefore, the pressure coefficient is positive below x_{opt}, and T_c changes as $t^2/|U|$, where *U* is the activation energy. Since at $x > x_{opt}$ T_c changes as $1/2zt$, the pressure coefficient is negative (as is the case in the BCS model) (Fig. 14). Near T_c^{max} the pressure derivative dT_c/dP goes to zero. Consequently, pressure causes T_c increase in the concentration range where there are two special characteristic temperatures, T^* and T_c. If $T^* = T_c$, then the pressure coefficient is negative and T_c decreases with pressure, as is the case for "classical" superconductors. This dependence has been experimentally confirmed for YBCO,[184] for which a positive and negative pressure derivative dT_c/dP at different values of *x* has been observed.
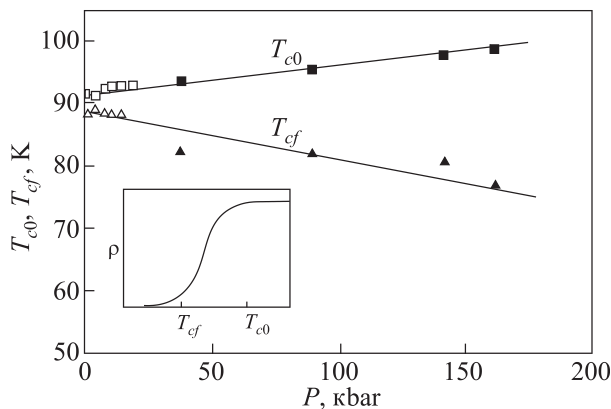

FIG. 12. T_{c0} and T_{cf} as functions of pressure, for YBaCuO.[23] On the inset: T_{c0} is the critical temperature at the start, T_{cf} is the temperature at the end of the SC transition.
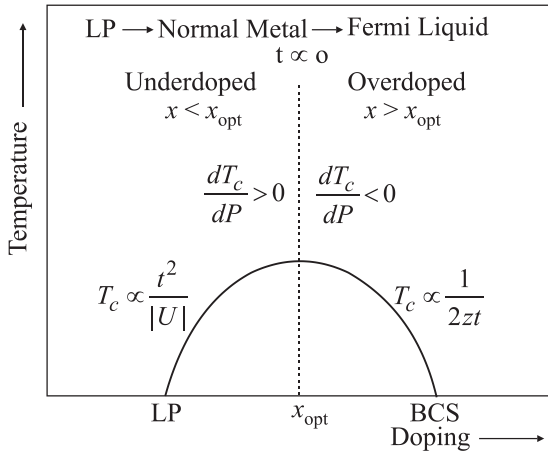
FIG. 14. The scaling of the pressure effect below ($x < x_{opt}$) and above ($x > x_{opt}$) the optimal carrier concentration.[180,183]

The calculations carried out in Ref. 185 show that the broadening of the pseudogap, associated with the overlapping of S- and D-wave components, causes an additional increase in T_c in the low-alloyed regime. Above the x_{opt} concentration, the lines $T^*(x)$ merge with the line $T_c(x)$, and Bose-Einstein condensation takes place in the metallic region, where the charge and phase fluctuations can be neglected, as in the case of the BCS model. Therefore, in this case the pressure effect is negative. However, the shift of x_{max} with respect to lower concentrations is still experimentally unconfirmed.

3.1.4. The high-pressure-induced diffusion of the labile component in YBa₂Cu₃O₇₋δ

In 1-2-3 system compounds, diffusing oxygen defects are usually already present as a result of the synthesis procedure.[64,172] Assuming that the total defect volume is zero, we can write[181]

$$\Delta V_A \approx \Delta V_M \approx N_A \frac{\partial E_A}{\partial P}, \qquad (18)$$

where N_A is Avogardo's number.

This expression for the migration volume has a simple physical interpretation. If the ion diffuses from one cell to another, it must overcome the energy barrier E_A, which exists due to its interaction with the ionic environment. Under pressure P, the free movement of ions inside the crystal is extremely difficult, since they must now work against the external pressure $\Delta E_A = P\Delta V_M$, which increases the activation energy by ΔE_A. In the hard sphere model,[181] each ion interacts with its neighbors as a rigid ball, with its ionic radius corresponding to its valence. At present, the ionic radii for ions relevant to this discussion have been calculated: $r(Cu^{1+}) = 0.96$ Å, $r(Cu^{2+}) = 0.72$ Å, $r(O^{2-}) = 1.32$ Å, $r(Ba^{2+}) = 1.34$ Å.[181] All ions are assumed to be solid spheres. The volume change due to the diffusion of ions through the "saddle point" is considered local.[181]

There is still no consensus in literature as to the dominant pathway of oxygen diffusion: different authors suggest different paths, but most believe that oxygen diffuses through the center of the cell in the Cu-O chain layer (Fig. 15).[181] Calculations of the migration volume give a value of
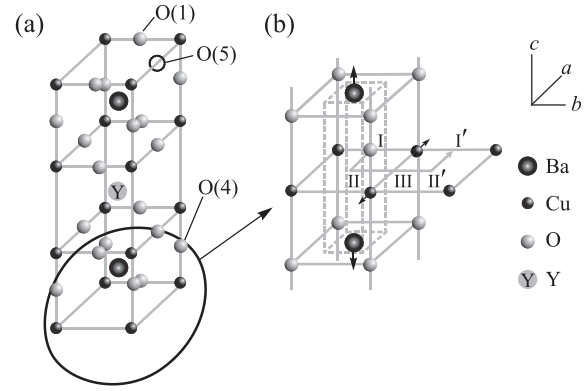

FIG. 15. Calculation of the migration volume in Y-123.[181] (a) The orthorhombic structure of Y-123. (b) The corresponding part of the Y-123 structure with Ba-O and Cu-O layers.

$\Delta V_M \approx 1.9$ cm³/mol for $YBa_2Cu_3O_{6.41}$ and $YBa_2Cu_3O_{6.45}$, which is approximately half the calculated value obtained in previous studies.[186]

At the same time, much less attention has been paid to studying the effect of pressure on the superconducting gap Δ[29] and the pseudogap Δ^*.[26,27]

4. The effect of pressure on the fluctuation conductivity and pseudogap of YBa₂Cu₃O₇₋δ single crystals with different levels of doping

As noted in the previous section, hydrostatic pressure is a powerful method for investigating the behavior of high-temperature superconductors.[120] It has been established that pressure markedly decreases cuprate resistance ρ and increases T_c. However, the mechanisms behind such behavior are not completely clear (see Sec. 3). As noted above, unlike classical superconductors, in cuprates the dependence of dT_c/dP is positive in an overwhelming majority of cases, while the derivative $d\ln\rho/dT$ is negative and relatively large. The mechanisms determining the effect of pressure on ρ are not fully understood, since the nature of HTSC transport properties, strictly speaking, is not entirely established. As is known, the main contribution to the conductivity of cuprates comes from CuO_2 planes, between which there is a relatively weak interplane interaction. Most likely, the pressure leads to an increase in the charge carrier concentration (n_f) in the CuO_2 conducting planes and, as a consequence, to a decrease in ρ. Obviously, an increase in n_f under pressure should also lead to an increase in T_c, i.e., to an experimentally observed positive dT_c/dP (Fig. 13). In this case, most likely one must take into account both the "true" and "relaxation" pressure effects.[23,24,50,173,174] Possible mechanisms behind the influence of pressure on T_c are considered in Sec. 3.

At the same time, the way in which pressure affects the magnitude and temperature dependence of the pseudogap has not been investigated before the publication of our studies. The increase in the PG under pressure was recorded for the first time in Ref. 26 (weakly doped YBCO single crystals) and Ref. 27 (optimally doped YBCO single crystals), both of which will be considered in this section.

4.1. The experiment

$Ya_2Cu_3O_{7-\delta}$ (YBCO) and $HoBa_2Cu_3O_{7-\delta}$ (HoBCO) single crystals are grown by gold crucible solution-melt

technology, according to the procedure in Refs. 187–190. As a result of annealing in an oxygen atmosphere at a temperature of 370–410 °C for three to five days, the single crystals have a pronounced twin structure (see Fig. 4).[191] Annealing is necessary to obtain samples with specific oxygen content.[187,188,191] As a result, twin boundaries are formed throughout the entire volume of the crystal (Fig. 4), which effectively minimizes the elastic energy of the crystal lattice during the transition from the tetra- to the ortho-phases (see Sec. 1.2.1).[188] Rectangular crystals with characteristic dimensions of about $2 \times 1.5 \times 0.5$ mm are selected in order to perform resistive measurements from a single batch. The minimum crystal size corresponds to the direction of the c-axis. The experiment geometry is set up such that the transport current is either parallel to the TB (YBCO) or flows at an angle of 45° to the TB (HoBCO). The electrical resistance in the ab-plane is measured using the four-probe method at a constant current of up to 10 mA, on a fully computerized set-up.[26,27,85,189] Current junctions are made using a silver paste along the edges of the single crystal to ensure a uniform distribution of the current across the central part of the sample, where potential contacts are located as two parallel strips. The contact resistance is less than 1 ohm, as detailed in Refs. 85 and 189. The temperature is measured by a Pt thermometer with an accuracy of 1 mK. At each level of pressure, the measurements are performed in temperature drift mode, which is about 0.1 K/min for measurements near T_c and about 5 K/min at $T \gg T_c$. The hydrostatic pressure is created in a Teflon chamber inside a piston-cylinder apparatus made of copper-beryllium, according to the procedure in Refs. 85 and 192. A manganin sensor prepared using a 25-ohm wire is used to measure the pressure. A mixture of transformer oil with kerosene 1:1 is used as a medium for transferring pressure, and the pressure change is always carried out at room temperature. In order to determine the impact of oxygen redistribution, the measurements are taken two-seven days after the pressure reduction, so that the relaxation processes could be completed.[26,27,85,187,188,193]
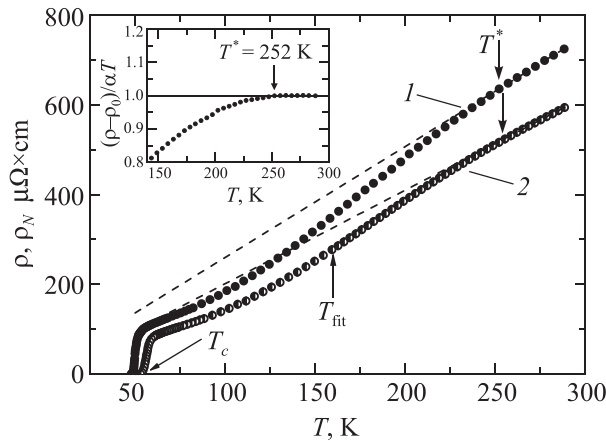

FIG. 16. The resistivity of a WD single crystal YBa$_2$Cu$_3$O$_{7-\delta}$ ($7-\delta \simeq 6.5$) as a function of temperature, $\rho(T)$, at $P = 0$ (curve 1, circles) and at $P = 1.05$ GPa (curve 2, half-circles). The dotted lines denote $\rho_N(T)$ extrapolated to the low-temperature region. T_{fit} is the temperature to which curve 2 was approximated by the polynomial. The temperature T^* is determined using the point at which $\rho(T)$ deviates from the linear dependence at high T, indicated by the dashed line. The inset shows a more accurate determination of the PG temperature T^* using the criterion $(\rho(T) - \rho_0)/aT = 1$,[128] $P = 0$.

TABLE 1. Parameters of FLC analysis for YBa$_2$Cu$_3$O$_{6.5}$ single crystals.

P, GPa	$\rho(100\,\text{K})$, $\mu\Omega$ cm	T_c, K	T_c^{mf}, K	T_{01}, K	T_G, K	ΔT_{fl}, K	d_1, Å	$\xi_c(0)$, Å
0	180.4	49.2	50.2	87.4	50.7	36.7	3.98	3.43
0.29	169.1	51.2	52.1	90.7	52.8	37.9	3.96	3.41
0.56	159.2	51.7	52.6	91.6	53.0	38.6	3.8	3.28
0.69	155.6	52.1	54.3	94.5	55.1	39.4	3.44	2.97
0.78	152.4	52.9	54.8	95.4	55.4	40.0	3.73	3.21
1.05	144.4	54.6	56.6	98.6	57.3	41.3	3.37	2.91

4.2. Weakly-doped single crystals

4.2.1. A study of resistance and critical temperature

The temperature dependences of resistivity $\rho(T) = \rho_{ab}(T)$ for a WD single crystal Ya$_2$Cu$_3$O$_{7-\delta}$ with $T_c \approx 49.2$ K ($P = 0$) and an oxygen index of $7-\delta \sim 6.5$, measured at $P = 0$ (curve 1) and $P = 1.05$ GPa (curve 2) are shown in Fig. 16.[26]

The $\rho(T)$ dependences for all applied pressures $P = 0$; 0.29; 0.56; 0.69; 0.78 and 1.05 GPa have an S-shape that is characteristic of WD HTSCs.[60,106] However, in the temperature interval above $T^* = (252 \pm 0.5)$ K ($P = 0$) and $T^* = (254 \pm 0.5)$ K to 300 K, all the $\rho(T)$ dependences are linear and have a slope $d\rho/dT = 2.48$, and 2.08 $\mu\Omega$ cm/K, at $P = 0$ and 1.05 GPa, respectively (Fig. 16). The slope is determined by approximating the experimental dependences $\rho(T)$ and confirms the excellent linearity of the dependences with an rms error of 0.009 ± 0.002 in the indicated interval T for all applied pressures. The pseudogap opening temperature $T^* \gg T_c$ is determined based on the deviation of $\rho(T)$ from this linear dependence towards the lower values (arrows in Fig. 16). A more accurate method for determining T^* is obtained by using the criterion $(\rho(T) - \rho_0)/aT = 1$, which is obtained by transforming the straight line equation,[128] where ρ_0 is the residual resistance cut off by this line on the Y axis at $T = 0$. In this case, T^* is defined as the temperature deviation of $\rho(T)$ from 1, as shown in the inset to Fig. 16. We emphasize that both methods give the same values of T^*.

In reality we analyzed 6 curves obtained at pressures $P = 0$; 0.29; 0.56; 0.69; 0.78 and 1.05 GPa, which can be considered as 6 different samples Y0-Y6. The corresponding resistive curves for intermediate pressures also have an S-shape and are located between the $\rho(T)$ curves at $P = 0$ and 1.05 GPa in Fig. 16, but are not shown so as not to overload the figure. The parameters of all the samples are given in Tables 1 and 2. We can see based on Table 2 that the pressure practically does not affect the value of T^*. At the same time, an increase in the hydrostatic pressure leads to a marked decrease in the resistance of the single crystal. Above 260 K, the decrease of $p(T)$ with increasing pressure is practically

TABLE 2. Parameters of PG analysis for YBa$_2$Cu$_3$O$_{6.5}$ single crystals.

P, GPa	ΔT_{cr}, K	T^*, K	D^*	$\Delta^*(T_c)$, K	Δ_{max}^c, K	T_{max}, K	T_{pair}, K
0	1.5	252	5	122.1	184.17	231.6	170
0.29	1.6	252	5.4	136.5	192.28	229.2	165
0.56	1.3	252	5.8	145.8	199.76	226.2	159
0.69	3.0	252	6.4	164.3	190.71	217.0	153
0.78	2.5	253	6.5	167.7	190.30	152.8	138
1.05	2.7	254	6.6	178.4	198.41	205.7	135

independent of the temperature and amounts to $d\ln\rho\,(300\,\mathrm{K})/$ $dP = -(19 \pm 0.2)\% \times \mathrm{GPa}^{-1}$ (Fig. 17, curve 1). This value is somewhat less than $d\ln\rho\;(300\,\mathrm{K})/dP = -(25 \pm 0.2)\% \times \mathrm{GPa}^{-1}$, usually reported for BiSCCO single crystals,[194] and $d\ln\rho\,(300\,\mathrm{K})/dP = -(33 \pm 0.2)\% \times \mathrm{GPa}^{-1}$, obtained by us for weakly doped HoBCO single crystals.[85] At the same time, at $T = 100\,\mathrm{K}$, we obtain $d\ln\rho\;(100\,\mathrm{K})/dP = (20 \pm 0.2)\% \times \mathrm{GPa}^{-1}$ (Fig. 17, curve 2), which is in good agreement with the data of Refs. 194 and 195 and the references therein.

Note that $d\ln\rho(100\,\mathrm{K})/dP$ (Fig. 17, curve 2) shows an almost linear dependence on P with a standard error of about 0.003, which is typical for HTSC single crystals. At the same time, $d\ln\rho(300\,\mathrm{K})/dP$ (Fig. 17, curve 1) demonstrates a marked deviation from linearity at ~ 0.7 GPa. The singularity at $P \sim 0.7$ GPa is also visible on the temperature dependence of the PG $\Delta^*(T)$, which could possibly be the specific behavior of the YBCO single crystals being studied.

Based on our measurements, (Fig. 16, Table 1) it also follows that T_c increases with pressure as $dT_c/dP = (5.1 \pm 0.2)$ K/GPa, which is in excellent agreement with the results obtained on WD single crystals HoBCO,[85,193] where $dT_c/dP = (4 \pm 0.2)$ K/GPa. This same value of $dT_c/dP = (4 \pm 0.2)$ K/GPa, obtained from experiments on muon scattering (μSR), is reported for a WD YBCO polycrystalline solid in,[196] but it is about 2 times larger than what is observed for BiSCCO single crystals.[194] These results support the assumption that the growth of T_c in cuprates occurs due to an increase in charge carrier density n_f in the CuO_2 planes subjected to pressure. Moreover, it seems that the oxygen vacancies in WD cuprates provide an opportunity for an easier redistribution of n_f,[181] than in OD cuprates[27] where the number of vacancies is small, and n_f is very large.

4.2.2. The impact of pressure on excess conductivity

The FLC at all applied pressures is determined based on excess conductivity, which is calculated according to Eq. (1) as the difference between the measured resistance $\rho(T)$ and the $\rho_N(T)$ extrapolated to the low temperature region. This approach is used to study various single crystals at all applied pressures. Going forward, we will consider the procedure for determining the FLC and PG for samples Y0 ($P = 0$) and Y6 ($P = 1.05$ GPa) in more detail. Note that in
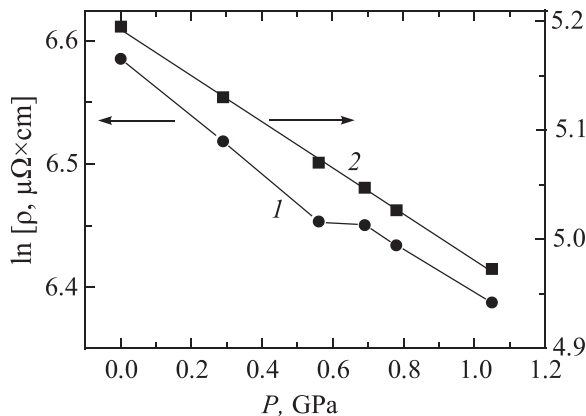
Secs. 4 and 5 FLC is denoted as $\sigma'(T)$, which is equivalent to $\Delta\sigma(T)$ (see Sec. 2.1.2).

According to the LP model, it is first of all necessary to determine the critical temperature in the mean field approximation T_c^{mf}, which separates the FLC domain from critical fluctuation region (see Sec. 2.1.2). T_c^{mf} is an important parameter for both FLC and PG analysis, since it determines the reduced temperature $\varepsilon = (T - T_c^{mf})/T_c^{mf}$. As noted in Sec. 2.1.2, near T_c, the FLC in HTSCs is always described by the Aslamazov-Larkin equation for 3D systems (2),[7,60] in which FLC $\sigma'(T) \sim \varepsilon^{-1/2}$. It is not difficult to show that in this case $\sigma'^{-2}(T) \sim \varepsilon \sim T - T_c^{mf}$. We can see here that σ'^{-2} (T) goes to 0 at $T = T_c^{mf}$ (Fig. 18), which allows us to determine T_c^{mf} with a high degree of accuracy.

In addition to T_c^{mf} and T_c, Fig. 18 shows the Ginzburg temperature T_G and the temperature of the 3D-2D crossover T_0, which limits the region of 3D AL fluctuations from above.[7,145,156]

Having determined T_c^{mf}, we construct $\ln\sigma'$ as a function of $\ln\varepsilon$, as shown in Fig. 19 for samples Y0 at $P = 0$ and Y6 at $P = 1.05$ GPa. It is seen that, as expected, close to T_c, the FLC is perfectly approximated by the 3D AL fluctuation contribution (2). In double logarithmic coordinates, these are the dashed lines (1) with the slope $\lambda = -1/2$. This means that the classical 3D FLC is always realized in HTSCs, when $T \to T_c$ and $\xi_c(T) > d$.[60,156] In the temperature range from T_0 to T_{01} (≈ 87.4 K for $P = 0$), where $d > \xi_c(T) > d_{01}$, the FLC is perfectly described by the 2D MT fluctuation theory (3) (Fig. 19, curves 2) with the parameters given in Table 1. Thus, at $T_0 = 54.5$ K ($P = 0$), there is a 3D-2D (AL-MT) crossover. Knowing T_0, we find $\xi_c(0) = (3.43 \pm 0.02)$ Å ($P = 0$) via Eq. (8). Using a similar approach for Y6 ($P = 1.05$ GPa), we obtain $\xi_c(0) = (2.91 \pm 0.02)$ Å, i.e., the pressure decreases $\xi_c(0)$ (Table 1). Note that in this case the transition from 3D to 2D fluctuations is very sharp (Fig. 19), which indicates that the structure quality of the single crystals is very good [there is no appreciable spread in the unit

FIG. 17. The dependence of $\ln\rho$ on pressure P for a $YBa_2Cu_3O_{6.5}$ single crystal at $T = 288$ K (1). The solid line is drawn for convenience. The squares (2) denote $\ln\rho(P)$ measured at $T = 100$ K. The solid line 2 is the least-squares fit.
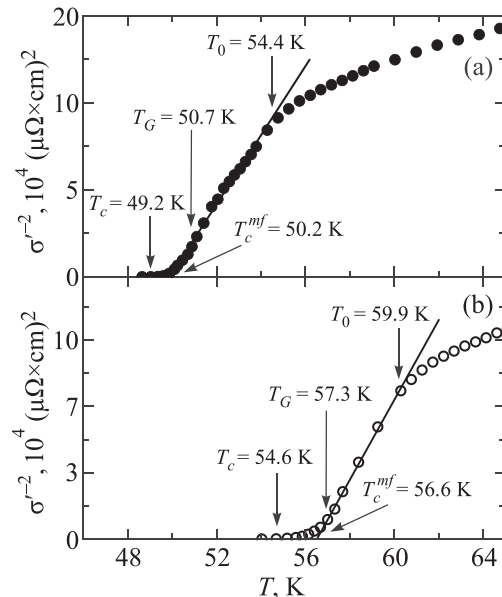

FIG. 18. The inverse square of excess conductivity as a function of temperature $\sigma'^{-2}(T)$ for a $YBa_2Cu_3O_{6.5}$ single crystal at $P = 0$ (a) and $P = 1.05$ GPa (b), which determine T_c^{mf}. The temperatures T_c, T_G and T_0 are also shown.
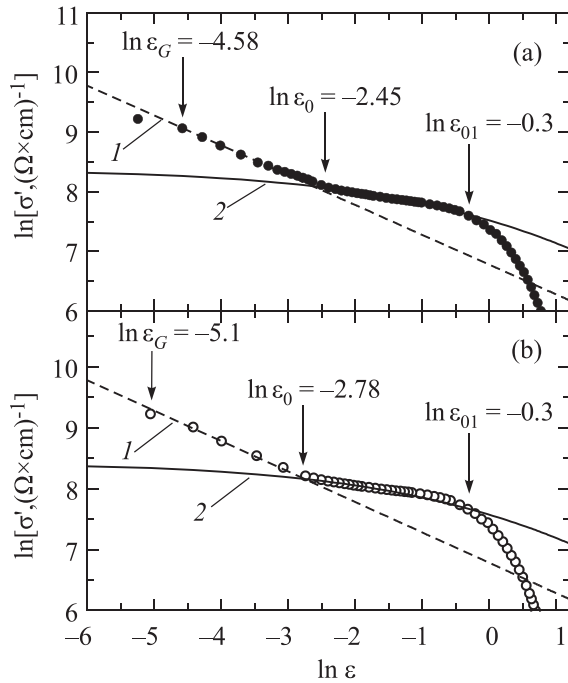
FIG. 19. $\ln \sigma'$ as a function of $\ln \varepsilon$, for a $YBa_2Cu_3O_{6.5}$ single crystal at $P = 0$ (a) and $P = 1.05$ GPa (b), in comparison with fluctuation theories: 3D AL (dashed lines 1); MT with $d = d_1$ (solid curves 2). $\ln\varepsilon_{01}$ determines T_{01}, which limits the range of SC fluctuations from above, $\ln \varepsilon_0$ determines the crossover temperature T_0, and $\ln\varepsilon_G$ determines the Ginzburg temperature T_G.

cell dimensions $d \sim 11.67$ Å (Ref. [95])]. Therefore, T_0 can be clearly determined from the point at which the temperature dependences of the AL and MT theories intersect ($\ln\varepsilon_0$ in Fig. 19).

Unfortunately, neither l nor $\xi_{ab}(T)$ is determined in the FLC experiments. In order to continue the analysis, we use the experimental fact that $\delta = 2$ when all parameters are selected correctly.[60,61] Thus, only the coupling parameter α needs to be determined, to calculate the MT contribution using Eq. (3). In order to achieve this, we use the fact that $\xi_c(0) = d\sqrt{\varepsilon_0}$ is already defined by the crossover temperature T_0. This means that the condition $\xi_c(0) = d\sqrt{\varepsilon_0} = d_{01}\sqrt{\varepsilon_{01}} = (3.43 \pm 0.02)$ Å is fulfilled, where d_{01} is the distance between the conducting CuO_2 planes in the HTSC. Assuming $d = c = 11.67$ Å (the unit cell size along the c-axis for YBCO and HoBCO cuprates), we obtain $d_{01} = d\sqrt{\varepsilon_0/\varepsilon_{01}} = (3.98 \pm 0.05)$ Å, which basically coincides with the inter-planar distance in WD YBCO, determined from structural measurements.[95] This means that ε_0 and ε_{01} are correctly defined. Accordingly, for Y6 ($P = 1.05$ GPa), we obtain $d_{01} = (3.37 \pm 0.02)$ Å, i.e., the pressure decreases the distance between the conducting planes in YBCO (Table 1), which is in good agreement with the conclusions of Sec. 3.

The fact that in the $\Delta T_{fl} = T_{01} - T_G$ interval the FLC obeys classical fluctuation theories means that up to T_{01}, there are SC fluctuations in the HTSC. This also indicates that phase rigidity of the order parameter wave function in HTSCs is conserved up to T_{01}.[40–42] In other words, as already noted above, this means that in this temperature range, the FCPs behave much like SCs, but not as coherent pairs (the so-called "short-range phase correlations"[3,5,8,9]).

Performing a similar analysis for all other applied pressures, we obtain the values of $\xi_c(0)$ and d_{01} for the rest of the

samples (Table 1). It can be seen from the table that pressure significantly reduces the resistance, but increases all characteristic temperatures. ΔT_{fl} also increases, which may indicate that there is an improvement in the structure of the HTSC under pressure. At the same time, both d_{01} and $\xi_c(0)$ decrease noticeably as pressure increases, i.e., apparently, such an increase somewhat reduces the size of the unit cell along the c-axis. At least, it reduces the distance between the internal conducting planes.

These results are in full agreement with the conclusions drawn in Sec. 3. It should be emphasized that, in contrast to the "magnetic" single crystals HoBCO (Sec. 5), pressure almost does not reduce $\sigma'(T)$ and does not change the shape of its experimental curve (Fig. 19).

4.2.3. The temperature dependence of the pseudogap in $YBa_2Cu_3O_{6.5}$ under pressure

The increase in the PG under pressure was observed by us for the first time when studying $YBa_2Cu_3O_{6.5}$ single crystals.[26] Information about the PG is obtained by analyzing the excess conductivity $\sigma'(T)$ that arises due to the PG opening at $T \leq T^*$, which, as noted above, is explained in the LP model.[7,60,142,183] The analysis is implemented using Eqs. (10) and (11). In addition to T_c, T^*, $\xi_c(0)$ and ε, the coefficient A_4 is included in both equations, which has the same meaning as the C-factor in FLC theory, as are $\Delta^*(T_c^{mf})$ and the theoretical parameter ε_{c0}^* (Ref. [168]) (see Sec. 2.1.3). In the analysis we developed, all the parameters are directly determined from the experiment,[7,61,62] which will be demonstrated below using sample Y1 ($P = 0$) as an example.

In the interval $\ln\varepsilon_{01} < \ln\varepsilon < \ln\varepsilon_{02}$ (Fig. 20), or, respectively, $\varepsilon_{01} < \varepsilon < \varepsilon_{02}$ (87.4 K $< T <$ 139 K) (the inset to Fig. 20), $\sigma'^{-1} \sim \exp \varepsilon$.[168] This type of excess conductivity behavior appears to be an intrinsic property of all HTSCs,[7,61,62] including iron-based superconductors (IBSC).[159] As a result, in this temperature interval $\ln\sigma'^{-1}$ is a linear function ε with a slope of $\alpha^* = 1.06$ at $P = 6$, which, according to Ref. [168], is what determines the parameter $\varepsilon_{c0}^* = 1/\alpha^* = 0.94$ (inset to
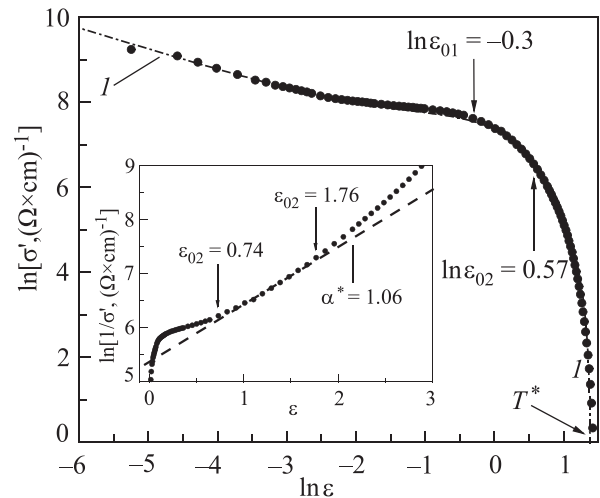
FIG. 20. $\ln \sigma'$ as a function of $\ln \varepsilon$ (dots), constructed over the entire temperature range from T^* to T_c^{mf} for $P = 0$. Curve 1 is an approximation of the data by Eq. (10). Inset: $\ln \sigma'^{-1}$ as a function of ε. The dashed line represents the linear part of the curve between $\varepsilon_{01} \simeq 0.74$ and $\varepsilon_{02} \simeq 1.76$. The corresponding values of $\ln\varepsilon_{01} \simeq 0.3$ and $\ln\varepsilon_{02} \simeq 0.57$ are indicated by arrows on the main panel. The slope $\alpha^* = 1.06$ determines the parameter $\varepsilon_{c0}^* = 1/\alpha^* = 0.94$.

Fig. 20). These same graphs, but with α that increases to 1.4 ($\varepsilon_{c0}^* = 0.71$) at $P = 1.05$ GPa, are obtained for all pressures (see Table 2). This made it possible to acquire reasonable values of ε_{c0}^*, which, as already shown, have a significant impact on the shape of the theoretical curves provided in Figs. 20 and 21.

To find the coefficient A_4, we calculate $\sigma'(\varepsilon)$ using Eq. (10) and approximate the experimental data in the 3D AL fluctuation region near T_c (Fig. 20), where $\ln\sigma'(\ln\varepsilon)$ is the linear function of the reduced temperature ε with the slope $\lambda = -1/2$. In addition, it is assumed that $\Delta^*(T_c^{mf}) = \Delta(0)$, where Δ is the SC gap.[70,146] To estimate $\Delta^*(T_c^{mf})$, which we use in Eq. (10), we construct $\ln\sigma'$ as a function of $1/T$ (Refs. 26 and 197) (Fig. 21, circles). In this case, the slope of the theoretical curve turns out to be very sensitive to $\Delta^*(T_c^{mf})$.[61,62] The best approximation is achieved with $\Delta^*(T_c^{mf}) = 2.5$ or $D^* = 2\Delta^*(T_c^{mf})/k_B T_c = (5.0 \pm 0.1)$ (curve 1 in Fig. 21), which is a typical value for d-wave superconductors in the strong-coupling limit.[26,36,62] Similar graphs for all pressure values make it possible to obtain reliable values of D^* (Table 2).

The data on Table 2 shows clearly that pressure significantly increases D^*. The same result, with similar values D^* is obtained for YBCO from μSR experiments, but for the SC gap Δ.[196] Having determined all the parameters, the dependences $\Delta^*(T)$ for all values of P (Fig. 22) are constructed using Eq. (11). At $P = 0$, Eq. (11) is analyzed with the following set of parameters: $T^* = 252$ K, $T_c^{mf} = 50.2$ K, $\xi_c(0) = 3.43$ Å, $\varepsilon_{c0}^* = 0.94$, $A_4 = 55$ and $\Delta^*(T_c^{mf})/k_B = 122.1$ K. Similar parameters for other samples are shown in Tables 1 and 2.

As can be seen in Fig. 22, there is a noticeable increase in the PG $\Delta^*(T)$ under pressure, which has been observed for the first time. It follows from Table 2 that the parameters of a single crystal, with the exception of T_{max} and T_{pair}, also increase with increasing pressure. Moreover, Δ^* and D^* increase with the same intensity $d\ln\Delta^*/dP = 0.36$ GPa^{-1}. At $P = 0$, the maximum at $T_{max} \approx 230$ K is observed along $\Delta^*(T)$, followed by a decreasing linear region ($\alpha_{max} = 1.28$), which seems to be a typical property of cuprate WD single
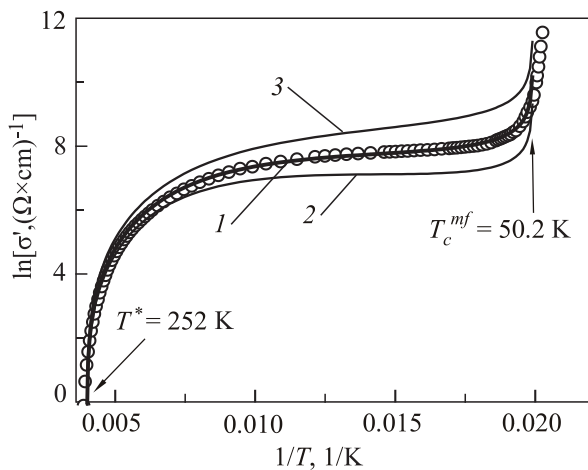

FIG. 22. The temperature dependences of the pseudogap $\Delta^*(T)$ of YBa$_2$Cu$_3$O$_{6.5}$ single crystal at different values of external hydrostatic pressure P, GPa: 0 ($\bullet$), 0.29 ($\circ$), 0.56 ($\blacksquare$), 1.05 ($\circleddash$).

crystals.[26] With an increase in P, the maximum is washed out, the inclined region disappears, and at $P = 1.05$ GPa, $\Delta^*(T)$ acquires a shape that is typical for YBCO films at $P = 0$.[61,62,106] At the same time, T_{max} and T_{pair} decrease.

The significant (about 46%) increase in the pseudogap caused by the application of pressure can be explained by the influence of both the "true" and "relaxation" pressure effects (Sec. 3). The latter is associated with a change in the number of holes under pressure, due to the redistribution of labile oxygen. These same effects should also lead to the observed pressure-induced increase in T_c. It was shown in Ref. 29 that the SC gap Δ in WD cuprates can increase due to the "softening" of the phonon spectrum. However, strictly speaking, a clear answer to these questions is currently absent.

It should also be noted that, regardless of the applied pressure, the transition to the SC state below T_{01} also occurs according to the same law (Fig. 22). All $\Delta^*(T)$ dependences show a minimum at $T \sim T_{01}$. Then a maximum occurs at $T \sim T_0$, followed by a minimum at $T \sim T_G$. All indicated features on the $\Delta^*(T)$ dependence below T_{01} are demonstrated even more clearly by optimally doped YBCO single crystals, as will be shown in the next section.

Thus, for the first time, the magnitude and temperature dependence of excess conductivity $\sigma'(T)$ and $\Delta^*(T)$, in weakly doped YBa$_2$Cu$_3$O$_{7-\delta}$ single crystals under hydrostatic pressure up to 1 GPa, are studied using the LP model.

It is found that with an increase in the hydrostatic pressure up to about 1 GPa, the resistance decreases as $d\ln\rho$ (300 K)$/dP = -(19 \pm 0.2)\% \times$ GPa^{-1}, at the same time as the critical temperature T_c increases as $dT_c/dP = +5.1$ K/GPa.

It is shown that, irrespective of pressure, near T_c, the excess conductivity $\sigma'(T)$ is well described by the Aslamazov-Larkin fluctuation theory for 3D systems, and by the 2D Maki-Thomson fluctuation theory at slightly higher values, demonstrating a 3D-2D crossover with increasing temperature.

It is shown for the first time that the pseudogap $\Delta^*(T)$ and the ratio $D^* = 2\Delta^*(T_c^{mf})/k_B T_c$ subjected to pressure both increase as $d\ln\Delta^*/dP = 0.36$ GPa^{-1}.

FIG. 21. $\ln \sigma'$ as a function of $1/T$ (circles) in the temperature ranging between T^* to T_c^{mf} at $P = 0$. The solid curves are approximations of the data from Eq. (10), at different values of Δ^*. The best result is obtained for $\Delta^*(T_c^{mf}) = 122.1$ K ($D^* = 2\Delta^*(T_c^{mf})/k_B T_c = 5.0$) (curve 1). Correspondingly, curves 2 and 3 are obtained for $D^* = 6$ and 4, which does not correspond to the experiment.
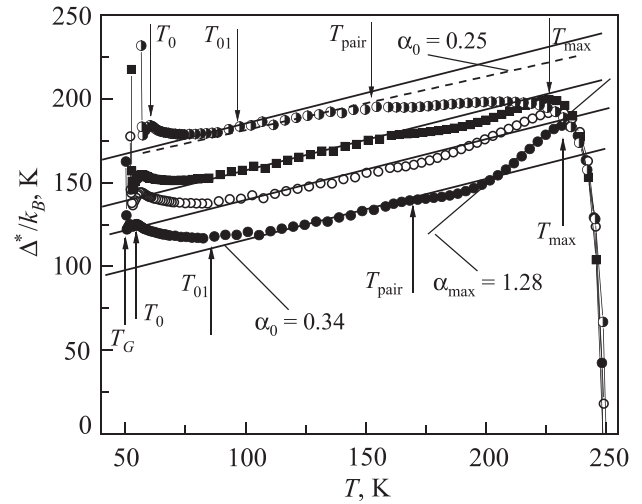
It is also discovered for the first time that, regardless of the applied pressure, the transition of $\Delta^*(T)$ to the superconducting state below T_{01} occurs in a similar fashion.

4.3. Features of optimally doped $YBa_2Cu_3O_{7-\delta}$ single crystal behavior under hydrostatic pressure up to 1 GPa

4.3.1. Study of resistance and critical temperature

Studies of OD single crystals confirm the effect of an increasing PG in $YBa_2Cu_3O_{7-\delta}$ subjected to pressure.[27] The measurements are carried out at hydrostatic pressures of $P = 0$; 0.25; 0.65 and 0.95 GPa. The temperature dependences of resistivity $\rho(T) = \rho_{ab}(T)$ for a $YBa_2Cu_3O_{7-\delta}$ single crystal with $T_c \approx 91.07$ K ($P = 0$) and an oxygen index of 7-$\delta \sim 6.94$, measured at $P = 0$ (curve 1) and $P = 0.95$ GPa (curve 2), are shown in Fig. 23. In contrast to the WD samples (Sec. 4.2.1), the curves for all applied pressures have a shape that is typical for OD HTSCs[61,106] with low values of T^*, as follows from the phase diagram (Fig. 3). In a wide temperature range from $T^* = (141 \pm 0.3)$ K ($P = 0$) and $T^* = (136 \pm 0.3)$ K ($P = 0.95$ GPa) to 300 K, the $\rho(T)$ curves are linear with a slope $d\rho/dT = 0.63$ and 0.54 $\mu\Omega$ cm/K, at $P = 0$ and 0.95 GPa, respectively (Fig. 23). In addition, the critical temperatures in this case are very high, and the resistive transitions are extremely narrow: $\Delta T_c(P = 0) = T_c$ $(0.9\rho'_N) - T_c(0.1\rho'_N) = 91.2 - 91.07$ K $= 0.13$ K and ΔT_c $(P = 0.95$ GPa$) = 92 - 91.76$ K $= 0.24$ K.

The most significant difference between the OD and WD single crystals is the very weak effect of pressure on T_c. In the first case, $dT_c/dP = +0.73$ K/GPa, whereas in WD single crystals, $dT_c/dP = +5$ K/GPa,[194] which is in complete agreement with the conclusions of Sec. 3. At the same time, the pressure still greatly reduces the resistance of the single crystal. In the first case, $d \ln\rho/dP = -(17 \pm 0.2)\% \times GPa^{-1}$, which is almost the same as in WD single crystals, where $d \ln\rho/dP = -(19 \pm 0.2)\% \; GPa^{-1}$. This result indicates that the mechanisms responsible for the impact of hydrostatic pressure on T_c and on the resistivity, are clearly different.[27] In OD single crystals, the planar charge carrier density n_f is maximal, and in YBCO systems it is practically saturated at oxygen index values of 7-$\delta \approx 6.94$, which occur in the studied samples. It is for this reason that in this case the pressure
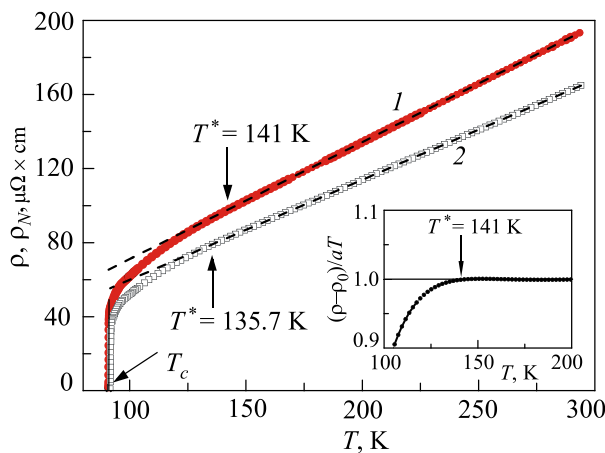
has almost no effect on n_f and the associated T_c (see Sec. 3, Figs. 13 and 14). Consequently, we can conclude that the observed decrease in $\rho(P)$ is caused not so much by a decrease in n_f, but is a result of a decrease in the number of structural defects[194] (Sec. 3), and of a "softening" of the phonon spectrum with increasing pressure.[29]

4.3.2. The effect of pressure on excess conductivity

As in the case of WD single crystals, the LP model[7,142] is used to obtain data on the FLC and the pseudogap $\Delta^*(T)$ from excess conductivity measurements in the sample at each pressure: $P = 0$; 0.25; 0.65 and 0.95 GPa. Next, the results obtained for the sample at $P = 0$ and 0.95 GPa are compared.

The first step of the LP model is the determination of the critical temperature in the mean-field approximation T_c^{mf}, which, as noted in Sec. 2.1.2, determines provides the reduced temperature $\varepsilon = (T - T_c^{mf})/T_c^{mf}$. T_c^{mf} is determined by the method considered in Sec. 4.2.2, which assumes that $\sigma'^{-2}(T) \sim \varepsilon \sim T - T_c^{mf}$, and goes to 0 at $T = T_c^{mf}$.[7,153] The dependence $\sigma'^{-2}(T)$ is shown in Fig. 24 for $P = 0$ and $P = 0.95$ GPa. The corresponding characteristic temperatures T_c, T_G and T_0 are also shown. A very narrow interval of SC fluctuations is specific to OD single crystals, as will be seen from the analysis of the dependence $\ln\sigma'(\ln\varepsilon)$.

The dependence $\ln \sigma'(\ln \varepsilon)$ is shown in Fig. 25 for $P = 0$ (a) and $P = 0.95$ GPa (b). In comparison with the WD YBCO single crystals (Sec. 4.2), both curves are noticeably shifted to the left, i.e., toward T_c, which points to the smallness of the sample's coherence length $\xi(T) = \xi(0)(T/T_c^{mf} - 1)^{-1/2}$.[21] Nevertheless, as expected, up to $T_0 \approx 91.15$ K ($\ln \varepsilon_0 \approx -7.11$) ($P = 0$), the experiment is extrapolated well by the 3D AL fluctuation contribution (2),[144] as shown by the dashed line with

FIG. 23. Temperature dependences of ρ and ρ_N for optimally doped $YBa_2Cu_3O_{7-\delta}$ (7-$\delta \sim 6.94$) single crystals at $P = 0$ (curve 1) and $P = 0.95$ GPa (curve 2). The dotted dashed lines denote $\rho_N(T)$. The inset shows the determination of T^* using $(\rho(T) - \rho_0)/aT = 1$ (Ref. 128) for $P = 0$.
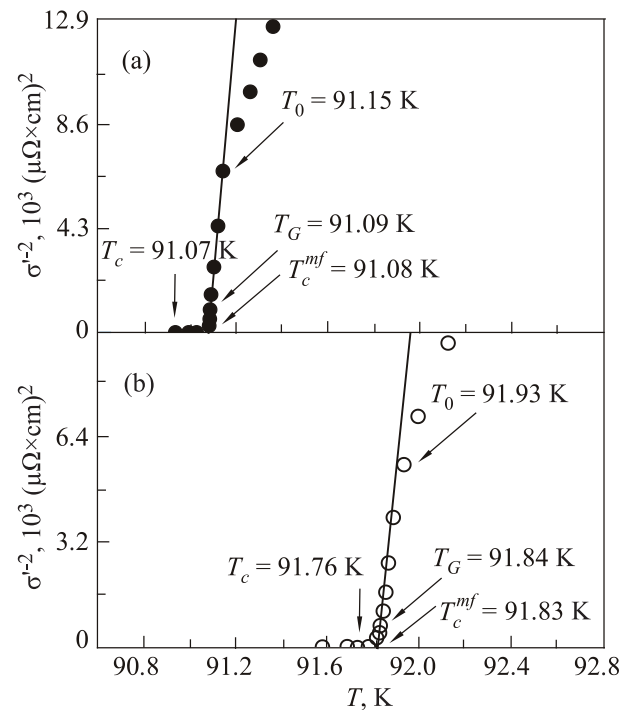

FIG. 24. The inverse square of excess conductivity $\sigma'^{-2}(T)$ as a function of temperature, for an OD $YBa_2Cu_3O_{6.94}$ single crystal at $P = 0$ (a), and $P = 0.95$ GPa (b), which determines T_c^{mf}. The temperatures T_c, T_G and T_0 are also shown.
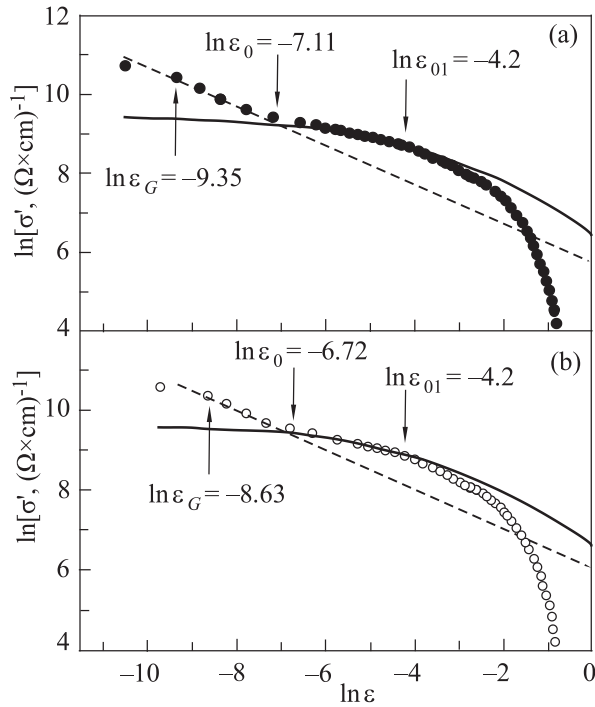
FIG. 25. Fluctuation conductivity σ' as a function of reduced temperature ε, in an optimally doped $YBa_2Cu_3O_{7-\delta}$ single crystal in double logarithmic coordinates at $P=0$ (a) and 0.95 GPa (b), in comparison with fluctuation theories: 3D AL (dashed lines); MT with $d=d_1$ (solid lines). $\ln\varepsilon_{01}$ defines T_{01}, which specifies the region of SC fluctuations above T_c, $\ln\varepsilon_0$ determines the crossover temperature T_0, and $\ln\varepsilon_G$ determines the Ginzburg temperature T_G.

slope $\lambda=-1/2$ in Fig. 25(a), and above T_0, to $T_{01} \approx 92.54$ K ($\ln\varepsilon_{01} \approx -4.2$), by the Maki-Thompson term of the Hikami-Larkin theory (3),[145] Fig. 25(a), shown by a solid curve.

Similar results are also obtained for all other pressures, including $P=0.95$ GPa [Fig. 25(b)], for which $T_0 \approx 91.93$ K ($\ln\varepsilon_0 \approx -6.72$) and $T_{01} \approx 93.2$ K ($\ln\varepsilon_{01} \approx -4.2$). At $T < T_0$, i.e., near T_c, the coherence length along the c-axis $\xi_c(T) > d$, where $d=11.67$ Å, is the size of the YBCO unit cell along the c-axis, and the FCPs can interact in the entire volume of the superconductor, forming a 3D state. That is, a HTSC always three-dimensionalizes before the SC transition, as required by theory.[126–131,165] As noted in Sec. 2.1.2, above $T_0 d > \xi_c(T) > d_{01}$ and the HTSC transforms into a quasi-two-dimensional state, which is described by the 2D MT fluctuation term of the HL theory (3). Having determined T_0, we use Eq. (8) to obtain $\xi_c(0)=(3.4 \pm 0.02) \times 10^{-1}$ Å at $P=0$, and $\xi_c(0)=(4.05 \pm 0.02) \times 10^{-1}$ Å at $P=0.95$ GPa (Table 3), which is very small. Figure 25 shows that, unlike WD single crystals, in this case the pressure has little effect on the value of the coherence length $\xi_c(0)$.[197] Usually, the cuprate coherence length in the ab-plane, which determines the size of the Cooper pair, is $\xi_{ab}(0) \sim 10$–15 Å.[132,133] For

TABLE 3. FLC analysis parameters of a $YBa_2Cu_3O_{6.94}$.

P, GPa	ρ (280 K), $\mu\Omega$ cm	T_c, K	T_c^{mf}, K	T_{01}, K	T_G, K	ΔT_{fl}, K	d_1, Å	$\xi_c(0)$, Å
0	187.6	91.07	91.08	92.54	91.09	1.45	2.72	0.334
0.25	175.9	91.12	91.3	92.6	91.3	1.3	2.73	0.335
0.65	168.2	91.51	91.58	92.9	91.6	1.3	3.34	0.47
0.95	157.3	91.76	91.83	91.84	1.34	1.34	3.3	0.405

example, in YBCO with a slightly less than optimal oxygen index, and with $T_c \approx 87.4$ K, $\xi_{ab}(0)$ is about 13 Å.[60,133,198] Accordingly, for the studied OD single crystal with $T_c \approx 91$ K, $\xi_{ab}(0) \approx 3.5$–5 Å at $P=0$. Therefore, we obtained a nontrivial result, a very small pair size at high T, where the LPs must exist in the form of SCBs. On the other hand, the smaller the $\xi_{ab}(0)$, the greater the coupling energy in the pair, $\varepsilon_b \sim (\xi_{ab}^2)^{-1}$,[126–129] which seems reasonable given the high T_c of the studied single crystals.

The second characteristic temperature in Fig. 25, which determines the region of superconducting fluctuations above T_c, is T_{01}. Having determined the values of $\ln\varepsilon_{01}$ from the graph, we obtain $T_{01} \approx 92.54$ K ($\ln\varepsilon_{01} \approx -4.2$) ($P=0$), and $T_{01} \approx 93.2$ K ($\ln\varepsilon_{01} \approx -4.2$) ($P=0.95$ GPa). As already mentioned, for $T_0 < T < T_{01}$, $\xi_c(T) < d$, but at the same time $\xi_c(T) > d_{01}$, i.e., the system is in a quasi-2D state and is described by Eq. (3).[145,156] Accordingly, above T_{01}, where $\xi_c(T) < d_{01}$, the pairs are located inside the planes and do not interact with each other. Therefore, above T_{01}, the fluctuation theories no longer describe the experiment, as is clearly seen in Fig. 25. Thus, it is clear that at $T = T_{01}$, $\xi_c(T_{01}) = d_{01}$. Obviously, $\xi_c(0)=$ const for a given pressure, so the condition $\xi_c(0) = d_{01}\sqrt{\varepsilon_{01}}$ must be satisfied. Since $\xi_c(0) = 3.34 \times 10^{-1}$ Å is already determined by the dimensional crossover temperature T_0 (8), we have the opportunity to estimate the value $d_{01} = \xi_c(0)(\sqrt{\varepsilon_{01}})^{-1}$. We get $d_{01} = 2.8$ Å ($P=0$) and $d_{01} = 3.3$ Å ($P=0.95$ GPa), which is close to the values of d_{01} that are determined via YBCO structural studies.[95] Thus, despite very small values of $\xi_c(0)$, an analysis of excess conductivity using the LP model allows us to obtain reasonable values of d_{01}. However, in contrast to the WD YBCO single crystals,[26] d_{01} increases insignificantly with increasing pressure. This may be due to errors in determining $\ln\varepsilon_{01}$ in Fig. 25. Another possible explanation is the specific behavior of the OD single crystal behavior when the sample under pressure is above the x_{opt} point (Figs. 13 and 14).

On the other hand, T_{01} is the temperature up to which, according to the theory in Ref. 40, the phase rigidity of the order parameter wave function in HTSCs is conserved, which is experimentally confirmed.[41,42] This means that in the interval from T_c to T_{01}, the Cooper pairs behave largely like superconducting pairs, but without long-range order. This leads to the unusual behavior of cuprates from the point of view of classical superconductivity. As shown in a number of studies,[70,125,146] the SC gap in HTSCs does not vanish at T_c, and the SC fluctuation region is preserved up to ≈ 120 K in YBCO (≈ 30 K above T_c) and up to ~ 150 K in Bi2223 (≈ 40 K above T_c). For example, in the WD YBCO single crystal studied by us, $T_c = 49.2$ K, and $T_{01} = 85.2$ K.[26] This means that the interval in which $\sigma'(T)$ is described by fluctuation theories, i.e., phase rigidity of the order parameter is preserved, $\Delta T_{fl} \approx 36$ K, is in good agreement with the results given above.

In the case of an OD single crystal, all the temperature intervals in which $\sigma'(T)$ can be described by fluctuation theories are extremely small.[27] The interval $\Delta T_{fl} = T_{01} - T_G = 92.54 - 91.09 = 1.45$ K is no exception. This seems somewhat surprising, since at first glance in OD systems with high T_c the interval ΔT_{fl} should be large. However, this agrees with theoretical conclusions: the higher the T_c, the shorter the SC fluctuation interval.[3,5,8,40] Indeed, the higher

the doping level, the higher the charge carrier density n_f and, as a consequence, the closer the HTSC is to a classical superconductor having a small SC fluctuation region,[3,131] which agrees with the conclusions of Sec. 3.1.3. The parameters of the FLC analysis for all samples are shown in Table 3.

4.3.3. The pseudogap as a function of temperature for YBa$_2$Cu$_3$O$_{6.94}$ subjected to pressure

As is the case in WD YBCO single crystals (Sec. 4.2.3), the authors of Ref. 27 first observed the increase in the PG, $\Delta^*(T)$, of an optimally doped single crystal YBa$_2$Cu$_3$O$_{6.94}$ subjected to pressure. To analyze the $\Delta^*(T)$ dependences, the authors of Ref. 27 used the results of excess conductivity $\sigma'(T)$ measurements, determined by Eq. (1). It should be emphasized that in fact these are the same values of $\sigma'(T)$ that were used to analyze the fluctuation conductivity of this same sample, which made it possible to use the FLC analysis parameters to calculate the pseudogap.

Using Eq. (10) for $\sigma'(T)$ (see Sec. 2.1.3), we obtain the temperature dependence of Δ^* (11), where $\sigma'(T)$ is the excess conductivity measured in the experiment. In both equations, T and T^* are determined from resistive measurements (Fig. 23), and the coherence length along the c-axis $\xi_c(0)$ is determined by the temperature of the 2D-3D crossover T_0, on the temperature dependence of the FLC (Fig. 25). Thus, in order to find $\Delta^*(T)$, the only things left to determine from the experiment are the theoretical parameters ε_{c0}^*, $\Delta^*(T_c^{mf})$, and the scaling coefficient A_4.

The algorithm for finding the listed parameters is described in detail in Sec. 4.2.3, therefore we will discuss only the main results. For cuprates, in some temperature range $\varepsilon_{c01}^* < \varepsilon < \varepsilon_{c02}^*$ ($T_{c01} < T < T_{c02}$) above T_{01}, the value $\sigma'^{-1} \sim \exp \varepsilon$, i.e., the dependence of $\ln(\sigma'^{-1})$ on ε, is linear.[168] The inverse of the slope of this line $\alpha^* = 6.5$ determines the parameter $\varepsilon_{c0}^* = 1/\alpha^* = 0.154$.[61,62] In order to define A_4, we use Eq. (10) in conjunction with the already determined parameters and calculate the $\sigma'(T)$ for all pressure values. We select A_4 before combining the calculated curves with the experimental dependences $\ln\sigma'(\ln\varepsilon)$ in the 3D AL fluctuation region near T_c,[7,61] as shown in Fig. 21, assuming that $\Delta^*(T_c) = \Delta(0)$.[70,146] For this, we must know $\Delta^*(T_c)$, which is a part of Eq. (10).

In order to find $\Delta^*(T_c)$, the experimental values of excess conductivity are constructed in terms of $\ln\sigma'$ vs. $1/T$,[61,62,167] and approximated by their values $\ln\sigma'(1/T)$, calculated by Eq. (10), as described in detail in the previous section. With this design, the shape of the curve determined by Eq. (10) (see Fig. 21) is sensitive to the value of $\Delta^*(T_c)$ (see Table 4). As is the case for a WD single crystal, the best result is obtained with $D^* = 2\Delta^*(T_c)/k_BT_c = 5$ ($P = 0$) and $D^* = 6.2$ ($P = 0.95$ GPa), which points to the strong coupling limit. This result seems reasonable considering that the sample is

optimally doped and has a very high $T_c \sim 91.1$ K. Analysis shows that under pressure, both D^* and Δ^* increase as $d \ln\Delta^*/dP = 0.32$ GPa^{-1}, which is comparable with $d\ln\Delta^*/dP = 0.36$ GPa^{-1}, obtained for WD single crystals. Thus, a hydrostatic pressure of 0.95 GPa increases D^* by 16%, which is in agreement with the results of Refs. 29 and 196, in which a similar increase in the SC gap Δ, and the BCS ratio $2\Delta(0)/k_BT_c$ under pressure, is reported.

When all the necessary parameters are found, we can construct the dependences $\Delta^*(T)$ for all pressure values. The dependence $\Delta^*(T)$, calculated using the LP model according to Eq. (11) for $P = 0$ with the experimentally determined parameters $T^* = 141$ K, $T_c^{mf} = 91.08$ K, $\xi_c(0) = 0.334$ Å, $\varepsilon_{c0}^* = 0.154$, and $A_4 = 4.7$, is represented by the dots in Fig. 26 (curve 1). A similar dependence for $P = 0.95$ GPa is shown in Fig. 26 using empty squares (curve 2). It is constructed using parameters $T^* = 135.7$ K, $T_c^{mf} = 91.83$ K, $\xi_c(0) = 0.405$ Å, $\varepsilon_{c0}^* = 0.147$, $A_4 = 12$. Similar dependences obtained for $P = 0.35$ and 0.65 GPa are located between these two curves, but are not shown so as not to overload the figure.

Figure 26 shows that the pressure significantly increases Δ^*, as $d \ln \Delta^*/dP \sim 0.32$ GPa^{-1}. At the same time, the ratio $D^* = 2\Delta^*(T_c)/k_BT_c$ also increases by 16%, as noted above. However, in general, in OD single crystals the pressure has little effect on the shape of the $\Delta^*(T)$ curve. Regardless of the pressure, the curve $\Delta^*(T)$ has a maximum at $T_{\text{pair}} \approx 129$ K ($P = 0$), in the temperature range $T^* \geq T \geq T_{\text{pair}}$, which is typical for high-quality thin YBCO films, where $T_{\text{pair}} = (131 \pm 1)$ K ($P = 0$) and does not depend on the oxygen concentration.[61,62,142] Recall that T_{pair} is the temperature at which the LPs transform from SCBs into FCPs. In other words, this is the temperature of the BEC-BCS crossover.[62,127–131] Below T_{pair}, the $\Delta^*(T)$ dependence becomes linear with a positive slope $\alpha_1 \approx 0.53$ ($P = 0$), which almost does not decrease with increasing pressure, i.e., in contrast to WD single crystals (Fig. 22), in this case the $\Delta^*(T)$ dependence is close to the similar dependence observed on well-structured YBCO films.[60–62,142] It can be seen that below T_{pair}, regardless of pressure, the linearity is conserved almost until 100 K. A small maximum at $T \approx 96$ K is most likely

FIG. 26. The temperature dependences of the pseudogap $\Delta^*(T)$ for an OD YBa$_2$Cu$_3$O$_{6.94}$ single crystal at $P = 0$ (curve 1) and $P = 0.95$ GPa (curve 2) calculated using the local pair model, according to Eq. (11), with the parameters given in the text.

TABLE 4. PG analysis parameters of a YBa$_2$Cu$_3$O$_{6.94}$ single crystal.

P, GPa	T^*, K	T_{pair}, K	$\Delta^*(T_G)$, K	$2\Delta^*/K_BT_c$	ε_{c0}^*	α_0
0	141	129	228	5	0.154	0.53
0.25	135	127	239	5.2	0.151	0.53
0.65	140	126	230	5.4	0.143	0.54
0.95	135.7	122	273	5.8	0.147	0.53

due to the specificity of this sample—a singularity along $\rho(T)$ in the region of $T \sim 96$ K, which is also visible in the form of a minimum along the $\ln \sigma'(\ln \varepsilon)$ dependence for $\ln \varepsilon \approx -2.6$ (Fig. 25).

Below T_{01} and up to T_c^{mf}, Fig. 26 shows an exceptionally sharp growth of $\Delta^*(T)$, which is observed for the first time, and is most likely a part of the specific behavior of the PG in OD single crystals.[199] This behavior is probably driven by the sample's transition into the SC fluctuation region, in which the excess conductivity $\sigma'(\varepsilon)$ (Fig. 25) obeys the classical fluctuation theories. The details of such a transition are shown in Fig. 27. As already noted, the phase rigidity of the SC order parameter wave function is conserved up to T_{01}.[40–42] This means that the superfluid density n_s retains a non-zero value up to T_{01}, i.e., up to T_{01}, the fluctuation pairs behave somewhat like ordinary SC pairs, but without long-range order, as noted in Sec. 4.2.2.[3,5,8,9,40] Accordingly, below T_0, local pairs are finally transformed into classical FCPs, and the system is three-dimensionalized,[7,61] i.e., the conditions necessary for the transition to the SC state are created (see Sec. 2).

At $T < T_{01}$, the shape of the $\Delta^*(T)$ dependence in Fig. 27 is actually the same as in a WD single crystal (Fig. 22, curve with $P = 0$). As is the case in a WD single crystal, $\Delta^*(T)$ increases rapidly, demonstrating a maximum in the T_0 region, and then a minimum at T_G, below which the fluctuation theories no longer work and a characteristic jump in $\Delta^*(T)$ is observed upon transition to the critical fluctuation region. Thus, it can be concluded that the transition to the SC state in both WD and OD YBCO single crystals obeys the same laws.

However, it is necessary to note at least two significant differences. In WD single-crystals, the SC fluctuation range is very large: $\Delta_{fl} = T_{01} - T_G = 36$ K, which coincides with the results of Refs. 29, 41, and 200. Whereas in OD single crystals, $\Delta_{fl} = T_{01} - T_G = 92.54 - 91.09$ K $= 1.45$ K ($P = 0$), and $\Delta_{fl} = 1.34$ K ($P = 0.95$ GPa), i.e., exceptionally small.[200] This result is also in agreement with the HTSC phase diagram in Fig. 3: the higher the charge carrier density n_f in the sample, the higher the T_c and the lower T^* and, as we can see, the smaller the region of SC fluctuations above T_c.

The second contrast is an exceptionally large difference in the increase of $\Delta^*(T)$ below T_{01}. In WD single crystals, $\Delta^*(T) = \Delta^*(T_G) - \Delta^*(T_{01}) \approx 5$ K ($P = 0$), i.e., it is relatively small, whereas the interval $\Delta_{fl} = 36$ K (Fig. 22), on the contrary, is very large. Accordingly, a very large increase of $\Delta^*(T) = \Delta^*(T_G) - \Delta^*(T_{01}) \approx 80$ K ($P = 0$) is observed in OD single crystals, but in an exceptionally narrow temperature range $\Delta_{fl} \approx 1.5$ K (Figs. 26 and 27).

In the OD sample, the charge carrier density n_f is at least 3 times greater than in a WD YBCO single crystal with $T_c \sim 49$ K.[3,61,71] Accordingly, the density of the superconducting carriers n_s, and hence the FCP density (short-range phase correlations) above T_c should also be much higher,[3,5,8,9,40] which can explain the observed sharp increase of Δ^* at $T < T_{01}$ (Fig. 26). In addition, an exceptionally short coherence length can also contribute to the formation of the SC correlations above T_c. It should also be noted that the absolute value of $\Delta^*(T_G) \approx 230$ K (Fig. 26) is actually 2 times larger than in WD single crystals. The sample parameters obtained from PG analysis for all values of P are given in Table 4.

It is worthwhile to note that the pressure-induced increase in Δ^* in OD samples is 1.12 times smaller than in YBCO single crystals. At the same time, the pressure-induced decrease in ρ is also 1.12 times lower than in WD samples (Tables 1–4). Thus, we can assume that both effects are based on the same physical mechanism, which is most likely rooted in the features of the electron-phonon interaction in cuprates.[29,30] Recently, a significant increase in both the SC gap $\Delta(0)$, and the $2\Delta(0)/k_B T_c$ ratio with increasing pressure was also observed in a WD polycrystalline Bi2223, together with a decrease in the frequencies of the superconductor's phonon spectrum.[29] Thus, most likely, the "softening" of the phonon spectrum is the most probable cause for the pressure-induced increase in both the SC gap Δ[29,196] and the PG Δ^*, and consequently, the ratio $D^* = 2\Delta^*(T_c)/k_B T_c$ detected in our experiments.[26,27] This "softening" of the phonon spectrum should also lead to an experimentally observed decrease in the resistance of HTSC cuprates under pressure.[29,85,194,200] It should be emphasized that, as our studies have shown (Figs. 16 and 23), the pressure-induced decrease in $\rho(T)$ is practically independent of the level of doping of HTSCs. At the same time, the dependence $T_c(P)$ has a significant dependence on doping (Tables 1 and 3). Consequently, it is most likely that the increase in T_c with increasing pressure occurs precisely as a result of the redistribution of the carrier density n_f, which leads to an increase in n_f of CuO_2 planes. This process likely occurs with more ease in WD cuprates,[26,62,194,201] where $dT_c/dP \sim 4$–5 K/GPa.[27,195,196] It can be assumed that in OD samples the pressure has little effect on the charge carrier density n_f of the CuO_2 planes, which is close to saturation in OD YBCO. As a consequence, the T_c in these samples is practically independent of pressure. The relatively weak effect of pressure on the value of T_c in OD samples can also be explained by the specific location of the Fermi level near the van Hove singularity in the charge carrier spectrum[123] (Sec. 3.1.2). However, strictly speaking, the mechanisms of both the pressure-induced increase in T_c and the decrease of ρ in HTSC are not completely clear.

Thus, for the first time the LP model is used to study the effect of hydrostatic pressure up to ~ 1 GPa on the excess
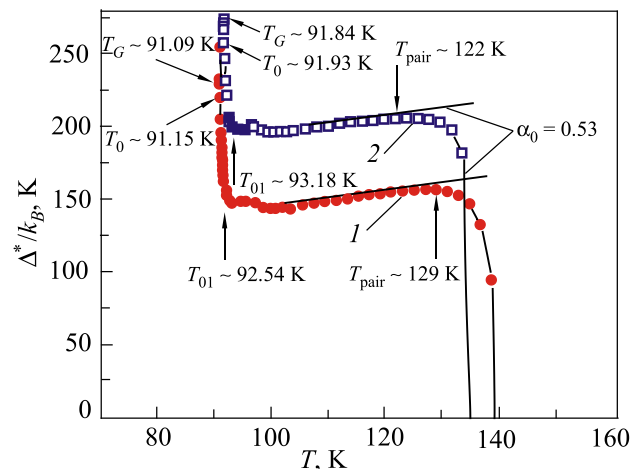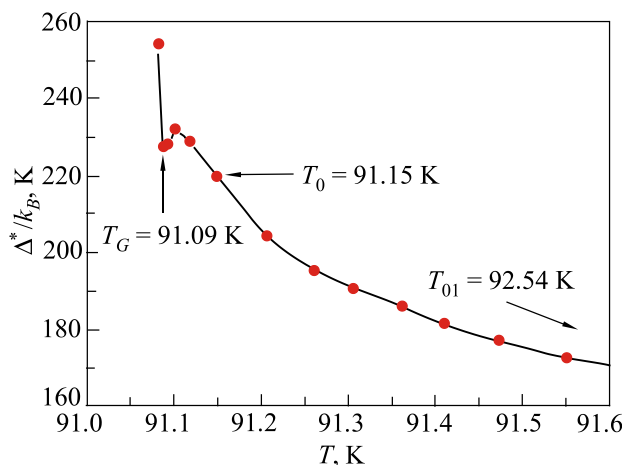

FIG. 27. The temperature dependence of the pseudogap $\Delta^*(T)$ for an OD YBa$_2$Cu$_3$O$_{6.94}$ single crystal at $P = 0$ (dots) in the $T < T_{01}$ temperature range. The solid curve is drawn for convenience.

conductivity $\sigma'(T)$ and the pseudogap $\Delta^*(T)$ of optimally doped $YBa_2Cu_3O_{7-\delta}$ single crystals with $T_c \sim 91.1\,K$ (for $P = 0$). It is found that the ratio $D^* = 2\Delta^*(T_c)/k_BT_c$, and also the PG increase as $d\ln\Delta^*/dP = 0.32\,GPa^{-1}$, which is of the same order as the increase in WD single crystals.

It is shown that the pressure impact in OD single crystals on T_c is very small: $dT_c/dP \approx 0.73\,K/GPa$, while $d\ln\rho/dP \approx -(17 \pm 0.2)\% \times GPa^{-1}$ is of the same order as in WD YBCO single crystals. Consequently, the mechanisms driving the effect of pressure on T_c and $\rho(T)$ are different. The increase in T_c is most likely due to the redistribution of charge carriers in the CuO_2 planes. The reduction of ρ and the increase in Δ^* is largely generated by a decrease in the frequencies of the phonon spectrum of the superconductor subjected to pressure.

It is shown that irrespective of the pressure, in the temperature range $T_c - T_{01}$ $\sigma'(T)$ is well described by the 3D AL and 2D MT fluctuation theories, demonstrating a 3D-2D crossover with increasing temperature.

The singularity in the form of a narrow minimum along the $\Delta^*(T)$ curve, corresponding to the temperature T_{01} (Figs. 25 and 27), which determines the SC fluctuation region above T_c, was clearly revealed for the first time. A sharp increase ($\sim 80\,K$) in $\Delta^*(T)$ is detected below T_{01}, in a narrow temperature range of $\sim 1.5\,K$, which is a specific feature of the PG behavior for OD YBCO single crystals.

It is shown that the transition of $\Delta^*(T)$ to the superconducting state below T_{01} actually occurs according to the same scenario as in WD single crystals.

5. The pressure-induced phase separation and diffusion of the labile component in $HoBa_2Cu_3O_{7-\delta}$ single crystals

In order to get a deeper understanding of HTSC physics, it is interesting to compare the results obtained above for $YBa_2Cu_3O_{7-\delta}$ single crystals in which no magnetism is expected, with $HoBa_2Cu_3O_{7-\delta}$ HTSCs, in which the magnetic subsystem can play a significant role. An important feature of HTSC compounds like $REBa_2Cu_3O_{7-\delta}$ ($RE = Y$, Ho, Dy …) is the possibility of them realizing a nonequilibrium state at a certain degree of oxygen deficiency, which can be induced by external conditions such as temperature,[187] or high pressure.[188] This state is accompanied by labile oxygen redistribution and structural relaxation (see Sec. 3), which, in turn, have a significant effect on electric transport system parameters.[187–189] The replacement of Y by Ho, which has a sufficiently large ($\mu_{Ho} = 10.6\ \mu_B$ and $\mu_{eff} = 9.7\ \mu_B$ in $HoBa_2Cu_3O_{7-\delta}$) magnetic moment,[202] allows to predict a qualitatively different system behavior due to the paramagnetism of HoBaCuO in the normal state. The study of samples that have a non-stoichiometric oxygen composition is of particular interest, because their rare-earth ion can serve as a probe, sensitive to the local symmetry of its environment and charge density distribution, since their change affects the crystal field that forms the electronic structure of such an ion.[36,189,194]

Our experiments[85,193] consider the influence hydrostatic pressures up to $\sim 0.5\,GPa$ have on the FLC $\sigma'(T)$ and the pseudogap $\Delta^*(T)$ in weakly doped $HoBa_2Cu_3O_{7-\delta}$ single crystals (HoBCO) with $T_c \approx 61.2\,K$ and an oxygen index $7-\delta \approx 6.65$. The measurements are made when the transport current flows both at an angle of $45°$ ($I\perp TB$) to the twin boundaries (sample S1)[85] and parallel to the TB: $I \parallel TB$ (sample S2), at which time the effect of twins on charge carrier scattering processes is minimized.[193] A comparison of these results with analogous data obtained for $YBa_2Cu_3O_{7-\delta}$ (Sec. 4) and iron-based superconductors such as $SmFeAsO_{0.85}$ (Ref. 203) and $EuFeAsO_{0.85}F_{0.15}$,[157] should help to elucidate the mutual influence mechanisms of superconductivity and magnetism in HTSCs.[159,204]

5.1. Specific features of the behavior of weakly doped $HoBa_2Cu_3O_{7-\delta}$ single crystals under hydrostatic pressure up to 0.5 GPa for current flowing at an angle of 45° to the twin boundaries

5.1.1. Studies of resistance and critical temperature

$HoYBa_2Cu_3O_{7-\delta}$ (HoBCO) single crystals, like YBCO single crystals, are grown using gold crucible solution-melt technology, according to the procedure in Refs. 187–189 (see Sec. 4.1). To carry out resistive measurements, rectangular crystals with typical dimensions of $1.9 \times 1.5 \times 0.3\,mm$ (S1) and $1.7 \times 1.2 \times 0.2\,mm$ (S2) are selected from one batch. The minimum crystal size corresponds to the direction of the c-axis. To determine the effect of oxygen redistribution, measurements were taken after two to seven days after the pressure application-relief so that the relaxation processes are complete.[85,187–190,193]

This section presents the results of measurements for $HoYBa_2Cu_3O_{7-\delta}$ single crystals with $T_c \approx 62\,K$ and an oxygen index of $7-\delta \approx 6.65$, when the transport current flows at an angle of $45°$ to the twin boundaries (S1) (sample S1).[85] In this case, oxygen-depleted TBs create additional defects (Fig. 4), which, as will be shown below, significantly affect the sample's ascending diffusion when pressure is applied (see Sec. 3.1.4). The temperature dependences of resistivity $\rho(T) = \rho_{ab}(T)$ are S-shaped,[85] which is typical for weakly doped YBCO films[61] and single crystals[106] (Fig. 28). In fact, we have four samples: H21 at $P = 0$, H22 ($P = 0.48\,GPa$), H23 ($P = 0.48\,GPa$ applied for 5 days) and H24 at $P = 0$, for measurement immediately after depressurization. We note that both the magnitude and the decrease in the resistivity under pressure are of the same order as in YBCO single crystals (Fig. 16), and above $T^* = 269\,K$ ($P = 0$) and $T^* = 265\,K$
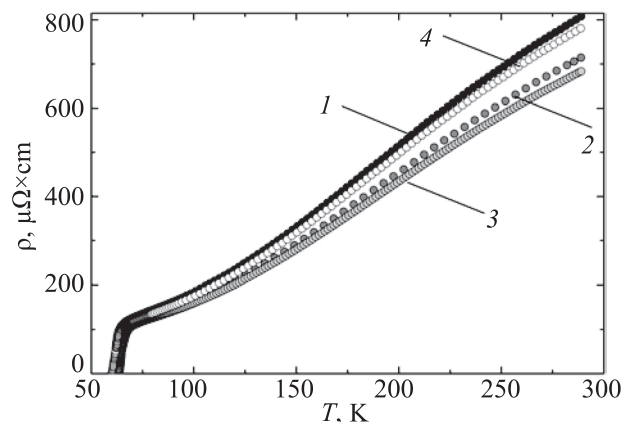

FIG. 28. The resistivity of a WD HoBCO single crystal as a function of temperature at different pressures and $I\perp TB$ for samples: H21, $P = 0$ (1); H22, $P = 0.48\,GPa$ (2); H23, after holding for 5 days at $P = 0.48\,GPa$ (3); H24, $P = 0$ immediately after depressurization (4).

TABLE 5. Parameters of the FLC analysis for the $HoBa_2Cu_3O_{6.65}$ single crystal.

P, GPa	$\rho(100K)$, $\mu\Omega$ cm	T_c, K	T^*, K	T_c^{mf}, K	T_G, K	Gi	T_0, K	T_{01}, K	$\xi_c(0)$, Å
0	186	61.2	269	61.9	62.3	0.006	65.3	99.5	2.72 ± 0.02
0.48	160	63.2	265	65.9	67.0	0.017	69.3	114	2.65 ± 0.02

($P = 0.48$ GPa) (Table 5), all the $\rho(T)$ dependences curves are linear[45] with a slope of $d\rho/dT = 3.1$ and 2.58 $\mu\Omega$ cm/K, for $P = 0$ and 0.48 GPa, respectively. As in all our experiments, the slope was determined by approximating the experimental dependences $\rho(T)$ on a computer and confirming the excellent linearity of the dependences with rms error of 0.009 $\pm$ 0.002 in the indicated temperature range for all applied pressures. Taking into account that the pressure in this case is 2.2 times less, we find that the decrease in $\rho(T)$ under pressure at $T > T^*$ is practically independent of the temperature and amounts to $d\ln\rho/dP = -(33 \pm 0.5)\% \times GPa^{-1}$. It is significant that this value appreciably exceeds the value $d\ln\rho/dP$ reported for various cuprates.[189,190,194–197,201] In particular, it is 1.7 times greater than in the YBCO single crystals studied by us (Sec. 4.2).

Figure 29 shows the superconducting transition curves at $P = 0$ (a) for sample H21 and $P = 0.48$ GPa (b) for sample H23, with indication of the characteristic temperatures. It is clear that the pressure increases both T_c and the width of the SC transition. The unusual shape of the $\rho(T)$ curve with several linear sections, especially at $P = 0.48$ GPa, indicates the possibility of phase separation in the sample due to
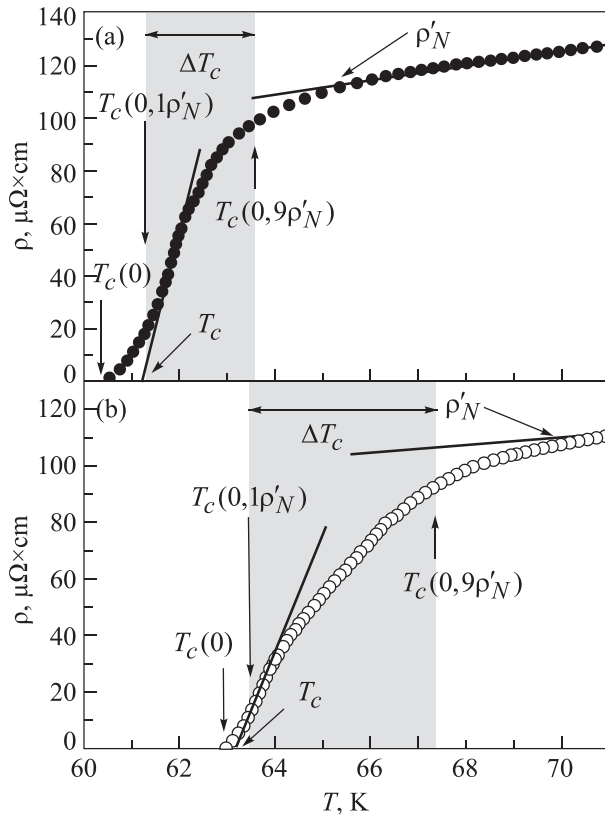
the enhancement of ascending diffusion processes under pressure.[187–190] From the data in Fig. 29 we see that T_c increases with pressure as $dT_c/dP \simeq 4.16$ K/GPa, which is in excellent agreement with the results obtained on weakly doped YBCO single crystals (Sec. 4), where $dT_c/dP \simeq 5.1$ K/GPa. The same value of $dT_c/dP \simeq 4$ K/GPa was obtained from experiments on muon scattering (μSR) in Ref. 196 for the WD YBCO polycrystalline solid. These results once again confirm the assumption that the growth of T_c in cuprates when pressure is applied, is most likely due to an increase in the carrier density n_f in the CuO_2 planes. Strictly speaking, the temperature dependences $\rho(T)$ of WD HoBCO single crystals, and their behavior under pressure, differ little from similar dependences of WD YBCO single crystals (Fig. 16). The main differences generated by the magnetism of HoBCO are found in the behavior of the FLC (Figs. 30 and 31) and, chiefly in the PG $\Delta^*(T)$ (Fig. 32).

5.1.2. The effect of pressure on excess conductivity

As in the case of WD YBCO single crystals (Sec. 4.2.2), the FLC is determined by excess conductivity analysis, which is calculated using Eq. (1), as the difference between the measured resistance $\rho(T)$ and the linear above T^* $\rho_N(T)$, extrapolated to low temperatures. This approach is used at all applied pressures. In a standard manner, all analysis is carried out using the LP model for all pressure values. However, we will consider the procedure for determining the FLC and PG in samples H21 ($P = 0$) and H23 ($P = 0.48$ GPa) in more detail, and compare the results.

FIG. 29. The superconducting transition of WD HoBCO single crystals at $I \perp TB$ and $P = 0$ (a) and after five days under a pressure of $P = 0.48$ GPa (b). ρ'_N is the resistance of the sample before the SC transition.
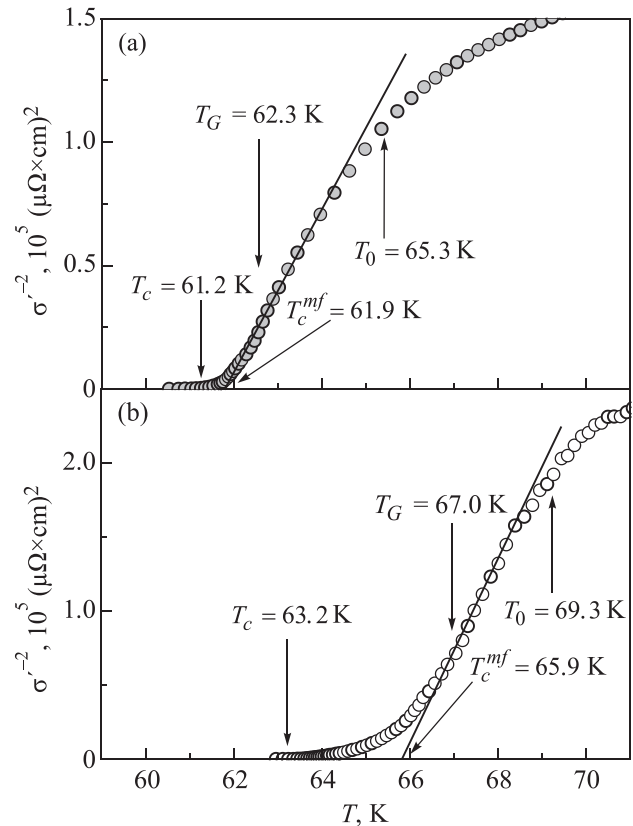

FIG. 30. The temperature dependences of the inverse square of the excess conductivity $\sigma'^{-2}(T)$ for a WD $HoBa_2Cu_3O_{6.65}$ single crystal at $P = 0$ (a) and $P = 0.48$ GPa (b), which determine T_c^{mf} ($I \perp TB$). T_c, T_G, and T_0 are also shown.
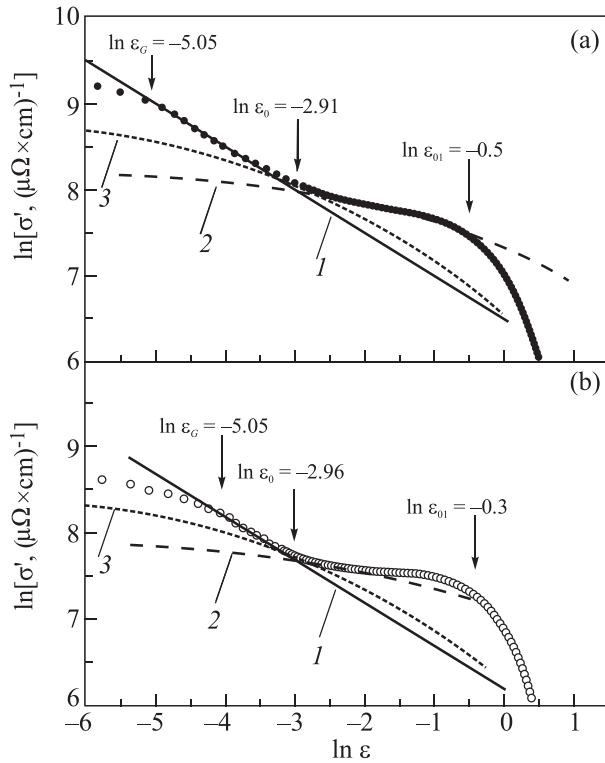
FIG. 31. $\ln\sigma'$ as a function of $\ln\varepsilon$ of a $HoBa_2Cu_3O_{6.65}$ single crystal at $P = 0$ (a) and $P = 1.05$ GPa (b) ($I\perp$TB) in comparison with fluctuation theories: 3D AL (1); MT with $d = d_{01}$ (2) and MT with $d = 11.67$ Å (3). $\ln\varepsilon_{01}$ determines T_{01}, which defines the region of SC fluctuations above T_c, $\ln\varepsilon 0$ determines the crossover temperature T_0, and $\ln\varepsilon_G$ determines the Ginzburg temperature T_G.

As in Sec. 4.2.2, the critical temperature in the mean-field approximation T_c^{mf} was determined from the $\sigma'^{-2}(T)$ dependence (Table 5). The corresponding $\sigma'^{-2}(T)$ dependences of the HoBCO single crystal at $P = 0$ (a) and $P = 0.48$ GPa (b) are shown in Fig. 30, which also marks the temperatures T_c, T_G, and T_0. The obtained values of T_c^{mf} allow us to determine $\varepsilon = (T - T_c^{mf})/T_c^{mf}$, after which it is possible to conduct a direct analysis of the FLC in the coordinates $\ln\sigma'$ versus $\ln\varepsilon$. In this case, the shape and behavior of the experimental curve, as well as its comparison with existing fluctuation theories, can give essential information about the test sample (see Secs. 4.2 and 4.3). The dependences of $\ln\sigma'$ on $\ln\varepsilon$ are shown in Fig. 31 for samples H21 at $P = 0$ (a) and H23 at $P = 0.48$ GPa (b). It is seen that, like in YBCO single crystals, close to T_c, the FLC is perfectly approximated by the 3D AL fluctuation contribution (2).[144] In double logarithmic coordinates, these are solid lines (1) with a slope $\lambda = -1/2$. This confirms that the classical 3D FLC is always realized in HTSCs, when $T \to T_c$, and where $\xi_c(T) > d$.[60,61] At $T_0 = 65.3$ K ($\ln\varepsilon_0 = -2.91$, $P = 0$), a 3D-2D (AL-MT) crossover occurs. Knowing T_0, according to Eq. (8), we find $\xi_c(0) = (2.72 \pm 0.02)$ Å ($P = 0$). Accordingly, $T_0 = 69.3$ K ($\ln\varepsilon_0 = -2.96$) and $\xi_c(0) = (2.65 \pm 0.02)$ Å ($P = 0.48$ GPa) (Table 5).

In the interval ranging from T_0 to $T_{01} \approx 99.5$ K, where $d > \xi_c(T) > d_{01}$, the FLC is perfectly described by the 2D MT fluctuation contribution of the HL theory[145] [Eq. (3)] (Fig. 31, dashed line 2) with the parameters given in Table 5. As already noted, neither l nor $\xi_{ab}(T)$ is determined in the FLC experiments. To continue the analysis, we use the

experimental fact that $\delta \approx 2$, if all the parameters are chosen correctly.[60,61] Thus, to calculate the MT contribution, according to Eq. (3), all we need to determine is the coupling parameter α (6). For this we use the experimental fact that $\xi_c(0)$ is already determined by the temperature of the 3D-2D crossover T_0.

This means that the condition $\xi_c(0) = d\sqrt{\varepsilon_0} = d_{01}\sqrt{\varepsilon_{01}} = (2.13 \pm 0.02)$Å$(P = 0)$ is fulfilled where, as before, d_{01} is the distance between the CuO_2 conducting planes in HTSCs. Assuming that the size of the unit cell along the c-axis for HoBCO and YBCO cuprates $d = c = 11.67$ Å, we get $d_{01} = d\sqrt{\varepsilon_0/\varepsilon_{01}} = (2.74 \pm 0.05)$Å$(P = 0)$, which is practically the inter-planar distance in WD HoBCO.[85,95] This means that ε_{01} is correctly defined. The fact that in the temperature interval $\Delta T_{fl} = T_{01} - T_G$ the FLC obeys the classical fluctuation theories, means that SC fluctuations exist up to T_{01} in HTSCs. In other words, as noted above, in the interval $\Delta T_{fl} = T_{01} - T_G \approx 37.2$ K ($P = 0$), which is of the same order as in the WD YBCO (Sec. 4.2), the phase rigidity of the order parameter wave function of HTSCs is conserved.[40–42]

In the framework of such an approach, it is assumed that below T_{01} $\xi_c(0) > d_1$ and connects the CuO_2 planes via Josephson interaction, which leads to the appearance of a FLC governed by 2D MT.[7,145,156] Obviously, in this case ε_{01} becomes the main parameter of Eq. (3), and its correct choice is crucial for the FLC analysis, which has already been discussed above. Thus, as is the case in all magnetic superconductors, it is precisely $d_1\sqrt{\varepsilon_{01}}$ that determines $\xi_c(0)$, and hence, the coupling parameter α (6). This is exactly why we substitute ε_{01} instead of ε_0 into Eq. (4) to find τ_φ(100 K) $\beta = (0.492 \pm 0.002) \times 10^{-13}$ s ($P = 0$). If $d = 11.67$ Å and $\varepsilon = \varepsilon_0$ are substituted into Eq. (4), then we obtain τ_φ(100 K) $\beta = (6.118 \pm 0.002) \times 10^{-13}$ s and curve 3 in Fig. 31(b), which clearly does not correspond to the experiment. This result confirms the correctness of our reasoning, and also indicates a strengthened 2D-MT contribution [denoted as Δ ($\ln\sigma'$) on Fig. 7 in Ref. 150] in FLC as compared to $YBa_2Cu_3O_{7-\delta}$. For the first time, the enhanced MT contribution to the 2D region of SC fluctuations above T_c was observed in a magnetic superconductor $SmFeAsO_{0.85}$,[7,203] and then in $EuFeAsO_{0.85}F_{0.15}$.[157] By comparing the results, it can be concluded that the enhanced fluctuation contribution to the 2D MT region can be considered to be the main feature of the specific FLC behavior caused by the influence of the HoBCO magnetic subsystem.

A few more distinct differences between the behavior of the FLC for WD HoBCO single crystals (Fig. 31) and YBCO (Sec. 4.2) are worth noting. In contrast to YBCO (Fig. 19), the HoBCO transition from 3D to 2D fluctuations is somewhat stretched in temperature (Fig. 31). This may be caused by the spread of unit cell sizes $d \sim 11.67$ Å due to defects induced by the TB, especially in the case of $I\perp$TB,[85,187–190] and also because of the possible enhancement of magnetic interactions in HoBCO. However, as before, T_0 ($\ln\varepsilon_0$ in Fig. 31) is clearly determined based on the point at which the temperature dependences of the AL and MT theories intersect. It should also be noted that pressure amplifies 2D fluctuations, as a result of which the data deviates upward from the theoretical MT curve above $\ln\varepsilon \sim -1.65$. Such a curve shape is typical for magnetic superconductors.[157,203] As will be shown below, the effect of the

HoBCO magnetic subsystem is even more clearly observed on the temperature dependence of the pseudogap for such single crystals.[85]

In addition to the apparent decrease in resistance and the increase in T_c, as well T_c^{mf}, T_c, T_0 and T_{01} and the SC fluctuation region $\Delta T_{fl} = T_{01} - T_G \approx 47$ K ($P = 0.48$ GPa) (Figs. 28–31), the pressure decreases $\tau_\varphi(100\,\text{K})\beta = (0.405 \pm 0.002) \times 10^{-13}$ s at $P = 0.48$ GPa, as well as the excess conductivity σ'. From the data shown in Fig. 31, it follows that $d\ln\sigma'/dP \approx -1.25$ GPa^{-1}. Whereas in YBCO, σ' is practically independent of pressure (Fig. 19). Also in HoBCO, $\xi_c(0)$, d_{01}, and both C-factors slightly decrease (see Tables 5 and 6), which indicates some improvement in the structure of the sample under pressure. The closer C_{3D} is to 1.0, the more homogeneous the structure of the sample.[7,60–62] This conclusion is supported by the experimental fact that the temperature interval of the "Anderson"-type metal-to-dielectric (MD) transition, which is most likely caused by the disordering of such systems,[205] smoothly decreases under pressure in HoBCO.[188] The pressure also increases T_G, and consequently, the so-called Ginzburg number: Gi = $(T_G - T_c^{mf})/T_c^{mf}$ (Table 5),[162] as shown in detail in our Ref. 85. However, this issue is outside the scope of this paper.

5.1.3. The temperature dependence of the HoBa$_2$Cu$_3$O$_{6.65}$ pseudogap, under pressure

In the framework of the LP model, information on the magnitude and temperature dependence of the PG in HoBa$_2$Cu$_3$O$_{6.65}$ is obtained from the temperature dependence of the excess conductivity $\Delta\sigma(T)$ with the aid of Eqs. (10) and (11).[85] In addition to T^*, $\xi_c(0)$, and ε, the values of the coefficients A_4 and ε_{c0}^*, which were experimentally determined using the LP model, as was the case with YBCO single crystals (see Fig. 20), are substituted into Eq. (11). The value $\Delta^*(T_c^{mf})$ was found based on the dependence $\Delta(1/T)$ (see Fig. 21). As expected, at $P = 0$ $D^* = 2\Delta^*(T_c^{mf})/k_B T_c = (5.0 \pm 0.05)$, though in contrast to YBCO, which is surprising, in HoBCO D^* is practically independent of pressure (Table 6). The dependences $\Delta^*(T)$, calculated according to Eq. (11) with the parameters $T^* = 269$ K, $T_c^{mf} = 61.9$ K, $\xi_c(0) = 2.72$ Å, $\varepsilon_{c0}^* = 0.76$, $A_4 = 35$, $\Delta^*(T_c) = 151$ K and $D^* = 5.0$ at $P = 0$, and accordingly $T^* = 265$ K, $T_c^{mf} = 65.9$ K, $\xi_c(0) = 2.65$ Å, $\varepsilon_{c0}^* = 0.806$, $A_4 = 23.8$, $\Delta^*(T_c) = 156.6$ K and $D^* = 5.0$ at $P = 0.48$ GPa are shown in Fig. 32.

As can be seen in the figure, the shape of the $\Delta^*(T)$ dependence of the HoBa$_2$Cu$_3$O$_{6.65}$ single crystal differs fundamentally from the analogous dependence observed for WD YBCO single crystals both without and without pressure (see Fig. 22). In addition, at $P = 0$, the $\Delta^*(T)$ dependence shows two unexpected maxima at $T_{m1} \approx 214$ K and $T_{m2} \approx 239$ K (Fig. 32, curve 1). The higher temperature maximum is expressed more clearly. Most likely, the maxima arise as a result of the single crystal's two-phase
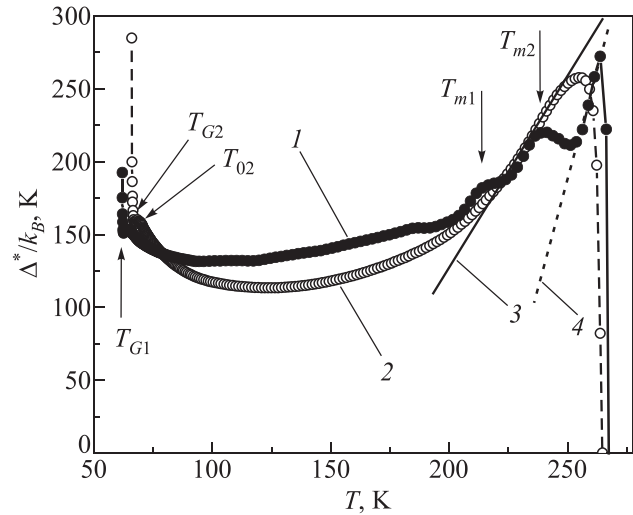

FIG. 32. The temperature dependences of the pseudogap $\Delta^*(T)$ for the WD HoBa$_2$Cu$_3$O$_{6.65}$ single crystal at $P = 0$ (1) and $P = 0.48$ GPa (2), calculated using the LP model (11) with the parameters given in the text. Line 3 marks the linear portion of curve 2 ($\mathbf{I} \perp$ TB). Dashed line 4 shows a slope that is expressed by magnetic superconductors such as SmFeAsO$_{0.85}$.[203] T_{m1} and T_{m2} are the maxima of $\Delta^*(T)$ on curve 1.

stratification, which is specific to HoBCO single crystals with pronounced TBs (see Fig. 4).[187,188] One of the possible causes of phase separation can be a lowered T_c in the TB region, which occurs due to an increased density of vortices in the TB regions.[206,207] In addition, at $P = 0$, there is a decreasing linear section marked by straight line 4, with a slope close to that observed in the IBSCs,[157,203] in the $T > T_{m2}$ range. These questions were considered in detail in Ref. 85. The pressure forces the ascending diffusion processes to operate in the sample, which leads to the redistribution of labile oxygen in a single crystal[187–190] (see Sec. 3.1.4). Ultimately, this leads to the disappearance of the maxima along $\Delta^*(T)$ and the appearance of a specific $\Delta^*(T)$ dependence with a decreasing linear region in the high temperature range (line 3 on Fig. 32), but one that is different from line 4.[85] We emphasize that in this case the maxima disappear only after keeping the sample under pressure for 5 days. It can be assumed that the specificity of the charge carrier distribution, which arises at the twin boundaries at $\mathbf{I} \perp$ TB, inhibits the ascending diffusion process in a single crystal.[85]

As noted above, similar dependences of $\Delta^*(T)$ are observed in SmFeAsO$_{0.85}$ (Refs. 7 and 203) and EuFeAsO$_{0.85}$F$_{0.15}$ (Ref. 157) IBSCs and are typical for magnetic superconductors.[159] Thus, the peculiarities observed in our experiments for the behavior of the FLC and PG in WD HoBCO single crystals can probably be explained by the enhancement of the magnetic interaction in such samples, due to the obvious influence of the intrinsic magnetism of Ho.[85,208] At the same time, the behavior of $\Delta^*(T)$ before the SC transition (Fig. 32) is the same as in all HTSCs that we investigated (Fig. 27).[159] Below $T_{01} \approx 114$ K ($P = 0.48$ GPa), $\Delta^*(T)$ increases appreciably, demonstrating a maximum at $T \sim T_{02}$ (T_0 for $P = 0$ is not shown). Then follows a minimum at T_G, below which there is a sharp increase in $\Delta^*(T)$ during the transition to the critical fluctuation regime immediately near T_c. All the results obtained confirm the above assumption that the excess conductivity reflects not

TABLE 6. Parameters of FLC and PG analysis of HoBa$_2$Cu$_3$O$_{6.65}$ single crystals.

P, GPa	d_I, Å	C_{3D}	C_{2D}	T_{M1}, K	T_{M2}, K	D^*	$\Delta^*(T_c)$, K	Δ^*_{max}, K
0	3.5	2.38	2.75	214	239	5.0 ± 0.05	151	271
0.48	3.09	1.72	2.18	…	…	5.0 ± 0.05	157	258

only the value of the PG, but also the features of the interaction, including magnetic, in the HTSC charge carrier system.

Unexpected and surprising is the fact that in this case, the PG $\Delta^*(T)$ practically does not increase under pressure, which sharply distinguishes the magnetic HoBCO from the nonmagnetic YBCO (Sec. 4). Moreover, in a significant temperature range, from ≈ 220 to ≈ 80 K, the $\Delta^*(T, P)$ dependence passes even below $\Delta^*(T, 0)$ (Fig. 32). However, $\Delta^*(T_G, P) \approx 156.6$ K (ln $\Delta^*(T_G, P) = 5.0536$) is still larger than $\Delta^*(T_G, 0) \approx 150.8$ K (ln$\Delta^*(T_G, P) = 5.0159$). This indicates an increase in $\Delta^*(T)$ with a velocity $d\ln\Delta^*/dP \approx 0.075$ GPa^{-1}, which is about 5 times smaller than in the WD YBCO single crystal, where $d\ln\Delta^*/dP \approx 0.36$ GPa^{-1} (Sec. 4.2.3). Even less, practically at the level of experimental error, is the pressure effect on $D^* = 2\Delta^*(T_c^{mf})/k_B T_c$, equal to $D^* = 5 \pm 0.05$, irrespective of pressure. Is this behavior a consequence magnetism in HoBCO, or is it generated by the defects created by TBs? The answer is unclear. To gain more insight, we measured the same HoBCO single crystals while passing a current parallel to the TBs, as shown in the next section.

5.2. The specific behavior of weakly doped HoBa$_2$Cu$_3$O$_{7-\delta}$ single crystals under hydrostatic pressure up to 0.5 GPa at a current parallel to the twin boundaries

5.2.1. A study of how pressure impacts resistance, critical temperature and fluctuation conductivity

For studies at a current parallel to the TB (**I** || TB) (sample S2),[193] single crystals are taken from the same batch as the samples used in the previous section. The measurements are also carried out at pressures $P = 0$ (sample H12) and $P = 0.48$ GPa after aging for five days (sample H32). That is, to determine the effect of oxygen redistribution, measurements are carried out at two to seven days after the pressure application-relief, so that the relaxation processes are completed.[85,187,188,193] In fact, as in the case of **I**⊥TB, we have four samples: H12 at $P = 0$, H22 ($P = 0.48$ GPa), H32 ($P = 0.48$ GPa applied for 5 days) and H42 at $P = 0$, measured immediately after depressurization.

The temperature dependences of resistivity $\rho(T) = \rho_{ab}(T)$ of the HoBa$_2$Cu$_3$O$_{7-\delta}$ single crystal with $T_c \approx 62$ K and oxygen index $7-\delta \approx 6.65$ for **I** ||TB are similar to those shown in Fig. 28 for measurements at a current with an angle of 45° to the TB (**I**⊥TB). As expected, they had the same S-shape,[85,193] characteristic of weakly doped HTSCs.[60,61,106] However, unlike the measurements for **I**⊥TB, T^* was noticeably lower: $T^* \approx 247.5$ K at $P = 0$, but also decreased insignificantly to $T^* \approx 242.7$ K at $P = 0.48$ GPa (Table 2). Accordingly, as can be seen from Table 7, at **I** || TB $dT_c/dP \approx 5.8$ K/GPa. We note that this is 1.4 times greater than for **I**⊥TB, but it is consistent with similar results obtained for other cuprates.[188,189,194–197,201] Above T^*, all the $\rho(T)$ dependences are linear with a slope $d\rho/dT \approx 3.0$ and ≈ 2.45 $\mu\Omega$ cm/K at $P = 0$ and $P = 0.48$ GPa,

respectively, as follows from the theory.[45] As in the case of **I**⊥TB (Sec. 5.1), the decrease in $\rho(T)$ under pressure at $T > T^*$ is practically independent of the temperature and amounts to $d \ln\rho(300\,\text{K})/dP = -(35 \pm 0.5)\% \times \text{GPa}^{-1}$, which is ~ 1.8 times larger than in our YBCO single crystals (Sec. 4.2). This value appreciably exceeds the value $d\ln\rho/dP$, reported for various cuprates.[189,190,194–197,201] Note that the detected large value of $d\ln\rho(300\text{K})/dP = -(34 \pm 1)\% \times \text{GPa}^{-1}$, observed for both **I**⊥TB and **I** || TB, is apparently specific to HoBCO single crystal behavior. The reason for this behavior requires further study.

The fluctuation conductivity for all P was determined in a standard manner based on excess conductivity $\sigma'(T)$, which is calculated from Eq. (1) as the difference between the measured resistance $\rho(T)$ and the linear above $T^* \rho_N(T)$, extrapolated to the low-temperature region.[193] As in other single crystals (Secs. 4 and 5.1), the analysis is carried out using the LP model for all values of pressure. The results obtained for the sample at $P = 0$ and 0.48 GPa applied for a week are compared. As in Sec. 5.1.2 (Fig. 30), the dependence $\sigma'^{-2}(T)$ is used to determine the critical temperature in the mean-field approximation $T_c^{mf} \approx 62.4\,K > T_c(P = 0)$ and $T_c^{mf} \approx 65.4\,K(P = 0.48)$ GPa, as well as T_G and T_0 (Table 7). As usual, T_c is determined by extrapolating the resistive transition to the value $\rho(T_c) = 0$. The dependences $\ln\sigma'(\ln\varepsilon)$ at $P = 0$ (a) and $P = 0.48$ GPa (b) are shown in Fig. 33. Let us consider the details of FLC behavior using the example
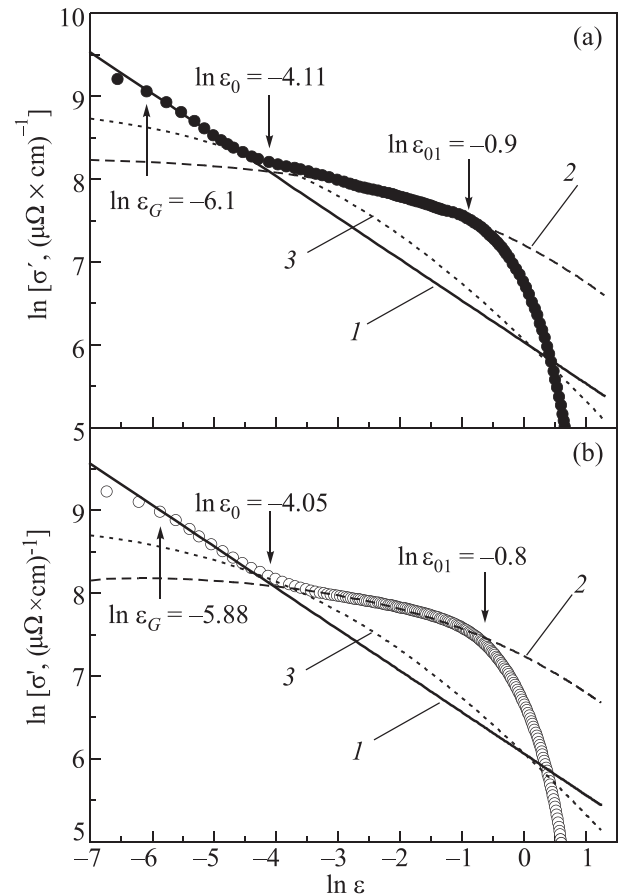
FIG. 33. ln σ' as a function of ln ε for a HoBa$_2$Cu$_3$O$_{6.65}$ single crystal at $P = 0$ (a) and $P = 1.05$ GPa (b) (**I** || TB) in comparison with fluctuation theories: 3D AL (1); MT with $d = d_{01}$ (2) and MT with $d = 11.67$ Å (3). In ε_{01} defines T_{01}, which gives the SC fluctuation region above T_c, lnε_0 determines the temperature of the crossover T_0 and lnε_G determines the Ginzburg temperature T_G.

TABLE 7. FLC analysis parameters for the HoBa$_2$Cu$_3$O$_{6.65}$ single crystal at **I** || TB.

P, GPa	$\rho(100\,\text{K})$, $\mu\Omega$ cm	T_c, K	T^*, k	T_c^{mf}, K	T_G, K	T_0, K	T_{01}, K	$\xi_c(0)$, Å
0	193	61.2	247.5	62.4	62.5	63.3	88.7	1.49 ± 0.05
0.48	172	64	242.7	65.4	65.6	66.5	95.6	1.53 ± 0.05

$P = 0.48$ GPa. Same as the other single crystals that were studied, up to $T_0 \approx 66.5$ K (ln $\varepsilon_0 \approx -4.05$), the experimental data are extrapolated well by 3D AL fluctuation contribution (2)[7,60,144] (solid line 1), and above T_0, to $T_{01} \approx 95.6$ K (ln $\varepsilon_{01} \approx -0.8$), by the 2D MT contribution to HL (3)[26,27,145,193] with $d = d_{01} = 2.29$ Å and τ_φ (100 K)$\beta = (0.665 \pm 0.002) \times 10^{-13}$ s (dashed curve 2), which is typical for magnetic HTSCs. Accordingly, curve 3, constructed with $d = 11.67$ Å, as in the case of $\mathbf{I}{\perp}TB$ (Fig. 31), passes much lower than the experimental points and has a completely different slope. However, somewhat unexpectedly, curve 3 describes the experiment quite well in the temperature interval between the region of 3D and 2D fluctuations. Nevertheless, T_0 is still defined as the point of intersection of the AL and MT curves, which seems logical. Thus, at $T = T_0$, a dimensional 3D-2D (AL-MT) crossover is also clearly observed (Fig. 33). Using Eq. (8), we use the crossover temperature to determine $\xi_c(0)$ $= d_{01}\varepsilon_{01}^{1/2} = d\varepsilon_0^{1/2} = (1.53 \pm 0.005)$ Å (Table 7), which, however, is 1.73 times smaller, than with $\mathbf{I}{\perp}TB$.

A similar dependence of ln σ'(ln ε) is obtained for $P = 0$ with the parameters given in Tables 7 and 8. It can be seen from the tables that the pressure leads to a noticeable increase in the SC fluctuation temperature interval, determined by T_{01}.[40–42] It is not difficult to calculate that $\Delta T_{fl} = T_{01} - T_G$ changes from $\Delta T_{fl} \approx 26.2$ K ($P = 0$) to $\Delta T_{fl} \approx 30$ K ($P = 0.48$ GPa), which is 17 K less than in the case of $\mathbf{I}{\perp}TB$ at that the same pressure (Sec. 5.1).

We note other measurement differences from the case of $\mathbf{I}{\perp}TB$. From Fig. 33 it is visible that at $\mathbf{I}\,\|\,TB$ the pressure does not distort the experimental dependence, and that the deviation of the experimental points from the MT curve in the high-temperature region observed for $\mathbf{I}{\perp}TB$ at $P = 0.48$ GPa above ln $\varepsilon \approx -1.65$ [Fig. 31(b)], is absent in this case. As is the case for WD YBCO (Fig. 19), the pressure practically does not affect the value of σ' at $\mathbf{I}\,\|\,TB$. It can be assumed that the decrease in σ' found for $\mathbf{I}{\perp}TB$ under pressure, $d\ln\sigma'/dP \sim -1.25$ GPa^{-1}, is a consequence of the specific distribution of charge carriers when the current is directed at an angle to the TB. At the same time, the transition from 3D to 2D fluctuations is even more prolonged for $\mathbf{I}\,\|\,TB$ (Fig. 33). This result is somewhat unexpected, since it suggests a greater spread of values of d in the sample, presumably due to structural distortions. At the same time, it was expected that for $\mathbf{I}\,\|\,TB$, the number of defects that are created by the TB should be smaller. However, this result is confirmed by the observed decrease in T^* by ~ 22 K compared with $\mathbf{I}{\perp}TB$ (Tables 6 and 7). A significant decrease in T^* was observed for the first time in $Y_{1-x}Pr_xBa_2Cu_3O_{7-\delta}$ films.[158] It is assumed that the dielectric cells of PrBCO, which arise during the manufacture of such films, create multiple defects in the conducting YBCO matrix, which prevent the appearance of phase coherence in the local pair

ensemble, thus lowering T^*. Consequently, the more defects, the lower the T^* should be, which is observed when $\mathbf{I}\,\|\,TB$.

We also note that, despite the same T_c, the entire curve $\sigma'(T)$ is shifted toward low temperatures for $\mathbf{I}\|TB$. When we compare the results shown in Figs. 31 and 33, we see that for $\mathbf{I}{\perp}TB$ the dimensional crossover occurs at ln$\varepsilon_0 \approx -3$, and for $\mathbf{I}\|TB$ at ln$\varepsilon_0 \approx -4$. Thus, we get a nontrivial result: when the direction of the current is changed relative to the TB, $\xi_c(0)$ decreases by almost 2 times in comparison with $\mathbf{I}{\perp}TB$, and by 2.3 times in comparison with the WD YBCO (Sec. 4.2). Accordingly, the distance between the conducting planes d_{01} surprisingly turned out to be ~ 1.5 times smaller (see tables). Also, note that in this case $C_{3D} = 0.82$ at $P = 0$, i.e., less than one, and increases somewhat under pressure (up to 0.87) (Table 8). Whereas for $\mathbf{I}{\perp}TB$, $C_{3D} = 2.38$ at $P = 0$, i.e., more than one, and under pressure it noticeably decreases (to 1.72) (Table 6). Recall that the closer the C_{3D} is to 1.0, the more uniform the structure of the sample is assumed to be.[7,60,61]

5.2.2. Influence of pressure on the pseudogap at I ∥ TB

As in Secs. 4.2, 4.3, and 5.1, the pseudogap in $HoBa_2Cu_3O_{6.65}$ single crystals at $\mathbf{I}\|TB$ is analyzed using the LP model. In a standard way, information on the magnitude and temperature dependence of the PG was determined from the temperature dependence of the excess conductivity $\Delta\sigma(T)$ with using Eqs. (10) and (11).[85] In addition to T^*, $\xi_c(0)$ and ε, defined above, the values of the coefficients A_4 and ε_{c0}^*, which are experimentally determined in the LP model (see Sec. 4, Fig. 20 and Sec. 5.1), enter into Eq. (11). The value $\Delta^*(T_c^{mf})$ is determined based on the dependence $\Delta^*(1/T)$ (see Fig. 21). As expected, at $P = 0$ $D^* = \Delta^*(T_c^{mf})/k_BT_c = (5.0 \pm 0.05)$, and just like for $\mathbf{I}{\perp}TB$, it is practically independent of pressure (Table 8). The dependences $\Delta^*(T)$, calculated according to (11) with the parameters $T^* = 247.5$ K, $T_c^{mf} = 62.4$ K, $\xi_c(0) = 1.49$ Å, $\varepsilon_{c0}^* = 0.78$, $A_4 = 12.7$, $\Delta^*(T_c) = 152.6$ K and $D^* = 5.0$ at $P = 0$ and, respectively, $T^* = 242.7$ K, $T_c^{mf} = 65.4$ K, $\xi_c(0) = 1.53$ Å, $\varepsilon_{c0}^* = 0.79$, $A_4 = 13.9$, $\Delta^*(T_c) = 160$ K and $D^* = 5.0$ at $P = 0.48$ GPa, are shown in Fig. 34 (curves 1 and 2, respectively).

As can be seen in Fig. 34, the dependences $\Delta^*(T)$ in the case of $\mathbf{I}\|TB$ are fundamentally the same as for $\mathbf{I}{\perp}TB$ (Fig. 32). Similarly, at $P = 0$, the $\Delta^*(T)$ curve shows two maxima, but at much lower temperatures $T_{m1} \approx 195$ K and $T_{m1} \approx 208$ K (Fig. 34, curve 1). Accordingly, the difference between the temperatures at which the maxima at $\mathbf{I}{\perp}TB$ and $\mathbf{I}\|TB$ appear is: $\Delta T_{m1} = 214 - 195$ K $= 19$ K and $\Delta T_{m2} = 239 - 208$ K $= 31$ K. We still assume that the maxima arise as a result of the single crystal's biphasic nature, which is specific to HoBCO single crystals with pronounced TBs (see Fig. 4).[187–189] The causes for the phase separation in such single crystals are considered in Sec. 5.1 and in detail in Ref. 85. The pressure forces the processes of ascending diffusion to kick into action, which leads to the redistribution of labile oxygen in the single crystal (Sec. 3.1.4).[187–190] Ultimately, this generates the disappearance of the maxima along $\Delta^*(T)$ (curve 2) and the appearance of a specific $\Delta^*(T)$ dependence with an extended decreasing linear region at high temperatures (straight line 3, Fig. 34). In contrast to

TABLE 8. The parameters of the FLC and PG analysis of $HoBa_2Cu_3O_{6.65}$ single crystal at $\mathbf{I}\,\|\,TB$.

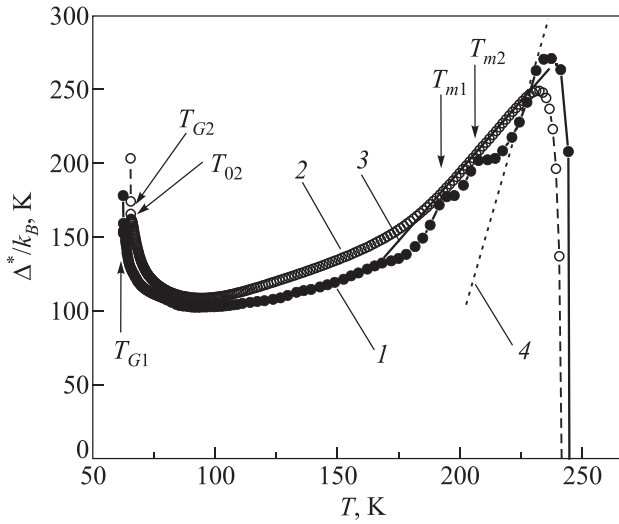| P, GPa	d_1,Å	C_{3D}	C_{2D}	T_{m1}, K	T_{m2}, K	D^*	$\Delta^*(T_c)$, K	Δ_{max}^*, K
0	2.34	0.82	1.29	195	208	5.0 ± 0.05	152.6	271

FIG. 34. The temperature dependences of the pseudogap $\Delta^*(T)$ for the WD HoBa$_2$Cu$_3$O$_{6.65}$ single crystal at $P=0$ (1) and $P=0.48$ GPa (2), calculated within the framework of the LP model, using Eq. (11) with the parameters given in the text (**I**||TB). Line 3 marks the linear portion of curve 2. The dashed line 4 shows the slope that is demonstrated by magnetic superconductors such as SMFeAsO$_{0.85}$.[203] T_{m1} and T_{m2} mark the maxima of $\Delta^*(T)$ on curve 1.

I⊥TB, in this case the maxima disappear immediately after the application of pressure, i.e., the process of ascending diffusion in this case flows much faster. Perhaps this explains the much lower values of ΔT_{m1} and ΔT_{m2} for **I**||TB. However, the physics of these processes are not completely clear.

The dependence of $\Delta^*(T)$ with the decreasing linear portion was observed by us in the IBSCs SmFeAsO$_{0.85}$ (Refs. 7 and 204) and EuFeAsO$_{0.85}$F$_{0.15}$, and is typical for magnetic superconductors.[159] The slope of the $\Delta^*(T)$ dependence with $d\Delta^*/dT \approx 5.8$, which is usually observed for the IBSCs,[159] is shown in Fig. 34 by the dashed line 4. It can be seen that in a relatively narrow temperature range of 231–221 K ∼ 10 K, the same slope is demonstrated by the experimental dependence of $\Delta^*(T)$ at $P=0$. And the same slope at $P=0$ is observed in the interval 275–265 K on the $\Delta^*(T)$ curve at **I**⊥D (Fig. 32). These results support the hypothesis of the enhanced role played by magnetic fluctuations in the WD HoBCO.[85] With increasing pressure, the slope decreases to ≈ 1.9 (line 3 in Fig. 34) and to ≈2.6 at **I**⊥TB (line 3 in Fig. 32). Strictly speaking, this dependence somewhat resembles the $\Delta^*(T)$ obtained for the WD YBCO single crystal at $P=0$ (Fig. 22). But there, the slope $d\Delta^*/dT \approx$ 1.28 is even less, and, as expected, there is no region with a "magnetic" slope $d\Delta^*/dT \approx 5.8$. Comparing all the results obtained, it can be assumed that pressure not only stimulates the ascending diffusion process, but also somewhat reduces the role of magnetic fluctuations in HoBCO single crystals. However, this issue requires further study.

It should be noted that, as in the case of **I**⊥TB, pressure practically does not affect the value of $\Delta^*(T)$ (Fig. 34), which, as already mentioned, distinguishes magnetic HoBCO (Sec. 5.1) from non-magnetic YBCO (Sec. 4). However, $\Delta^*(T_G, P) \approx 160$ K (ln $\Delta^*(T_G, P) = 5.075$) is still larger than $\Delta^*(T_G, 0) \approx 152.6$ K (ln $\Delta^*(T_G, P) = 5.0278$), and curve 2 ($P=0.48$ GPa) in this case passes somewhat higher than curve 1 ($P=0$) (Fig. 34) This indicates the growth of $\Delta^*(T)$ at the rate of $d\ln\Delta^*/dP = 0.0472/0.48 \approx 0.098$ GPa^{-1},

which is 3.7 times lower than in the WD YBCO single crystals, where $d\ln \Delta^*/dP \approx 0.36$ GPa^{-1} (Sec. 4.2.3). As before, the pressure effect on $D^* = 2\Delta^*(T_c^{mf})/k_B T_c$, equal to $D^*=5 \pm 0.05$ is small, almost at the level of experiment error (Table 8) regardless of pressurization. Despite a number of distinct differences noted above in the behavior of $\Delta^*(T)$ for both **I**||TB and **I**⊥TB from the $\Delta^*(T)$ observed in WD YBCO, it is still not clear whether such behavior is a consequence of magnetism in HoBCO single crystals or if it is due to defects created by the TB. Most likely, both mechanisms contribute to the observed behavior of $\Delta^*(T)$ in both cases.[85,193,208] Obviously, in order to shed light on this question, it is necessary to perform measurements for both **I**||TB and **I**⊥TB at even larger (at least ∼1 GPa) values of hydrostatic pressure.

Taking into account the above facts, we can consider the significant decrease (more than 1.7 times in comparison with YBCO) of $\rho(T)$ in HoBCO under pressure, keeping in mind that in this case the PG remains practically unchanged. We recall that when studying the OD YBCO single crystals, we found that $\rho(T)$ and PG strongly change with pressure, whereas T_c increases very slightly. The last result means that in the OD YBCO, the pressure practically does not increase the charge carrier density n_f in CuO$_2$ planes, which close to saturation in OD HTSCs. In this case, the decrease in $\rho(T)$ and the considerable growth of the PG were attributed to a decrease in the frequencies of the phonon spectrum of the HTSC under pressure. This effect is reported in Ref. 29. In WD HoBCO single crystals, the PG practically does not depend on pressure, calling into question the possibility of the phonon spectrum softening in this case. At the same time, $\rho(T)$ decreases significantly, and T_c increases with the same intensity as in YBCO. As can be seen in Fig. 4, WD HoBCO single crystals have a pronounced twin boundary structure. As our investigations have shown (Sec. 5), when pressure is applied, an appreciable role is played by the process of ascending diffusion in such samples. As a result of applying pressure to the single crystal, there remains only one high-temperature phase enriched in oxygen, and therefore charge carriers,[187,188] and the number of defects (Sec. 3) is also reduced. It is likely that the decrease in resistance and the growth of T_c in HoBCO single crystals are largely caused by these processes.

We also note that, as expected, the behavior of $\Delta^*(T)$ before the SC transition (Fig. 34) is the same as in all HTSCs (Fig. 27).[159] Below $T_{01} \approx 95.6$ K ($P=0.48$ GPa), $\Delta^*(T)$ appreciably increases, demonstrating a maximum at $T \sim T_{02}$ (T_0 for $P=0$ is not shown). Then follows a minimum at T_G, below which there is a sharp increase at $P=0$ in the transition to the critical fluctuation regime immediately near T_c. All the results once again confirm the above assumption that excess conductivity reflects not only the value of the PG, but also the features of the interaction in the system of HTSC charge carriers, including when magnetic interaction is present.[85,193]

Thus, for the first time the LP model is used to study the influence of hydrostatic pressure up to ∼0.5 GPa on the excess conductivity $\sigma'(T)$ and the pseudogap $\Delta^*(T)$ of weakly doped HoBa$_2$Cu$_3$O$_{7-\delta}$ single crystals with T_c ∼ 61.2 K (at $P=0$) and an intrinsic magnetic moment of $\mu_{eff} = 9.7$ μ_B.

For the first time, it is discovered that, regardless of the direction of the transport current with respect to the TB,

hydrostatic pressure up to ~ 0.5 GPa has almost no impact either on $\Delta^*(T)$, or the ratio $D^* = 2\Delta^*(T_c^{mf})/k_B T_c$.

It is shown that this behavior of $\Delta^*(T)$ is most likely due both to the influence of intrinsic magnetism in HoBCO and the defects created by pronounced twin boundaries (TB) in such single crystals. At the same time, the role of the phonon spectrum "softening", which plays a decisive role in the observed significant increase of $\Delta^*(T)$ in YBCO single crystals (Sec. 4), in this case is not clear.

It was found that the effect of pressure on T_c, $dT_c/dP = +(4.2–5.7)$ K/GPa, is of the same order as that of WD YBCO single crystals, while the decrease in the resistivity $d\ln\rho/dP \approx -(33 \pm 0.2)\% \times$ GPa^{-1} is ~ 1.8 times higher. In such samples a significant role is played by the process of ascending diffusion under pressure, as a result of which only one oxygen-enriched, and therefore charge carrier-enriched, high-temperature phase remains, and the number of defects also decreases. It is most likely that the decrease in resistance and the growth of T_c in the HoBCO single crystal are caused by these processes.

This assumption is confirmed by the observation of two maxima on the $\Delta^*(T)$ dependence at high T, which disappear under pressure due to the ascending diffusion process. This leads to a noticeable change in the shape of the $\Delta^*(T)$ dependence, in which an extended linear portion arises at the site of the maxima.

It is shown that at $P = 0$ the slope of the $\Delta^*(T)$ dependence at high T, $d\Delta^*/dT \approx 5.8$, is the same as that observed in the IBSCs, which indicates that magnetic fluctuations play an appreciable role in the formation of the PG in WD HoBCO single crystals.

Note that the slope of this linear section $d\Delta^*/dT \approx 2.6$ (for $\mathbf{I}\bot$ TB) is 2.2 times smaller than $d\Delta^*/dT \approx 5.8$, observed in magnetic HTSCs, but 2 times greater than $d\Delta^*/dT \approx 1.28$, found in non-magnetic YBCO (Sec. 4). This also indicates that the unusual behavior of the PG in pressurized HoBCO single crystals is a consequence of changes to the magnetic interactions, the redistribution of charge carriers, and a decrease in the role of defects as a result of the pressure exerted on the TB.

It is shown that, regardless of pressure, in the temperature range T_c–T_{01} the excess conductivity $\sigma'(T)$ is well described by 3D AL and 2D MT fluctuation theories, demonstrating a 3D-2D crossover with increasing temperature.

Despite the pressure applied to HoBCO single crystals, the transition $\Delta^*(T)$ to the superconducting state below T_{01} actually takes place according to the same law as in all the other high-temperature superconductors studied by us.

Conclusion

In this review, an attempt is made to consider the main problems facing high-temperature superconductor physics, and to analyze the different mechanisms of how hydrostatic pressure affects the electric transport and pseudogaps in HTSCs, taking into account the various possible defects, and using YBa$_2$Cu$_3$O$_{7-\delta}$ and HoBa$_2$Cu$_3$O$_{7-\delta}$ single crystal samples. At present, HTSCs are the main object of research in the field of fundamental and applied superconductivity, which informs the relevance of this study. In order to improve the characteristics of existing HTSCs, and to search for new materials with even higher superconducting parameters, it is necessary to not only develop the

technology, but also to properly understand the physics of the processes that lead up to the appearance of superconductivity at temperatures $T_c \sim 100$ K. However, despite intense investigation of HTSCs for more than 30 years, the superconducting pairing mechanism in such compounds is still very controversial. It is believed that the ability to understand an unusual phenomenon like the pseudogap, observed in cuprate HTSCs at $T \gg T_c$, would make it possible to answer the question of the SC pairing mechanism. Unfortunately the physics behind the appearance of the PG are not completely clear.

By studying the properties of both WD and OD YBa$_2$Cu$_3$O$_{7-\delta}$ and HoBa$_2$Cu$_3$O$_{7-\delta}$ single crystals under hydrostatic pressure, we obtained a number of new and unusual results. It was shown that pressure significantly reduces the resistance of such single crystals. Moreover, this effect in HoBa$_2$Cu$_3$O$_{7-\delta}$ is almost 2 times greater than in YBa$_2$Cu$_3$O$_{7-\delta}$, which has not yet been explained. It is also shown that pressure increases the T_c in WD samples as $dT_c/dP = +(4.2–5.7)$ K/GPa, but practically does not affect T_c in OD single crystals. This result is in agreement with the conclusions of other articles that consider the possible mechanisms of pressure influence on T_c, and account for the role of the defective ensemble of a particular sample.

For the first time, it has been demonstrated that an increase of the PG under pressure $d\ln\Delta^*/dP \approx 0.32$ GPa^{-1} in YBa$_2$Cu$_3$O$_{7-\delta}$ single crystals is practically independent of doping. Taking into account the results on the increase in the SC gap of Bi2223,[29] it can be assumed that the observed effect is due to a pressure-induced decrease in the frequencies of the YBCO phonon spectrum. However, since there is no strict theory devoted to this question, the issue remains open. One more interesting result is the lack of pressure impact on the PG in HoBa$_2$Cu$_3$O$_{7-\delta}$ single crystals, which turned out to be quite unexpected against the backdrop of a strong increase in the PG of pressurized YBa$_2$Cu$_3$O$_{7-\delta}$ single crystals. Considering the number of unusual properties that have been observed for Ho single crystals, such as the strongest decrease in the resistance under pressure, and the specific shape of the $\Delta^*(T)$ dependence, both at $P = 0$ and under applied pressure, and also the fact that Ho has a large intrinsic magnetic moment ($\mu_{Ho} = 10.6$ μ_B and $\mu_{eff} = 9.7$ μ_B in HoBa$_2$Cu$_3$O$_{7-\delta}$),[202] it can be assumed that the observed effects are a consequence of changes in magnetic interactions, a specific redistribution of charge carriers, and a decrease in the role of defects as a result of pressure being applied to the TB.

In general, our studies have shown that excess conductivity, determined from resistive measurements in the LP model, contains information not only on the magnitude and temperature dependence of the FLC and the PG, but also on the forces of interaction, including those that are magnetic, which take place in specific sample.

a)Email: solovjov@ilt.kharkov.ua

[1]J. G. Bednorz and K. A. Müller, Z. Phys. B **64**, 189 (1986).
[2]*The Physics of Superconductors. Conventional and High-Tc Superconductors*, edited by K. H. Bennemann and J. B. Katterson (Springer, New York, 2003), Vol. 1.

[3]M. Randeria, Nat. Phys. **6**, 561 (2010).

[4]S. Badoux, W. Tabis, F. Laliberte, G. Grissonnanche, B. Vignolle, D. Vignolles, J. Beard, D. A. Bonn, W. N. Hardy, R. Liang, N. Doiron-Leyraud, L. Taillefer, and C. Proust, Nature **531**, 210 (2016).

[5]A. A. Kordyuk, Fiz. Nizk. Temp. **41**, 417 (2015) [Low Temp. Phys. **41**, 319 (2015)].

[6]R. V. Vovk, N. R. Vovk, G. Ya. Khadzhai, and A. V. Dobrovolskiy, Solid State Commun. **204**, 64 (2015).

[7]A. L. Solovjov, *Superconductors - Materials, Properties and Applications. Chapter 7: Pseudogap and Local Pairs in High-Tc Superconductors*, edited by A. M. Gabovich, (InTech, Rijeka, 2012), p. 137.

[8]L. Taillefer, Annu. Rev. Condens. Matter Phys. **1**, 51 (2010).

[9]R. Peters and J. Bauer, Phys. Rev. B **92**, 014511 (2015).

[10]Rui-Hua He, M. Hashimoto, H. Karapetyan, J. D. Koralek, J. P. Hinton, J. P. Testaud, V. Nathan, Y. Yoshida, Hong Yao, K. Tanaka, W. Meevasana, R. G. Moore, D. H. Lu, S.-K. Mo, M. Ishikado, H. Eisaki, Z. Hussain, T. P. Devereaux, S. A. Kivelson, J. Orenstein, A. Kapitulnik, and Z.-X. Shen, Science **331**, 1579 (2011).

[11]M. V. Sadovsky, UFN **171**, 539 (2001).

[12]Z. C. Gu and Y. Z. Weng, Phys. Rev. B **72**, 104520 (2005).

[13]P. W. Anderson, *The Theory of Superconductivity in the High-Tc Cuprates* (Princeton University Press, Princeton, NJ, 1997), p. 446.

[14]P. W. Anderson and Z. Zou, Phys. Rev. Lett. **60**, 132 (1988).

[15]L. A. Boyarsky, S. P. Gabuda, and S. G. Kozlova, FNT **31**, 405 (2005) [Low Temp. Phys. **31**, 308 (2005)].

[16]Y. Ma, P. Ye, and Z.-Y. Weng, New J. Phys. **16**, 083039 (2014).

[17]C. M. Varma, Phys. Rev. B **73**, 155113 (2006).

[18]P. Pieri, G. C. Strinati, and D. Moroni, Phys. Rev. Lett. **89**, 127003 (2002).

[19]H. Alloul, T. Ohno, and P. Mendels, Phys. Rev. Lett. **63**, 1700 (1989).

[20]T. Kondo, A. D. Palczewski, Y. Hamay, T. Kondo, A. D. Palczewski, Y. Hamaya, T. Takeuchi, J. S. Wen, Z. J. Xu, G. Gu, and A. Kaminski, preprint arXiv:1208.3448v1 (2012).

[21]P. G. De Gennes, *Superconductivity of Metals and Alloys* (W.A. Benjamin, INC., New York-Amsterdam, 1966), p. 280.

[22]R. V. Vovk, M. A. Obolenskii, A. A. Zavgorodniy, I. L. Goulatis, V. I. Beletskii, and A. Chroneos, Physica C **469**, 203 (2009).

[23]A. Driessen, R. Griessen, N. Koeman, E. Salomons, R. Brouwer, D. G. De Groot, K. Heeck, H. Hemmes, and J. Rector, Phys. Rev. B **36**, 5602 (1987).

[24]R. Griessen, Phys. Rev. B **36**, 5284 (1987).

[25]J. Metzler, T. Weber, W. H. Fietz, K. Grube, H. A. Ludwig, T. Wolf, and H. Wühl, Physica C **214**, 371 (1993).

[26]A. L. Solovjov, L. V. Omelchenko, R. V. Vovk, O. V. Dobrovolskiy, Z. F. Nazyrov, S. N. Kamchatnaya, and D. M Sergeyev, Physica B **493**, 58 (2016).

[27]A. L. Solovjov, L. V. Omelchenko, R. V. Vovk, O. V. Dobrovolskiy, Z. F. Nazyrov, S. N. Kamchatnaya, and D. M. Sergeyev, Curr. Appl. Phys. **16**, 931 (2016).

[28]E. G. Maksimov, Phys.-Usp. **43**, 965 (2000).

[29]A. I. Dyachenko and V. Yu. Tarenkov, FTVD **24**(2), 24 (2014).

[30]E. E. Zubov, Physica C **497**, 67 (2014).

[31]R. J. Cava, Science **243**, 656 (1990).

[32]M. Asta, D. de Futaine, G. Ceder, E. Salomons, and M. Kraitchman, J. Less. Common Met. **168**, 39 (1991).

[33]R. V. Vovk, N. R. Vovk, and O. V. Dobrovolskiy, J. Low Temp. Phys. **175**, 614 (2014).

[34]R. V. Vovk, Z. F. Nazyrov, M. A. Obolenskii, I. L. Goulatis, A. Chroneos, and V. M. Pinto Simoes, J. Alloys Compd. **509**, 4553 (2011).

[35]S. V. Savich, A. V. Samoilov, R. V. Vovk, O. V. Dobrovolskiy, S. N. Kamchatna, Ya. V. Dolgopolova, and O. A. Chernovol-Tkachenko, Mod. Phys. Lett. B **30**, 1650034 (2016).

[36]K. W. Wang and W. Y. Ching, Physica C **416**, 47 (2004).

[37]V. Mishra, U. Chatterjee, J. C. Campusano, and M. R. Norman, Nat. Phys. Lett. **1**, 1 (2014).

[38]I. O. Kulik and A. G. Pedan, FNT **14**, 700 (1988) [Low Temp. Phys. **14**, 384 (1988)].

[39]P. W. Anderson, Science **235**, 1196 (1987).

[40]V. J. Emery and S. A. Kivelson, Nature **374**, 434 (1995).

[41]J. Corson, R. Mallozzi, J. Orenstein, J. N. Eckstein, and I. Bozovic, Nature **398**, 221 (1999).

[42]K. Kawabata, S. Tsukui, Y. Shono, O. Mishikami, H. Sasakura, K. Yoshiara, Y. Kakehi, and T. Yotsuya, Phys. Rev. B **58**, 2458 (1998).

[43]Q. Chen, I. Kosztin, B. Janko, and K. Levin, Phys. Rev. Lett. **81**, 4708 (1998).

[44]J. R. Engelbrecht, A. Nazarenko, M. Randeria, and E. Dagotto, Phys. Rev. B **57**, 13406 (1998).

[45]B. P. Stojkovic and D. Pines, Phys. Rev. B **55**, 8576 (1997).

[46]A. V. Chubukov and J. Schmalian, Phys. Rev. B **57**, R11085 (1998).

[47]D. J. Scalapino, Rev. Mod. Phys. **84**, 1383 (2012).

[48]S. Dzhumanov, O. K. Ganiev, and S. S. Djumanov, Physica B **440**, 17 (2014).

[49]K. Efetov, H. Meier, and C. Pin, Nat. Phys. **9**, 442 (2013).

[50]M. A. Obolenskii, A. V. Bondarenko, R. V. Vovk, and A. A. Prodan, FNT **23**, 1178 (1997) [Low Temp. Phys. **23**, 882 (1997)].

[51]R. V. Vovk, N. R. Vovk, O. V. Shekhovtsov, I. L. Goulatis, and A. Chroneos, Supercond. Sci. Technol. **26**, 085017 (2013).

[52]R. V. Vovk, N. R. Vovk, I. L. Goulatis, and A. Chroneos, Mod. Phys. Lett. B **27**, 1350198 (2013).

[53]R. V. Vovk, M. A. Obolenskii, A. A. Zavgorodniy, Z. F. Nazyrov, I. L. Goulatis, V. V. Kruglyak, and A. Chroneos, Mod. Phys. Lett. B **25**, 2131 (2011).

[54]R. V. Vovk, G. Ya. Khadzhai, O. V. Dobrovolskiy, N. R. Vovk, and Z. F. Nazyrov, J. Mater. Sci.: Mater. Electron. **26**, 1435 (2015).

[55]R. V. Vovk, M. A. Obolenskii, Z. F. Nazyrov, I. L. Goulatis, and A. Chroneos, J. Mater. Sci.: Mater. Electron. **23**, 1255 (2012).

[56]A. Chroneos, I. L. Goulatis, and R. V. Vovk, Acta Chim. Slovaca **54**, 179 (2007).

[57]R. V. Vovk, Z. F. Nazyrov, I. L. Goulatis, and A. Chroneos, Mod. Phys. Lett. B **26**, 1250163 (2012).

[58]R. V. Vovk, N. R. Vovk, and O. V. Dobrovolskiy, Adv. Condens. Matter Phys. **2013**, 931726 (2013).

[59]B. Ya. Sukharevsky, I. V. Zhikharev, and S. I. Khokhlova, preprint 91-10, DonFTI (1990).

[60]A. L. Solovjov, H.-U. Habermeier, and T. Haage, FNT **28**, 24 (2002) , [Low Temp. Phys. **28**, 17 (2002)]; FNT **28**, 144 (2002) [Low Temp. Phys. **28**, 99 (2002)].

[61]A. L. Soloviev and V. M. Dmitriev, FNT **35**, 227 (2009) [Low Temp. Phys. **35**, 168 (2009)].

[62]A. L. Soloviev and V. M. Dmitriev, FNT **32**, 139 (2006) [Low Temp. Phys. **32**, 99 (2006)].

[63]D. A. Lotnyk, R. V. Vovk, M. A. Obolenskii, A. A. Zavgorodniy, J. Kováč, M. Kaňuchová, M. Šefciková, V. Antal, P. Diko, A. Feher, and A. Chroneos, J. Low Temp. Phys. **161**, 4387 (2010).

[64]A. V. Bondarenko, V. A. Shklovsky, R. V. Vovk, M. A. Obolenskii, and A. A. Prodan, FNT **23**, 1281 (1997) [Low Temp. Phys. **23**, 962 (1997)].

[65]V. V. Kvardakov, V. A. Somenkov, and S. Sh. Schillstein, SFHT **5**, 624 (1992).

[66]V. M. Molchanov, L. A. Muradyan, and V. I. Simonov, JETP Lett. **48**, 222 (1989).

[67]J. Eturno, *Structure of High-Temperature Superconductive Oxides* (Physics Abroad, Mir, Moscow, 1989), p. 25.

[68]M. Imada, A. Fujimori, and Y. Tokura, Rev. Mod. Phys. **70**, 1040 (1998).

[69]M. Suzuki and T. Watanabe, Phys. Rev. Lett. **85**, 4787 (2000).

[70]Y. Yamada, K. Anagawa, T Shibauchi, T. Fujii, T. Watanabe, A. Matsuda, and M. Suzuki, Phys. Rev. B **68**, 054533 (2003).

[71]Y. Iye, "Transport properties of high-Tc cuprates," in *Physics Properties of High-Temperature Superconductors*, edited by D. M. Ginsberg (World Scientific, Singapore, 1992), Vol. 3, p. 285.

[72]Yu. A. Izyumov, UFN **167**, 465 (1997).

[73]N. Bulut, Turk. J. Phys. **20**, 548 (1996).

[74]V. M. Loktev, FNT **22**, 3 (1996) [Low Temp. Phys. **22**, 1 (1996)].

[75]V. V. Eremenko, V. N. Samovarov, V. N. Svishchev, V. L. Vakula, M. Yu. Libin, and S. A. Uyutnov, FNT **26**, 739 (2000) [Low Temp. Phys. **26**, 541 (2000)].

[76]A. Bianconi, "Linear array of homogeneous Cu sites in the CuO_2 plane," in *Phase Separation in Cuprate Superconductors*, edited by D. M. Ginsberg (World Scientific, Singapore, 1992), T. 1, p. 3.

[77]H.-U. Habermeier, in *Proceedings of ESF International Workshop on Superconductivity in Reduced Dimensions Sulzburg*, Austria (2010), p. 33.

[78]Y. Zha, S. L. Cooper, and D. Pines, Phys. Rev. B **53**, 8253 (1996).

[79]V. M. Loktev, UFZ Look Back **1**, 10 (2004).

[80]G. Koren, Supercond. Sci. Technol. **30**, 045008 (2017).

[81]*The Physics of Superconductors, Vol. 1, Conventional and High-Tc Superconductors*, edited by K. H. Bennemann and J. B. Katterson (Springer, Berlin, 2003).

[82]R. J. Birgineau and G. Shirane, "Neutron scattering studies of structural and magnetic excitations in lamellar copper oxides," in *Physical Properties of High-Temperature Superconductors*, edited by D. M. Ginsberg (World Scientific, Singapore, 1989), p. 152.

[83]S. M. Quinlan, D. J. Scalapino, and N. Bulut, Phys. Rev. B **49**, 1470 (1994).

[84]T. Kemin, H. Meisheng, and W. Yening, J. Phys.: Condens. Matter **1**, 1049 (1989).

[85]A. L. Solovjov, M. A. Tkachenko, R. V. Vovk, and A. Chroneos, Physica C **501**, 24 (2014).

[86]R. V. Vovk, G. Ya. Khadzhai, O. V. Dobrovolskiy, Z. F. Nazyrov, and A. Chroneos, Physica C **516**, 58 (2015).

[87]G. Lacayc, R. Hermann, and G. Kaestener, Physica C **192**, 207 (1992).

[88]R. V. Vovk, N. R. Vovk, I. L. Goulatis, and A. Chroneos, J. Low Temp. Phys. **174**, 214 (2014).

[89]V. Selvamanickam, M. Mironova, and S. Son, Physica C **208**, 238 (1993).

[90]A. V. Bondarenko, B. I. Verkin, M. O. Zubarev, and M. A. Obolenskii, preprint 41-88, ILTPE of the Academy of Sciences of the USSR (1998).

[91]W. Gawalek, W. Schueppel, and R. Hergt, Supercond. Sci. Technol. **5**, 407 (1992).

[92]A. Ono and T. Tanaka, Jpn. J. Appl. Phys. **26**, 825 (1987).

[93]V. Selvamanickam, M. Mironova, and S. Son, Physica C **208**, 238 (1993).

[94]G. Roth, G. Heger, and P. Schweiss, Zh. Phys. **152**, 329 (1988).

[95]G. D. Chryssikos, E. I. Kamitsos, J. A. Kapoutsis, A. P. Patsis, V. Psycharis, A. Kafoudakis, C. Mitros, G. Kallias, E. Gamari-Seale, and D. Niarchos, Physica C **254**, 44 (1995).

[96]A. V. Bondarenko, A. A. Prodan, Yu. T. Petrusenko, V. N. Borisenko, F. Dworschak, and U. Dedek, *Magnetic and Superconducting Materials* (World Scientific, 1999), p. 499.

[97]A. V. Bondarenko, A. A. Prodan, Yu. T. Petrusenko, V. N. Borisenko, F. Dworschak, and U. Dedek, Phys. Rev. B **64**, 92513 (2001).

[98]D. M. Ginsberg, *Physical Properties of High-Temperature Superconductor* (Mir, Moscow, 1991).

[99]M. A. Obolenskii, R. V. Vovk, A. V. Bondarenko, and N. N. Chebotaev, Fiz. Nizk. Temp. **32**, 746 (2006) [Low Temp. Phys. **32**, 571 (2006)].

[100]R. V. Vovk, M. A. Obolenskii, A. A. Zavgorodniy, A. V. Bondarenko, I. L. Goulatis, and A. I. Chroneos, J. Mater. Sci.: Mater. Electron. **18**, 811 (2007).

[101]R. V. Vovk, G. Ya. Khadzhai, O. V. Dobrovolskiy, S. N. Kamchatnaya, and Z. F. Nazyrov, J. Low Temp. Phys. **183**, 59 (2016).

[102]R. V. Vovk, N. R. Vovk, G. Ya. Khadzhai, I. L. Goulatis, and A. Chroneos, Physica B: Condens. Matter **422**, 33 (2013).

[103]R. V. Vovk, J. Phys. Chem. Solids **8**, 500 (2007).

[104]R. V. Vovk, M. A. Obolenskii, A. A. Zavgorodniy, A. V. Bondarenko, I. L. Goulatis, and A. I. Chroneos, J. Mater. Sci.: Mater. Electron. **18**, 811 (2007).

[105]R. V. Vovk, M. A. Obolenskii, A. A. Zavgorodniy, A. V. Bondarenko, I. L. Gulatis, and N. N. Chebotaev, FNT **33**, 931 (2007) [Low Temp. Phys. **33**, 710 (2007)].

[106]Y. Ando, S. Komiya, K. Segawa, S. Ono, and Y. Kurita, Phys. Rev. Lett. **93**, 267001 (2004).

[107]R. V. Vovk, Z. F. Nazyrov, I. L. Goulatis, and A. Chroneos, Physica C **485**, 89 (2013).

[108]R. B. Van Dover, L. F. Schneemeyer, J. V. Waszczak, D. A. Rudman, J. Y. Juang, and J. A. Cutro, Phys. Rev. **39**, 2932 (1989).

[109]N. E. Alekseevsky, A. V. Mitin, V. I. Nizhankovskii, E. P. Khlybov, V. V. Evdokimova, and G. M. Kuzmichev, SFHT **2**, 40 (1989).

[110]R. V. Vovk, Z. F. Nazyrov, M. A. Obolenskii, V. M. Pinto Simoes, M. Januszczyk, and J. N. Latosińska, Acta Phys. Pol. A **120**, 512 (2011).

[111]A. Matsuda, K. Kinoshita, T. Ishii, H. Shibata, T. Watanabe, and T. Yamada, Phys. Rev. B **38**, 2910 (1988).

[112]Y. X. Jia, J. Z. Liu, M. D. Lan, and R. N. Shelton, Phys. Rev. B **47**, 6043 (1993).

[113]A. L. Solojov and V. M. Dmitriev, FNT **32**, 753 (2006) [Low Temp. Phys. **32**, 576 (2006)].

[114]R. Fehrenbacher and T. M. Rice, Phys. Rev. Lett. **70**, 3471 (1993).

[115]A. I. Liechtenstein and I. I. Mazin, Phys. Rev. Lett. **74**, 1000 (1995).

[116]Y. Yu, G. Cao, and Z. Jiao, Phys. Rev. **59**, 3845 (1999).

[117]Z. Zou, J. Ye, K. Oka, and Y. Nishihara, Phys. Rev. Lett. **80**, 1074 (1998).

[118]V. V. Moshchalkov, I. G. Muttik, and N. A. Samarin, FNT **14**, 988 (1988) [Low Temp. Phys. **14**, 543 (1988)].

[119]R. V. Vovk, M. A. Obolenskii, A. V. Bondarenko, I. L. Goulatis, M. R. Levy, and A. I. Chroneos, Acta Phys. Pol. A **111**, 123 (2007).

[120]C. W. Chu, P. H. Hor, R. L. Meng, L. Gao, A. J. Huang, and Y. Q. Wang, Phys. Rev. Lett. **58**, 405 (1988).

[121]M. A. Obolenskii, D. D. Balla, A. V. Bondarenko, R. V. Vovk, A. A. Prodan, and T. Φ. Ivanova, FNT **25**, 1259 (1999)

[122]Z. Z. Wang, J. Clayhold, N. P. Ong, J. M. Tarascon, L. H. Greene, W. R. McKinnon, and G. W. Hull, Phys. Rev. B **36**, 7222 (1987).

[123]Y. Kubo, Y. Shimakawa, N. Manako, and H. Igarashi, Phys. Rev. B **43**, 7875 (1991).

[124]T. Timusk and B. Statt, Rep. Prog. Phys. **62**, 161 (1999).

[125]J. L. Tallon, F. Barber, J. G. Storey, and J. W. Loram, Phys. Rev. B **87**, 140508 (2013). [Low Temp. Phys. **25**, 943 (1999)].

[126]V. M. Loktev, FNT **22**, 490 (1996) [Low Temp. Phys. **22**, 376 (1996)].

[127]R. Haussmann, Phys. Rev. B **49**, 12975 (1994).

[128]E. V. L. de Mello, M. T. D. Orlando, J. L. Gonzalez, E. S. Caixeiro, and E. Baggio-Saitovich, Phys. Rev. B **66**, 092504 (2002).

[129]J. R. Engelbrecht, M. Randeria, and C. A. R. Sa de Melo, Phys. Rev. B **55**, 15153 (1997).

[130]V. N. Bogomolov, JTF Lett. **33**(1), 30 (2007).

[131]V. P. Gusynin, V. M. Loktev, and S. G. Sharapov, JETP Lett. **65**, 170 (1997).

[132]Y. Matsuda, T. Hirai, S. Komiyama, T. Terashima, Y. Bando, K. Iijima, K. Yamamoto, and K. Hirata, Phys. Rev. B **40**, 5176 (1989).

[133]J. Sugawara, H. Iwasaki, N. Kabayashi, H. Yamane, and T. Hirai, Phys. Rev. B **46**, 14818 (1992).

[134]T. Ito, K. Takenaka, and S. Uchida, Phys. Rev. Lett. **70**, 3995 (1993).

[135]B. Wuyts, V. V. Moshchalkov, and Y. Bruynseraede, Phys. Rev. B **53**, 9418 (1996).

[136]E. A. Pashitsky and V. I. Pentegov, UFZH **50**, A77 (2005).

[137]A. S. Alexandrov, A. M. Bratkovsky, and N. F. Mott, Phys. Rev. Lett. **72**, 1734 (1994),

[138]A. S. Alexandrov, Phys. Rev. B **53**, 2863 (1996).

[139]A. M. Gabovich, M. S. Li, H. Szymczak, and A. I. Voitenko, Phys. Rev. B **92**, 054512 (2015).

[140]I. A. Nekrasov, N. S. Pavlov, M. V. Sadovskii, and A. A. Slobodchikov, Fiz. Nizk. Temp. **42**, 1137 (2016) [Low Temp. Phys. **42**, 891 (2016)].

[141]K. Morawetz, B. Schmidt, M. Schreiber, and P. Lipavsky, Phys. Rev. B **72**, 174504 (2005).

[142]A. L. Solovjov and M. A. Tkachenko, preprint arXiv:1112.3812v1 [cond-mat.supr-con] (2011); Metallofiz. Noveishie Tekhnol. **35**, 19 (2013).

[143]T. Kondo, Y. Hamaya, A. D. Palczewski1, T. Takeuchi, J. S. Wen, Z. J. Xu, G. Gu, J. Schmalian, and A. Kaminski, Nat. Phys. **7**, 21 (2011).

[144]L. G. Aslamazov and A. L. Larkin, Phys. Lett. **26A**, 238 (1968); FTT **10**, 1104 (1968).

[145]S. Hikami and A. I. Larkin, Mod. Phys. Lett. B **2**, 693 (1988).

[146]E. Stajic, A. Iyengar, K. Levin, B. R. Boyce, and T. R. Lemberger, Phys. Rev. B **68**, 024520 (2003).

[147]A. N. Pasupathy, A. Pushp, K. K. Gomes, C. V. Parker, J. Wen, Z. Xu, G. Gu, S. Ono, Y. Ando, and Ali Yazdani, Science **320**, 146 (2008).

[148]K. Nakayama, T. Sato, Y. Sekiba, K. Terashima, P. Richard, T. Takahashi, K. Kudo, N. Okumura, T. Sasaki, and N. Kobayashi, Phys. Rev. Lett. **102**, 227006 (2009).

[149]K. Nakayama, T. Sato, Y.-M. Xu, Z.-H. Pan, P. Richard, H. Ding, H.-H. Wen, K. Kudo, T. Sasaki, N. Kobayashi, and T. Takahashi, e-print arXiv:1105.5865 [cond-mat.supr-con].

[150]S. Ideta, T. Yoshida, A. Fujimo, H. Anzai, T. Fujita, A. Ino, M. Arita, H. Namatame, M. Taniguchi, Z.-X. Shen, K. Takashima, K. Kojima, and S. Uchida, Phys. Rev. B **85**, 104515 (2012).

[151]T. Kondo, A. D. Palczewski, Y. Hamaya, T. Takeuchi, J. S. Wen, Z. J. Xu, G. Gu, and A. Kaminski, Phys. Rev. Lett. **111**, 157,003 (2013).

[152]W. Lang, G. Heine, P. Schwab, X. Z. Wang, and D. Bauerle, Phys. Rev. B **49**, 4209 (1994).

[153]B. Oh, K. Char, A. D. Kent, M. Naito, M. R. Beasley, T. H. Geballe, R. H. Hammond, J. M. Graybeal, and A. Kapitulnik, Phys. Rev. B **37**, 7861 (1988).

[154]W. E. Lawrence and S. Doniach, in *Proceedings of the Twelfth International Conference on Low Temperature Physics*, Kyoto, Japan, edited by E. Kanda (1970), p. 361.

[155]J. B. Bieri, K. Maki, and R. S. Thompson, Phys. Rev. B **44**, 4709 (1991).

[156]Y. B. Xie, Phys. Rev. B **46**, 13997 (1992).

[157]A. L. Solovjov, L. V. Omelchenko, A. V. Terekhov, K. Rogacki, R. V. Vovk, E. P. Khlybov, and A. Chroneos, Mater. Res. Express **3**, 076001 (2016).

[158]A. L. Solovjov, Fiz. Nizk. Temp. **28**, 1138 (2002) [Low Temp. Phys. **28**, 812 (2002)].

[159]A. L. Solovjov, L. V. Omelchenko, V. B. Stepanov, R. V. Vovk, H.-U. Habermeier, H. Lochmajer, P. Przyslupski, and K. Rogacki, Phys. Rev. B **94**, 224505 (2016).

[160]V. L. Ginzburg and L. D. Landau, JETP **20**, 1064 (1950).

[161]E. M. Lifshitz and L. P. Pitaevskii, *Statistical Physics* (Moscow, 1978), Vol. 2.

[162] A. Kapitulnik, M. R. Beasley, C. Castellani, and C. Di Castro, Phys. Rev. B **37**, 537 (1988).

[163] A. A. Varlamov and D. V. Livanov, JETP **98**, 584 (1990).

[164] L. Reggani, R. Vaglio, and A. A. Varlamov, Phys. Rev. B **44**, 9541 (1991).

[165] O. Tchernyshyov, Phys. Rev. B **56**, 3372 (1997).

[166] A. C. Bódi, R. Laiho, and E. Lähderanta, Physica C **411**, 107 (2004).

[167] D. D. Prokofiev, M. P. Volkov, and Yu. A. Boykov, FTT **45**, 1168 (2003).

[168] B. Leridon, A. Defossez, J. Dumont, J. Lesueur, and J. P. Contour, Phys. Rev. Lett. **87**, 197007 (2001).

[169] J. D. Jorgencen, P. Shiyou, P. Lightfoot, H. Shi, A. P. Paulikas, and B. M. W. Veal, Physica C **167**, 571 (1990).

[170] M. A. Obolenskii, R. V. Vovk, and A. V. Bondarenko, FNT **32**, 802 (2006) [Low Temp. Phys. **32**, 614 (2006)].

[171] D. J. L. Hong and D. M. Smith, J. Am. Ceram. Soc. **74**, 1751 (1991).

[172] D. D. Balla, A. V. Bondarenko, R. V. Vovk, M. A. Obolenskii, and A. A. Prodan, FNT **23**, 1035 (1997) [Low Temp. Phys. **23**, 777 (1997)].

[173] R. P. Gupta and M. Gupta, Phys. Rev. B **51**, 11760 (1995).

[174] A. P. Saiko and V. E. Gusakov, FNT **22**, 748 (1996) [Low Temp. Phys. **22**, 575 (1996)].

[175] I. V. Aleksandrov, A. F. Goncharov, and S. M. Stishov, JETP Lett. **47**, 357 (1988).

[176] U. Welp, M. Grimsditch, S. Flesher, W. Nessler, J. Downey, G. W. Crabtree, and J. Guimpel, Phys. Rev. Lett. **69**, 2130 (1992).

[177] J. Labbe and J. Bok, Europhys. Lett. **3**, 1225 (1987).

[178] R. V. Vovk, G. Ya. Khadzhai, Z. F. Nazyrov, I. L. Goulatis, and A. Chroneos, Physica B **407**, 4470 (2012).

[179] V. M. Gvozdikov, FNT **19**, 1285 (1993) [Low Temp. Phys. **19**, 914 (1993)].

[180] J. Stankowski, M. Krupski, and R. Micnas, Mater. Sci. Pol. **22**, 175 (2004).

[181] S. Sadewasser, J. S. Schilling, A. P. Paulicas, and B. M. Veal, Phys. Rev. B **61**, 741 (2000).

[182] A. A. Abrikosov, Phys. Rev. B **63**, 134518 (2001); **64**, 104521 (2001).

[183] R. Micnas and S. Robaszkiewicz, *High-Tc Superconductivity*, NATO ASI Series E, edited by E. Kaldis, E. Liarokapis, and K. A. Miller (Kluwer Academic Publishers, The Netherlands, 1997), Vol. 343, p. 31.

[184] M. Krupski, J. Stankowski, S. Przybyl, B. Andrzejewski, A. Kaczmarek, B. Hilcer, J. Marfaing, and C. Caranoni, Physica C **320**, 120 (1999).

[185] R. Micnas and B. Tobijaszewska, Acta Phys. Pol. B **32**, 3233 (2001).

[186] M. S. Islam, Supercond. Sci. Technol **3**, 531 (1990).

[187] R. V. Vovk, M. A. Obolenskii, A. A. Zavgorodniy, I. L. Goulatis, and A. I. Chroneos, J. Mater. Sci.: Mater. Electron. **20**, 853 (2009).

[188] R. V. Vovk, M. A. Obolenskii, A. A. Zavgorodniy, A. V. Bondarenko, I. L. Goulatis, A. V. Samoilov, and A. I. Chroneos, J. Alloys and Compd. **453**, 69 (2008).

[189] R. V. Vovk, Z. F. Nazyrov, M. A. Obolenskii, I. L. Goulatis, A. Chroneos, and S. V. Pinto, Philos. Mag. **91**, 2291 (2011).

[190] R. V. Vovk, M. A. Obolenskii, Z. F. Nazyrov, I. L. Goulatis, A. Chroneos, and V. M. Pinto Simoes, J. Mater. Sci.: Mater. Electron. **23**, 1255 (2012).

[191] R. V. Vovk, A. A. Zavgorodniy, M. A. Obolenskii, I. L. Goulatis, A. Chroneos, and V. P. Pinto Simoes, J. Mater. Sci.: Mater. Electron. **22**, 20 (2011).

[192] J. D. Thompson, Rev. Sci. Instrum. **55**, 231 (1984).

[193] A. L. Solovjov, M. A. Tkachenko, R. V. Vovk, and M. A. Obolenskii, FNT **37**, 1053 (2011) [Low Temp. Phys. **37**, 840 (2011)].

[194] H. J. Liu, Q. Wang, G. A. Saunders, D. P. Almond, B. Chapman, and K. Kitahama, Phys. Rev. B **51**, 9167 (1995).

[195] L. M. Ferreira, P. Pureur, H. A. Borges, and P. Lejay, Phys. Rev. B **69**, 212505 (2004).

[196] A. Maisuradze, A. Shengelaya, A. Amato, E. Pomjakushina, and H. Keller, Phys. Rev. B **84**, 184523 (2011).

[197] L. J. Shen, C. C. Lam, J. Q. Li, J. Feng, Y. S. Chen, and H. M. Shao, Supercond. Sci. Technol. **11**, 1277 (1998).

[198] K. Winzer and G. Kumm, Z. Phys. B **82**, 317 (1991).

[199] A. L. Solovjov, L. V. Omelchenko, R. V. Vovk, and S. N. Kamchatnaya, FNT **43**, 1050 (2017) [Low Temp. Phys. **43**, 841 (2017)].

[200] M. S. Grbić, M. Požek, D. Paar, V. Hinkov, M. Raichle, D. Haug, B. Keimer, N. Barišić, and A. Dulčić, Phys. Rev. B **83**, 144508 (2011).

[201] Q. Wang, G. A. Saunders, H. J. Liu, M. S. Acres, and D. P. Almond, Phys. Rev. B **55**, 8529–8543 (1997).

[202] B. N. Goshchitskii, V. L. Kozhevnikov, and M. V. Sadovskii, Int. J. Mod. Phys. B **2**, 1331 (1988).

[203] A. L. Solovjov, V. N. Svetlov, V. B. Stepanov, S. L. Sidorov, V. Yu. Tarenkov, A. I. D'yachenko, and A. B. Agafonov, FNT **37**, 703 (2011) [Low Temp. Phys. **37**, 557 (2011)].

[204] K. Rogacki, Phys. Rev. B **68**, 100507(R) (2003).

[205] N. F. Mott, *Metal-Insulator Transition* (World Scientific, London, 1974).

[206] L. Ya. Vinnikov, L. A. Gurevich, G. A. Yemelchenko, and Yu. A. Ossipyan, Solid State Commun. **67**, 421 (1988).

[207] C. Duran, P. L. Gammel, and R. Wolfe, Nature **357**, 474 (1992).

[208] A. J. Drew, Ch. Niedermayer, P. J. Baker, F. L. Pratt, S. J. Blundell, T. Lancaster, R. H. Liu, G. Wu, X. H. Chen, I. Watanabe, V. K. Malik, A. Dubroka, M. Rössle, K. W. Kim, C. Baines, and C. Bernhard, Nat. Mater. **8**, 310 (2009).

Translated by A. Bronskaya